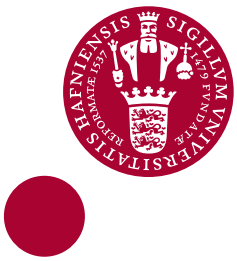

Performance of pile-up mitigation techniques for jets in pp collisions at root s=8 TeV using the ATLAS detector

Aad, G.; Abbott, B.; Abdallah, J.; Abdinov, O.; Aben, R.; Abolins, M.; AbouZeid, O.S.; Abramowicz, H.; Abreu, H.; Abreu, R.; Adye, T.; Adams, David L.; Dam, Mogens; Hansen, Jørn Dines; Hansen, Jørgen Beck; Xella, Stefania; Hansen, Peter Henrik; Petersen, Troels Christian; Thomsen, Lotte Ansgaard; Pingel, Almut Maria; Løvschall-Jensen, Ask Emil; Alonso Diaz, Alejandro; Monk, James William; Pedersen, Lars Egholm; Wiglesworth, Graig; Galster, Gorm Aske Gram Krohn

Published in:
European Physical Journal C

DOI:
10.1140/epjc/s10052-016-4395-z

Publication date:
2016

Document version
Publisher's PDF, also known as Version of record

Eur. Phys. J. C (2016) 76:581
DOI 10.1140/epjc/s10052-016-4395-z

THE EUROPEAN PHYSICAL JOURNAL C

Regular Article - Experimental Physics

Performance of pile-up mitigation techniques for jets in pp collisions at $\sqrt{s} = 8$ TeV using the ATLAS detector

ATLAS Collaboration[*]

CERN, 1211 Geneva 23, Switzerland

Received: 14 October 2015 / Accepted: 26 September 2016 / Published online: 27 October 2016

Abstract The large rate of multiple simultaneous proton–proton interactions, or pile-up, generated by the Large Hadron Collider in Run 1 required the development of many new techniques to mitigate the adverse effects of these conditions. This paper describes the methods employed in the ATLAS experiment to correct for the impact of pile-up on jet energy and jet shapes, and for the presence of spurious additional jets, with a primary focus on the large 20.3 fb^{-1} data sample collected at a centre-of-mass energy of $\sqrt{s} = 8$ TeV. The energy correction techniques that incorporate sophisticated estimates of the average pile-up energy density and tracking information are presented. Jet-to-vertex association techniques are discussed and projections of performance for the future are considered. Lastly, the extension of these techniques to mitigate the effect of pile-up on jet shapes using subtraction and grooming procedures is presented.

Contents

[*] e-mail: atlas.publications@cern.ch

1 Introduction

The success of the proton–proton (pp) operation of the Large Hadron Collider (LHC) at $\sqrt{s} = 8$ TeV led to instantaneous luminosities of up to 7.7×10^{33} cm^{-2} s^{-1} at the beginning of a fill. Consequently, multiple pp interactions occur within each bunch crossing. Averaged over the full data sample, the mean number of such simultaneous interactions (pile-up) is approximately 21. These additional collisions are uncorrelated with the hard-scattering process that typically triggers the event and can be approximated as contributing a background of soft energy depositions that have particularly adverse and complex effects on jet reconstruction. Hadronic jets are observed as groups of topologically related energy deposits in the ATLAS calorimeters, and therefore pile-up affects the measured jet energy and jet structure observables. Pile-up interactions can also directly generate additional jets. The production of such *pile-up jets* can occur from additional $2 \rightarrow 2$ interactions that are independent of the hard-scattering and from contributions due to soft energy deposits that would not otherwise exceed the threshold to be considered a jet. An understanding of all of these effects is therefore critical for precision measurements as well as searches for new physics.

The expected amount of pile-up (μ) in each bunch crossing is related to the instantaneous luminosity ($\mathcal{L}_0$) by the following relationship:

$$\mu = \frac{\mathcal{L}_0 \sigma_{\mathrm{inelastic}}}{n_{\mathrm{c}}\, f_{\mathrm{rev}}} \tag{1}$$

where n_{c} is the number of colliding bunch pairs in the LHC, $f_{\mathrm{rev}} = 11.245$ kHz is the revolution frequency [1], and $\sigma_{\mathrm{inelastic}}$ is the pp inelastic cross section. When the instan-

taneous luminosity is measured by integrating over many bunch crossings, Eq. (1) yields the average number of interactions per crossing, or $\langle\mu\rangle$. The so-called *in-time pile-up* due to additional pp collisions within a single bunch crossing can also be accompanied by *out-of-time pile-up* due to signals from collisions in other bunch crossings. This occurs when the detector and/or electronics integration time is significantly larger than the time between crossings, as is the case for the liquid-argon (LAr) calorimeters in the ATLAS detector. The measured detector response as a function of $\langle\mu\rangle$ in such cases is sensitive to the level of out-of-time pile-up. The distributions of $\langle\mu\rangle$ for both the $\sqrt{s} = 7$ TeV and $\sqrt{s} = 8$ TeV runs (collectively referred to as Run 1) are shown in Fig. 1. The spacing between successive proton bunches was 50 ns for the majority of data collected during Run 1. This bunch spacing is decreased to 25 ns for LHC Run 2. Out-of-time pile-up contributions are likely to increase with this change. However, the LAr calorimeter readout electronics are also designed to provide an optimal detector response for a 25 ns bunch spacing scenario, and thus the relative impact of the change to 25 ns may be mitigated, particularly in the case of the calorimeter response (see Sect. 2).

The different responses of the individual ATLAS subdetector systems to pile-up influence the methods used to mitigate its effects. The sensitivity of the calorimeter energy measurements to multiple bunch crossings, and the LAr EM calorimeter in particular, necessitates correction techniques that incorporate estimates of the impact of both in-time and out-of-time pile-up. These techniques use the average deposited energy density due to pile-up as well as track-based quantities from the inner tracking detector (ID) such as the number of reconstructed primary vertices (N_{PV}) in an event. Due to the fast response of the silicon tracking detectors, this quantity is not affected by out-of-time pile-up, to a very good approximation.

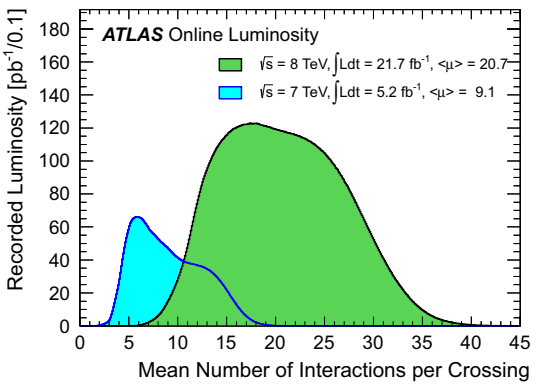

Fig. 1 The luminosity-weighted distribution of the mean number of interactions per bunch crossing for the 2011 ($\sqrt{s} = 7$ TeV) and 2012 ($\sqrt{s} = 8$ TeV) pp data samples

Resolving individual vertices using the ATLAS ID is a critical task in accurately determining the origin of charged-particle tracks that point to energy deposits in the calorimeter. By identifying tracks that originate in the hard-scatter primary vertex, jets that contain significant contamination from pile-up interactions can be rejected. These approaches provide tools for reducing or even obviating the effects of pile-up on the measurements from individual subdetector systems used in various stages of the jet reconstruction. The result is a robust, stable jet definition, even at very high luminosities.

The first part of this paper describes the implementation of methods to partially suppress the impact of signals from pile-up interactions on jet reconstruction and to directly estimate event-by-event pile-up activity and jet-by-jet pile-up sensitivity, originally proposed in Ref. [2]. These estimates allow for a sophisticated pile-up subtraction technique in which the four-momentum of the jet and the jet shape are corrected event-by-event for fluctuations due to pile-up, and whereby jet-by-jet variations in pile-up sensitivity are automatically accommodated. The performance of these new pile-up correction methods is assessed and compared to previous pile-up corrections based on the number of reconstructed primary vertices and the instantaneous luminosity [3,4]. Since the pile-up subtraction is the first step of the jet energy scale (JES) correction in ATLAS, these techniques play a crucial role in establishing the overall systematic uncertainty of the jet energy scale. Nearly all ATLAS measurements and searches for physics beyond the Standard Model published since the end of the 2012 data-taking period utilise these methods, including the majority of the final Run 1 Higgs cross section and coupling measurements [5–9].

The second part of this paper describes the use of tracks to assign jets to the hard-scatter interaction. By matching tracks to jets, one obtains a measure of the fraction of the jet energy associated with a particular primary vertex. Several track-based methods allow the rejection of spurious calorimeter jets resulting from local fluctuations in pile-up activity, as well as real jets originating from single pile-up interactions, resulting in improved stability of the reconstructed jet multiplicity against pile-up. Track-based methods to reject pile-up jets are applied after the full chain of JES corrections, as pile-up jet tagging algorithms.

The discussion of these approaches proceeds as follows. The ATLAS detector is described in Sect. 2 and the data and Monte Carlo simulation samples are described in Sect. 3. Section 4 describes how the inputs to jet reconstruction are optimised to reduce the effects of pile-up on jet constituents. Methods for subtracting pile-up from jets, primarily focusing on the impacts on calorimeter-based measurements of jet kinematics and jet shapes, are discussed in Sect. 5. Approaches to suppressing the effects of pile-up using both the subtraction techniques and charged-particle tracking information are then presented in Sect. 6. Lastly, techniques

that aim to correct jets by actively removing specific energy deposits that are due to pile-up, are discussed in Sect. 7.

2 The ATLAS detector

The ATLAS detector [10,11] provides nearly full solid angle coverage around the collision point with an inner tracking system covering the pseudorapidity range $|\eta| < 2.5$,[1] electromagnetic and hadronic calorimeters covering $|\eta| < 4.9$, and a muon spectrometer covering $|\eta| < 2.7$.

The ID comprises a silicon pixel tracker closest to the beamline, a microstrip silicon tracker, and a straw-tube transition radiation tracker at radii up to 108 cm. These detectors are layered radially around each other in the central region. A thin superconducting solenoid surrounding the tracker provides an axial 2 T field enabling the measurement of charged-particle momenta. The overall ID acceptance spans the full azimuthal range in ϕ for particles originating near the nominal LHC interaction region [12–14]. Due to the fast readout design of the silicon pixel and microstrip trackers, the track reconstruction is only affected by in-time pile-up. The efficiency to reconstruct charged hadrons ranges from 78% at $p_{\mathrm{T}}^{\mathrm{track}} = 500$ MeV to more than 85% above 10 GeV, with a transverse impact parameter (d_0) resolution of 10 μm for high-momentum particles in the central region. For jets with p_{T} above approximately 500 GeV, the reconstruction efficiency for tracks in the core of the jet starts to degrade because these tracks share many clusters in the pixel tracker, creating ambiguities when matching the clusters with track candidates, and leading to lost tracks.

The high-granularity EM and hadronic calorimeters are composed of multiple subdetectors spanning $|\eta| \leq 4.9$. The EM barrel calorimeter uses a LAr active medium and lead absorbers. In the region $|\eta| < 1.7$, the hadronic (Tile) calorimeter is constructed from steel absorber and scintillator tiles and is separated into barrel ($|\eta| < 1.0$) and extended barrel ($0.8 < |\eta| < 1.7$) sections. The calorimeter end-cap ($1.375 < |\eta| < 3.2$) and forward ($3.1 < |\eta| < 4.9$) regions are instrumented with LAr calorimeters for EM and hadronic energy measurements. The response of the calorimeters to single charged hadrons—defined as the energy (E) reconstructed for a given charged hadron momentum (p), or E/p—ranges from 20 to 80% in the range of charged hadron momentum between 1–30 GeV and is well described by Monte Carlo (MC) simulation [15]. In contrast to the pixel and microstrip tracking detectors, the LAr calorimeter readout is sensitive to signals from the preceding 12 bunch crossings during 50 ns bunch spacing operation [16,17]. For the 25 ns bunch spacing scenario expected during Run 2 of the LHC, this increases to 24 bunch crossings. The LAr calorimeter uses bipolar shaping with positive and negative output which ensures that the average signal induced by pile-up averages to zero in the nominal 25 ns bunch spacing operation. Consequently, although the LAr detector will be exposed to more out-of-time pile-up in Run 2, the signal shaping of the front-end electronics is optimised for this shorter spacing [16,18], and is expected to cope well with the change. The fast readout of the Tile calorimeter, however, makes it relatively insensitive to out-of-time pile-up [19]. The LAr barrel has three EM layers longitudinal in shower depth (EM1, EM2, EM3), whereas the LAr end-cap has three EM layers (EMEC1, EMEC2, EMEC3) in the range $1.5 < |\eta| < 2.5$, two layers in the range $2.5 < |\eta| < 3.2$ and four hadronic layers (HEC1, HEC2, HEC3, HEC4). In addition, there is a pre-sampler layer in front of the $\mathrm{LA_r}$ barrel and end-cap EM calorimeter (PS). The transverse segmentation of both the EM and hadronic LAr end-caps is reduced in the region between $2.5 < |\eta| < 3.2$ compared to the barrel layers. The forward LAr calorimeter has one EM layer (FCal1) and two hadronic layers (FCal2, FCal3) with transverse segmentation similar to the more forward HEC region. The Tile calorimeter has three layers longitudinal in shower depth (Tile1, Tile2, Tile3) as well as scintillators in the gap region spanning ($0.85 < |\eta| < 1.51$) between the barrel and extended barrel sections.

3 Data and Monte Carlo samples

This section provides a description of the data selection and definitions of objects used in the analysis (Sect. 3.1) as well as of the simulated event samples to which the data are compared (Sect. 3.2).

3.1 Object definitions and event selection

The full 2012 pp data-taking period at a centre-of-mass energy of $\sqrt{s} = 8$ TeV is used for these measurements presented here. Events are required to meet baseline quality criteria during stable LHC running periods. The ATLAS data quality (DQ) criteria reject data with significant contamination from detector noise or issues in the read-out [20] based upon individual assessments for each subdetector. These criteria are established separately for the barrel, end-cap and forward regions, and they differ depending on the trigger

[1] The ATLAS reference system is a Cartesian right-handed coordinate system, with the nominal collision point at the origin. The anticlockwise beam direction defines the positive z-axis, while the positive x-axis is defined as pointing from the collision point to the centre of the LHC ring and the positive y-axis points upwards. The azimuthal angle ϕ is measured around the beam axis, and the polar angle θ is measured with respect to the z-axis. Pseudorapidity is defined as $\eta = -\ln[\tan(\theta/2)]$, rapidity is defined as $y = 0.5\ \ln[(E + p_z)/(E - p_z)]$, where E is the energy and p_z is the z-component of the momentum, and the transverse energy is defined as $E_{\mathrm{T}} = E \sin\theta$.

conditions and reconstruction of each type of physics object (for example jets, electrons and muons). The resulting dataset corresponds to an integrated luminosity of 20.3 ± 0.6 fb^{-1} following the methodology described in Ref. [21].

To reject non-collision backgrounds [22], events are required to contain at least one primary vertex consistent with the LHC beam spot, reconstructed from at least two tracks each with $p_{\mathrm{T}}^{\mathrm{track}} > 400$ MeV. The primary hard-scatter vertex is defined as the vertex with the highest $\sum (p_{\mathrm{T}}^{\mathrm{track}})^2$. To reject rare events contaminated by spurious signals in the detector, all anti-k_t [23,24] jets with radius parameter $R = 0.4$ and $p_{\mathrm{T}}^{\mathrm{jet}} > 20$GeV (see below) are required to satisfy the jet quality requirements that are discussed in detail in Ref. [22] (and therein referred to as the "looser" selection). These criteria are designed to reject non-collision backgrounds and significant transient noise in the calorimeters while maintaining an efficiency for good-quality events greater than 99.8% with as high a rejection of contaminated events as possible. In particular, this selection is very efficient in rejecting events that contain fake jets due to calorimeter noise.

Hadronic jets are reconstructed from calibrated three-dimensional topo-clusters [25]. Clusters are constructed from calorimeter cells that are grouped together using a topological clustering algorithm. These objects provide a three-dimensional representation of energy depositions in the calorimeter and implement a nearest-neighbour noise suppression algorithm. The resulting topo-clusters are classified as either electromagnetic or hadronic based on their shape, depth and energy density. Energy corrections are then applied to the clusters in order to calibrate them to the appropriate energy scale for their classification. These corrections are collectively referred to as *local cluster weighting*, or LCW, and jets that are calibrated using this procedure are referred to as LCW jets [4].

Jets can also be built from charged-particle tracks (track-jets) using the identical anti-k_t algorithm as for jets built from calorimeter clusters. Tracks used to construct track-jets have to satisfy minimal quality criteria, and they are required to be associated with the hard-scatter vertex.

The jets used for the analyses presented here are primarily found and reconstructed using the anti-k_t algorithm with radius parameters $R = 0.4, 0.6$ and 1.0. In some cases, studies of *groomed* jets are also performed, for which algorithms are used to selectively remove constituents from a jet. Groomed jets are often used in searches involving highly Lorentz-boosted massive objects such as W/Z bosons [26] or top quarks [27]. Unless noted otherwise, the jet trimming algorithm [28] is used for groomed jet studies in this paper. The procedure implements a k_t algorithm [29,30] to create small *subjets* with a radius $R_{\mathrm{sub}} = 0.3$. The ratio of the p_{T} of these subjets to that of the jet is used to remove constituents from the jet. Any subjets with $p_{\mathrm{T}i}/p_{\mathrm{T}}^{\mathrm{jet}} < f_{\mathrm{cut}}$ are removed, where $p_{\mathrm{T}i}$ is the transverse momentum of the ith subjet, and $f_{\mathrm{cut}} = 0.05$ is determined to be an optimal setting for improving mass resolution, mitigating the effects of pile-up, and retaining substructure information [31]. The remaining constituents form the trimmed jet.

The energy of the reconstructed jet may be further corrected using subtraction techniques and multiplicative jet energy scale correction factors that are derived from MC simulation and validated with the data [3,4]. As discussed extensively in Sect. 5, subtraction procedures are critical to mitigating the jet energy scale dependence on pile-up. Specific jet energy scale correction factors are then applied after the subtraction is performed. The same corrections are applied to calorimeter jets in MC simulation and data to ensure consistency when direct comparisons are made between them.

Comparisons are also made to jets built from particles in the MC generator's event record ("truth particles"). In such cases, the inputs to jet reconstruction are stable particles with a lifetime of at least 10 ps (excluding muons and neutrinos). Such jets are referred to as *generator-level jets* or *truth-particle jets* and are to be distinguished from *parton-level jets*. Truth-particle jets represent the measurement for a hermetic detector with perfect resolution and scale, without pile-up, but including the underlying event.

Trigger decisions in ATLAS are made in three stages: Level-1, Level-2 and the Event Filter. The Level-1 trigger is implemented in hardware and uses a subset of detector information to reduce the event rate to a design value of at most 75 kHz. This is followed by two software-based triggers, Level-2 and the Event Filter, which together reduce the event rate to a few hundred Hz. The measurements presented in this paper primarily use single-jet triggers. The rate of events in which the highest transverse momentum jet is less than about 400 GeV is too high to record more than a small fraction of them. The triggers for such events are therefore pre-scaled to reduce the rates to an acceptable level in an unbiased manner. Where necessary, analyses compensate for the pre-scales by using weighted events based upon the pre-scale setting that was active at the time of the collision.

3.2 Monte Carlo simulation

Two primary MC event generator programs are used for comparison to the data. PYTHIA 8.160 [32] with the ATLAS A2 tunable parameter set (tune) [33] and the CT10 NLO parton distribution function (PDF) set [34] is used for the majority of comparisons. Comparisons are also made to the HERWIG++ 2.5.2 [35] program using the CTEQ6L1 [36] PDF set along with the UE7- 2 tune [37], which is tuned to reproduce underlying-event data from the LHC experiments. MC events are passed through the full GEANT4 [38] detector simulation of ATLAS [39] after the simulation of the parton shower and hadronisation processes. Identical reconstruction

and trigger, event, quality, jet and track selection criteria are then applied to both the MC simulation and to the data.

In some cases, additional processes are used for comparison to data. The Z boson samples used for the validation studies are produced with the POWHEG-BOX v1.0 generator [40–42] and the SHERPA 1.4.0 [43] generator, both of which provide NLO matrix elements for inclusive Z boson production. The CT10 NLO PDF set is also used in the matrix-element calculation for these samples. The modelling of the parton shower, multi-parton interactions and hadronisation for events generated using POWHEG-BOX is provided by PYTHIA 8.163 with the AU2 underlying-event tune [33] and the CT10 NLO PDF set. These MC samples are thus referred to as POWHEG+PYTHIA 8 samples. PYTHIA is in turn interfaced with PHOTOS [44] for the modelling of QED final-state radiation.

Pile-up is simulated for all samples by overlaying additional soft pp collisions which are also generated with PYTHIA 8.160 using the ATLAS A2 tune and the MSTW2008LO PDF set [45]. These additional events are overlaid onto the hard-scattering events according to the measured distribution of the average number $\langle\mu\rangle$ of pp interactions per bunch crossing from the luminosity detectors in ATLAS [21,46] using the full 8 TeV data sample, as shown in Fig. 1. The proton bunches were organised in four trains of 36 bunches with a 50 ns spacing between the bunches. Therefore, the simulation also contains effects from out-of-time pile-up. The effect of this pile-up history for a given detector system is then determined by the size of the readout time window for the relevant electronics. As an example, for the central LAr calorimeter barrel region, which is sensitive to signals from the preceding 12 bunch crossings during 50 ns bunch spacing operation, the digitization window is set to 751 ns before and 101 ns after the simulated hard-scattering interaction.

4 Topological clustering and cluster-level pile-up suppression

The first step for pile-up mitigation in ATLAS is at the level of the constituents used to reconstruct jets. The topological clustering algorithm incorporates a built-in pile-up suppression scheme to limit the formation of clusters produced by pile-up depositions as well as to limit the growth of clusters around highly energetic cells from hard-scatter signals. The key concept that allows this suppression is the treatment of pile-up as noise, and the use of cell energy thresholds based on their energy significance relative to the total noise.

Topological clusters are built using a three-dimensional nearest-neighbour algorithm that clusters calorimeter cells with energy significance $|E_{\text{cell}}|/\sigma^{\text{noise}} > 4$ for the seed, iterates among all neighbouring cells with $|E_{\text{cell}}|/\sigma^{\text{noise}} > 2$, and that finally adds one additional layer of cells $|E_{\text{cell}}|/\sigma^{\text{noise}} > 0$ when no further nearest-neighbours exceed the 2σ threshold at the boundary (not allowed to extend to next-to-nearest neighbours). The total cell noise, σ^{noise}, is the sum in quadrature of the cell noise due to the readout electronics and the cell noise that is due to pile-up ($\sigma^{\text{noise}}_{\text{pile-up}}$). The pile-up noise for a given cell is evaluated from Monte Carlo simulation and is defined to be the RMS of the energy distribution resulting from pile-up particles for a given number of pp collisions per bunch crossing (determined by $\langle\mu\rangle$) and a given bunch spacing Δt. It is technically possible to adjust the pile-up noise for specific data-taking periods depending on $\langle\mu\rangle$, but it was kept fixed for the entire Run 1 8 TeV dataset.

By adjusting the pile-up noise value, topological clustering partially suppresses the formation of clusters created by pile-up fluctuations, and it reduces the number of cells included in jets. Raising the pile-up noise value effectively increases the threshold for cluster formation and growth, significantly reducing the effects of pile-up on the input signals to jet reconstruction.

Figure 2 shows the electronic and pile-up noise contributions to cells that are used to define the thresholds for the topological clustering algorithm. In events with an average of 30 additional pile-up interactions ($\langle\mu\rangle = 30$), the noise from pile-up depositions is approximately a factor of 2 larger than the electronic noise for cells in the central electromagnetic calorimeter, and it reaches 10 GeV in FCal1 and FCal2. This high threshold in the forward region translates into a reduced topo-cluster occupancy due to the coarser segmentation of the forward calorimeter, and thus a smaller probability that a given event has a fluctuation beyond 4σ. The implications of this behaviour for the pile-up p_{T} density estimation are discussed in Sect. 5.1.

The value of $\langle\mu\rangle$ at which $\sigma^{\text{noise}}_{\text{pile-up}}$ is evaluated for a given data-taking period is chosen to be high enough that the number of clusters does not grow too large due to pile-up and at the same time low enough to retain as much signal as possible. For a Gaussian noise distribution the actual 4σ seed threshold leads to an increase in the number of clusters by a factor of 5 if the noise is underestimated by 10%. Therefore $\sigma^{\text{noise}}_{\text{pile-up}}$ was set to the pile-up noise corresponding to the largest expected $\langle\mu\rangle$ rather than the average or the lowest expected value. For 2012 (2011) pile-up conditions, $\sigma^{\text{noise}}_{\text{pile-up}}$ was set to the value of $\sigma^{\text{noise}}_{\text{pile-up}}$ corresponding to $\langle\mu\rangle = 30$ ($\langle\mu\rangle = 8$).

The local hadron calibration procedure for clusters depends on the value of σ^{noise} since this choice influences the cluster size and thus the shape variables used in the calibration. Therefore, the calibration constants are re-computed for each σ^{noise} configuration. For this reason, a single, fixed value of σ^{noise} is used for entire data set periods in order to maintain consistent conditions.

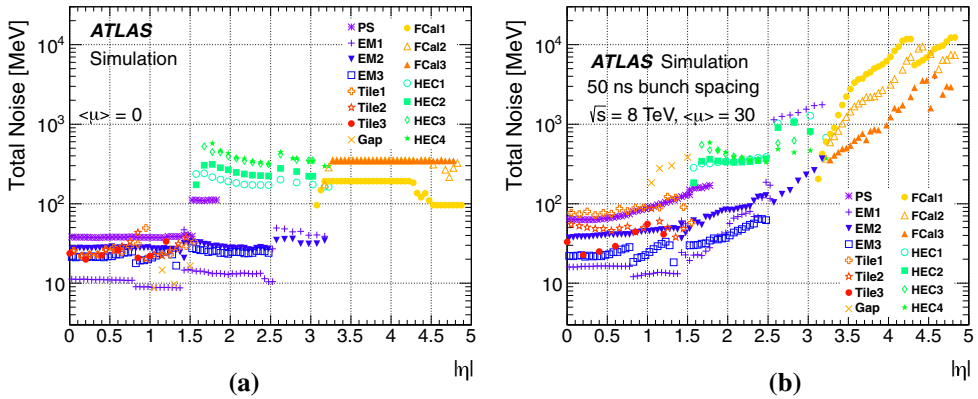

Fig. 2 **a** Per-cell electronic noise ($\langle\mu\rangle = 0$) and **b** total noise per cell at high luminosity corresponding to $\langle\mu\rangle = 30$ interactions per bunch crossing with a bunch spacing of $\Delta t = 50$ ns, in MeV, for each calorimeter layer. The *different colours* indicate the noise in the pre-sampler (PS), the up to three layers of the LAr calorimeter (EM), the up to three layers of the Tile calorimeter (Tile), the four layers of the hadronic endcap calorimeter (HEC), and the three layers of the forward calorimeter (FCal). The total noise, σ^{noise}, is the sum in quadrature of electronic noise and the expected RMS of the energy distribution corresponding to a single cell

5 Pile-up subtraction techniques and results

The independence of the hard-scattering process from additional pile-up interactions in a given event results in positive or negative shifts to the reconstructed jet kinematics and to the jet shape. This motivates the use of subtraction procedures to remove these contributions to the jet. Early subtraction methods [3,4] for mitigating the effects of pile-up on the jet transverse momentum in ATLAS relied on an average offset correction ($\langle\mathcal{O}^{\text{jet}}\rangle$),

$$p_{\text{T}}^{\text{corr}} = p_{\text{T}}^{\text{jet}} - \langle\mathcal{O}^{\text{jet}}(\langle\mu\rangle, N_{\text{PV}}, \eta)\rangle. \tag{2}$$

In these early approaches, $\langle\mathcal{O}^{\text{jet}}\rangle$ is determined from in-situ studies or MC simulation and represents an average offset applied to the jet p_{T}. This offset is parametrised as a function of η, N_{PV} and $\langle\mu\rangle$. Such methods do not fully capture the fluctuations of the pile-up energy added to the calorimeter on an event-by-event basis; that component is only indirectly estimated from its implicit dependence on N_{PV}. Moreover, no individual jet's information enters into this correction and thus jet-by-jet fluctuations in the actual offset of that particular jet p_{T}, $\mathcal{O}^{\text{jet}}$, or the jet shape, cannot be taken into account. Similar methods have also been pursued by the CMS collaboration [47], as well a much more complex approaches that attempt to mitigate the effects of pile-up prior to jet reconstruction [48,49].

The approach adopted for the final Run 1 ATLAS jet energy scale [4] is to estimate $\mathcal{O}^{\text{jet}}$ on an event-by-event basis. To accomplish this, a measure of the jet's susceptibility to soft energy depositions is needed in conjunction with a method to estimate the magnitude of the effect on a jet-by-jet and event-by-event basis. A natural approach is to define a jet *area* (A^{jet}) [50] in η–ϕ space along with a pile-up p_{T} density, ρ. The offset can then be determined dynamically for each jet [2] using

$$\mathcal{O}^{\text{jet}} = \rho \times A^{\text{jet}}. \tag{3}$$

Nearly all results published by ATLAS since 2012 have adopted this technique for correcting the jet kinematics for pile-up effects. The performance of this approach, as applied to both the jet kinematics and the jet shape, is discussed below.

5.1 Pile-up event p_{T} density ρ

One of the key parameters in the pile-up subtraction methods presented in this paper is the estimated pile-up p_{T} density characterised by the observable ρ. The pile-up p_{T} density of an event can be estimated as the median of the distribution of the density of many k_t jets, constructed with no minimum p_{T} threshold [29,30] in the event. Explicitly, this is defined as

$$\rho = \text{median}\left\{\frac{p_{\text{T},i}^{\text{jet}}}{A_i^{\text{jet}}}\right\}, \tag{4}$$

where each k_t jet i has transverse momentum $p_{\text{T},i}^{\text{jet}}$ and area A_i^{jet}, and it is defined with a nominal radius parameter $R_{k_t} = 0.4$. The chosen radius parameter value is the result of a dedicated optimisation study, balancing two competing effects: the sensitivity to biases from hard-jet contamination in the ρ calculation when R_{k_t} is large, and statistical fluctuations when R_{k_t} is small. The sensitivity to the chosen radius value is not large, but measurably worse performance was

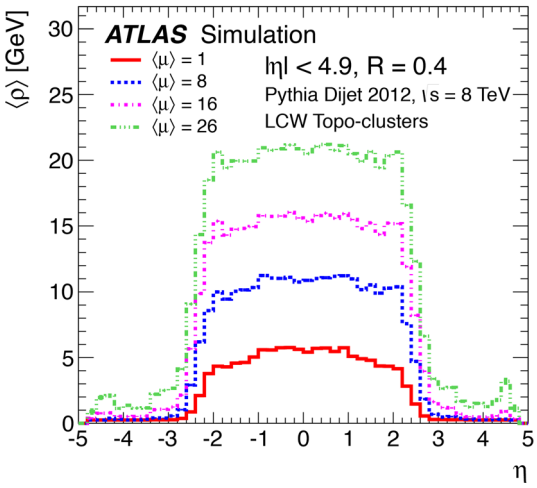

Fig. 3 The mean estimated pile-up p_{T} density, ρ as a function of η, in simulated PYTHIA 8 dijet events

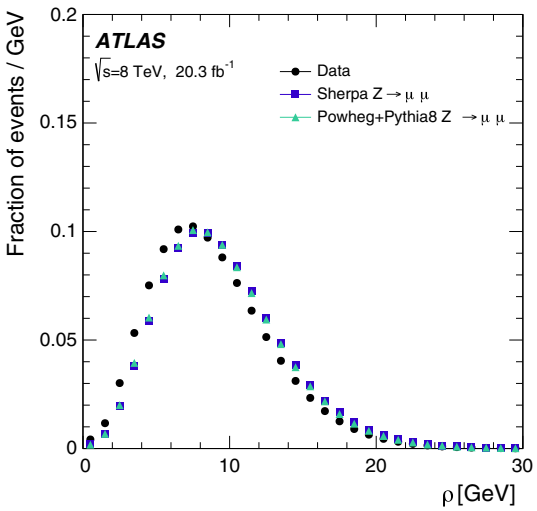

Fig. 4 The distribution of estimated pile-up p_{T} density, ρ, in $Z(\rightarrow \mu\mu)$+jets events using data and two independent MC simulation samples (SHERPA and POWHEG+PYTHIA 8). Both MC generators use the same pile-up simulation model (PYTHIA 8.160), and this model uses the $\langle\mu\rangle$ distribution for 8 TeV data shown in Fig. 1. ρ is calculated in the central region using topo-clusters with positive energy within $|\eta| \leq 2.0$

observed for radius parameters larger than 0.5 and smaller than 0.3.

The use of the k_t algorithm in Eq. (4) is motivated by its sensitivity to soft radiation and thus no minimum p_{T} selection is applied to the k_t jets that are used. In ATLAS, the inputs to the k_t jets used in the ρ calculation are positive-energy calorimeter topo-clusters within $|\eta| \leq 2.0$. The η range chosen for calculating ρ is motivated by the calorimeter occupancy, which is low in the forward region relative to the central region. The cause of the low occupancy in the forward region is complex and is intrinsically related to the calorimeter segmentation and response. The coarser calorimeter cell size at higher $|\eta|$ [10], coupled with the noise suppression inherent in topological clustering, plays a large role. Since topo-clusters are seeded according to significance relative to (electronic and pile-up) noise rather than an absolute threshold, having a larger number of cells (finer segmentation) increases the probability that the energy of one cell fluctuates up to a significant value due to (electronic or pile-up) noise. With the coarser segmentation in the end-cap and forward regions beginning near $|\eta| = 2.5$ (see Fig. 2), this probability becomes smaller, and clusters are predominantly seeded only by the hard-scatter signal. In addition, the likelihood that hadronic showers overlap in a single cell increases along with the probability that fluctuations in the calorimeter response cancel, which affects the energy deposited in the cell. The mean ρ measured as a function of η is shown in Fig. 3. The measurements are made in narrow strips in η which are $\Delta\eta = 0.7$ wide and shifted in steps of $\delta\eta = 0.1$ from $\eta = -4.9$ to 4.9. The η reported in Fig. 3 is the central value of each strip. The measured ρ in each strip quickly drops to nearly zero beyond $|\eta| \simeq 2$. Due to this effectively stricter suppression in the forward region, a calculation of ρ in the central region gives a more meaningful measure of the pile-up activity than the median over the entire η range, or an η-dependent ρ calculated in slices across the calorimeter.

Distributions of ρ in both data and MC simulation are presented in Fig. 4 for SHERPA and POWHEG+PYTHIA 8. Both MC generators use the same pile-up simulation model. The event selection used for these distributions corresponds to $Z(\rightarrow \mu\mu)$+jets events where a Z boson ($p_{\mathrm{T}}^{Z} > 30$ GeV) and a jet ($|\eta| < 2.5$ and $p_{\mathrm{T}} > 20$ GeV) are produced back-to-back ($\Delta\phi(Z, \text{leading jet}) > 2.9$). Both MC simulations slightly overestimate ρ, but agree well with each other. Small differences between the MC simulations can be caused by different modelling of the soft jet spectrum associated with the hard-scattering and the underlying event.

Since ρ is computed event-by-event, separately for data and MC, a key advantage of the jet area subtraction is that it reduces the pile-up uncertainty from detector mismodelling effects. This is because different values of ρ are determined in data and simulation depending on the measured pile-up activity rather than using a predicted value for ρ based on MC simulations.

5.2 Pile-up energy subtraction

The median p_{T} density ρ provides a direct estimate of the global pile-up activity in each event, whereas the jet area provides an estimate of an individual jet's susceptibility to pile-up. Equation (2) can thus be expressed on a jet-by-jet basis using Eq. (3) instead of requiring an average calculation of the offset, $\langle\mathcal{O}\rangle$. This yields the following pile-up subtraction scheme:

$$p_{\mathrm{T}}^{\mathrm{corr}} = p_{\mathrm{T}}^{\mathrm{jet}} - \rho \times A^{\mathrm{jet}}. \quad (5)$$

There are two ways in which pile-up can contribute energy to an event: either by forming new clusters, or by overlapping with signals from the hard-scattering event. Because of the noise suppression inherent in topological clustering, only pile-up signals above a certain threshold can form separate clusters. Low-energy pile-up deposits can thus only contribute measurable energy to the event if they overlap with other deposits that survive noise suppression. The probability of overlap is dependent on the transverse size of EM and hadronic showers in the calorimeter, relative to the size of the calorimeter cells. Due to fine segmentation, pile-up mainly contributes extra clusters in the central regions of the calorimeter where ρ is calculated ($|\eta| \lesssim 2$).

As discussed in Sect. 2, the details of the readout electronics for the LAr calorimeter can result in signals associated with out-of-time pile-up activity. If out-of-time signals from earlier bunch crossings are isolated from in-time signals, they may form negative energy clusters, which are excluded from jet reconstruction and the calculation of ρ. However, overlap between the positive jet signals and out-of-time activity results in both positive and negative modulation of the jet energy. Due to the long negative component of the LAr pulse shape, the probability is higher for an earlier bunch crossing to negatively contribute to signals from the triggered event than a later bunch crossing to contribute positively. This feature results in a negative dependence of the jet p_{T} on out-of-time pile-up. Such overlap is more probable at higher $|\eta|$, due to coarser segmentation relative to the transverse shower size. In addition, the length of the bipolar pulse is shorter in the forward calorimeters, which results in larger fluctuations in the out-of-time energy contributions to jets in the triggered event since the area of the pulse shape must remain constant. As a result, forward jets have enhanced sensitivity to out-of-time pile-up due to the larger impact of fluctuations of pile-up energy depositions in immediately neighbouring bunch crossings.

Since the ρ calculation is dominated by lower-occupancy regions in the calorimeter, the sensitivity of ρ to pile-up does not fully describe the pile-up sensitivity of the high-occupancy region at the core of a high-p_{T} jet. The noise suppression provided by the topological clustering procedure has a smaller impact in the dense core of a jet where significant nearby energy deposition causes a larger number of small signals to be included in the final clusters than would otherwise be possible. Furthermore, the effects of pile-up in the forward region are not well described by the median p_{T} density as obtained from positive clusters in the central region. A residual correction is therefore necessary to obtain an average jet response that is insensitive to pile-up across the full p_{T} range.

Figure 5 shows the η dependence of the transverse momentum of anti-k_t $R = 0.4$ jets on N_{PV} (for fixed $\langle\mu\rangle$) and on $\langle\mu\rangle$ (for fixed N_{PV}). Separating these dependencies probes the effects of in-time and out-of-time pile-up, respectively, as a function of η. These results were obtained from linear fits to the difference between the reconstructed and the true jet p_{T} (written as $p_{\mathrm{T}}^{\mathrm{reco}} - p_{\mathrm{T}}^{\mathrm{true}}$) as a function of both N_{PV} and $\langle\mu\rangle$. The subtraction of $\rho \times A^{\mathrm{jet}}$ removes a significant fraction of the sensitivity to in-time pile-up. In particular, the dependence decreases from nearly 0.5 GeV per additional vertex to $\lesssim 0.2$ GeV per vertex, or a factor of 3–5 reduction in pile-up sensitivity. This reduction in the dependence of the p_{T} on pile-up does not necessarily translate into a reduction of the pile-up dependence of other jet observables. Moreover, some residual dependence on N_{PV} remains. Figure 5b shows that $\rho \times A^{\mathrm{jet}}$ subtraction has very little effect on the sensitivity to out-of-time pile-up, which is particularly significant in the forward region. The dependence on N_{PV} is evaluated in bins of $\langle\mu\rangle$, and vice versa. Both dependencies are evaluated in bins of $p_{\mathrm{T}}^{\mathrm{true}}$ and η as well. The slope of the linear fit as a function of N_{PV} does not depend significantly on $\langle\mu\rangle$, or vice versa, within each ($p_{\mathrm{T}}^{\mathrm{true}}$, η) bin. In other words, there is no statistically significant evidence for non-linearity or cross-terms in the sensitivity of the jet p_{T} to in-time or out-of-time pile-up for the values of $\langle\mu\rangle$ seen in 2012 data. A measurable effect of such non-linearities may occur with the shorter bunch spacing operation, and thus increased out-of-time pile-up effects, expected during Run 2 of the LHC. Measurements and validations of this sort are therefore important for establishing the sensitivity of this correction technique to such changes in the operational characteristics of the accelerator.

After subtracting $\rho \times A^{\mathrm{jet}}$ from the jet p_{T}, there is an additional subtraction of a residual term proportional to the number ($N_{\mathrm{PV}} - 1$) of reconstructed pile-up vertices, as well as a residual term proportional to $\langle\mu\rangle$ (to account for out-of-time pile-up). This residual correction is derived by comparison to truth particle jets in simulated dijet events, and it is completely analogous to the average pile-up offset correction used previously in ATLAS [4]. Due to the preceding $\rho \times A^{\mathrm{jet}}$ subtraction, the residual correction is generally quite small for jets with $|\eta| < 2.1$. In the forward region, the negative dependence of jets on out-of-time pile-up results in a significantly larger residual correction. The $\langle\mu\rangle$-dependent term of the residual correction is approximately the same size as the corresponding term in the average offset correction of Eq. (2), but the N_{PV}-dependent term is significantly smaller. This is true even in the forward region, which shows that ρ is a useful estimate of in-time pile-up activity even beyond the region in which it is calculated.

Several additional jet definitions are also studied, including larger nominal jet radii and alternative jet algorithms. Prior to the jet area subtraction, a larger sensitivity to in-time pile-up is observed for larger-area jets, as expected. Follow-

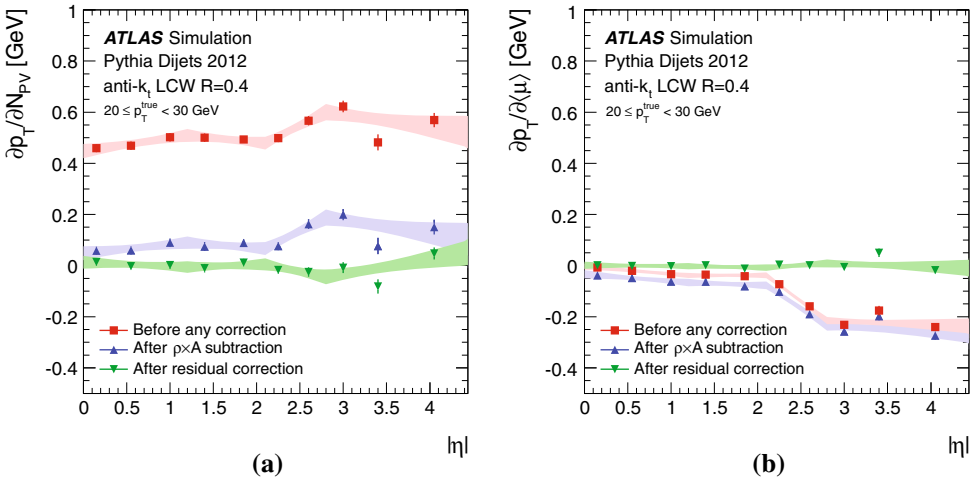

Fig. 5 Dependence of the reconstructed jet p_{T} (anti-k_t, $R = 0.4$, LCW scale) on **a** in-time pile-up measured using N_{PV} and **b** out-of-time pile-up measured using $\langle\mu\rangle$. In each case, the dependence of the jet p_{T} is shown for three correction stages: before any correction, after the $\rho \times A^{\mathrm{jet}}$ subtraction, and after the residual correction. The error bands show the 68% confidence intervals of the fits. The dependence was obtained by comparison with truth-particle jets in simulated dijet events, and corresponds to a truth-jet p_{T} range of 20–30 GeV

ing the subtraction procedure in Eq. (5) similar results are obtained even for larger-area jet definitions. These results demonstrate that $\rho \times A^{\mathrm{jet}}$ subtraction is able to effectively reduce the impact of in-time pile-up regardless of the jet definition, although a residual correction is required to completely remove the dependence on N_{PV} and $\langle\mu\rangle$.

In addition to the slope of the p_{T} dependence on N_{PV}, the RMS of the $p_{\mathrm{T}}^{\mathrm{reco}} - p_{\mathrm{T}}^{\mathrm{true}}$ distribution is studied as a function of $\langle\mu\rangle$ and η in Fig. 6. For this result, anti-k_t $R = 0.6$ jets are chosen due to their greater susceptibility to pile-up and the greater challenge they therefore pose to pile-up correction algorithms. The RMS width of this distribution is an approximate measure of the jet p_{T} resolution for the narrow truth-particle jet p_{T} ranges used in Fig. 6. These results show that the area subtraction procedure provides an approximate 20% reduction in the magnitude of the jet-by-jet fluctuations introduced by pile-up relative to uncorrected jets and approximately a 10% improvement over the simple offset correction. Smaller radius $R = 0.4$ jets exhibit a similar relative improvement compared to the simple offset correction. It should be noted that the pile-up activity in any given event may have significant local fluctuations similar in angular size to jets, and a global correction such as that provided by the area subtraction procedure defined in Eq. (3) cannot account for them. Variables such as the *jet vertex fraction* JVF, *corrected* JVF or corrJVF, or the *jet vertex tagger* JVT may be used to reject jets that result from such fluctuations in pile-up p_{T} density, as described in Sect. 6.

Two methods of in-situ validation of the pile-up correction are employed to study the dependence of jet p_{T} on N_{PV} and $\langle\mu\rangle$. The first method uses track-jets to provide a measure of the jet p_{T} that is pile-up independent. This requires the presence of track-jets and so can only be used in the most central region of the detector for $|\eta| < 2.1$. It is not statistically limited. The second method exploits the p_{T} balance between a reconstructed jet and a Z boson, using the p_{T}^{Z} as a measure of the jet p_{T}. This enables an analysis over the full ($|\eta| < 4.9$) range of the detector, but the extra selections applied to the jet and Z boson reduce its statistical significance. The N_{PV} dependence must therefore be evaluated inclusively in $\langle\mu\rangle$ and vice versa. This results in a degree of correlation between the measured N_{PV} and $\langle\mu\rangle$ dependence.

While the pile-up residual correction is derived from simulated dijet events, the in-situ validation is done entirely using Z+jets events. In the track-jet validation, although the kinematics of the Z boson candidate are not used directly, the dilepton system is relied upon for triggering, thus avoiding any potential bias from jet triggers.

Figure 7a shows the results obtained when matching anti-k_t $R = 0.4$, LCW reconstructed jets to anti-k_t $R = 0.4$ track-jets. No selection is applied based on the calorimeter-based jet p_{T}. Good agreement is observed between data and MC simulation; however, a small overcorrection is observed in the N_{PV} dependence of each. For the final uncertainties on the method, this non-closure of the correction is taken as an uncertainty in the jet p_{T} dependence on N_{PV}.

In events where a Z boson is produced in association with one jet, momentum conservation ensures balance between the Z boson and the jet in the transverse plane. In the direct p_{T} balance method, this principle is exploited by using p_{T}^{Z} as a proxy for the true jet p_{T}. In the case of a perfect measurement of lepton energies and provided that all particles recoiling against the Z boson are included in the jet cone, the jet is expected to balance the Z boson. Therefore the estimated Z boson p_{T} is used as the reference scale, denoted by $p_{\mathrm{T}}^{\mathrm{ref}}$.

Taking the mean, $\langle\Delta p_{\mathrm{T}}\rangle$, of the ($\Delta p_{\mathrm{T}} = p_{\mathrm{T}} - p_{\mathrm{T}}^{\mathrm{ref}}$) distribution, the slope $\partial\langle\Delta p_{\mathrm{T}}\rangle/\partial\langle\mu\rangle$ is extracted and plotted as a function of $p_{\mathrm{T}}^{\mathrm{ref}}$, as shown in Fig. 7b. A small residual slope is observed after the jet-area correction, which is well modelled by the MC simulation, as can be seen in Fig. 7b. The mismodelling is quantified by the maximum differences between data and MC events for

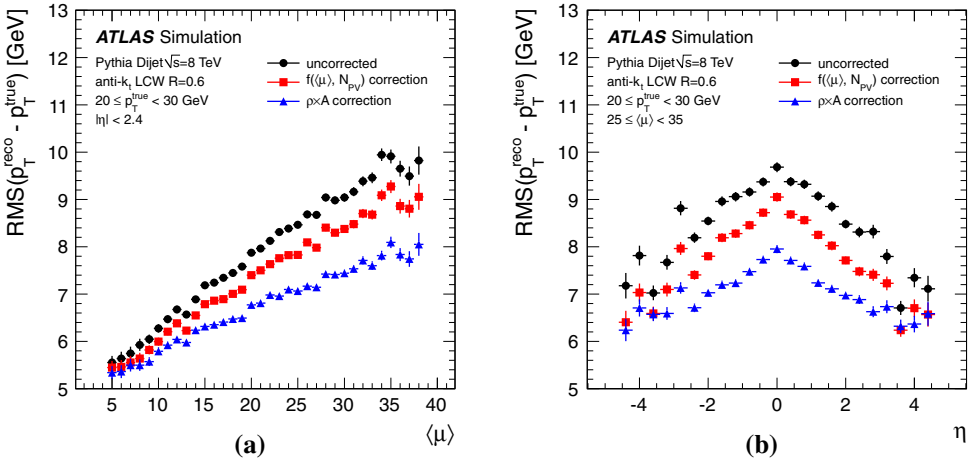

Fig. 6 **a** RMS width of the $p_{\mathrm{T}}^{\mathrm{reco}} - p_{\mathrm{T}}^{\mathrm{true}}$ distribution versus $\langle\mu\rangle$ and **b** versus pseudorapidity η, for anti-k_t $R = 0.6$ jets at the LCW scale matched to truth-particle jets satisfying $20 < p_{\mathrm{T}}^{\mathrm{true}} < 30\,\mathrm{GeV}$, in simulated dijet events. A significant improvement is observed compared to the previous subtraction method (shown in *red*) [4]

both $\partial\langle\Delta p_{\mathrm{T}}\rangle/\partial N_{\mathrm{PV}}$ and $\partial\langle\Delta p_{\mathrm{T}}\rangle/\partial\langle\mu\rangle$. These differences (denoted by $\Delta\,(\partial\langle\Delta p_{\mathrm{T}}\rangle/\partial N_{\mathrm{PV}})$ and $\Delta\,(\partial\langle\Delta p_{\mathrm{T}}\rangle/\partial\langle\mu\rangle)$) are included in the total systematic uncertainty.

The systematic uncertainties are obtained by combining the measurements from Z–jet balance and track-jet in-situ validation studies. In the central region ($|\eta| < 2.1$) only the track-jet measurements are used whereas Z–jet balance is used for $2.1 < |\eta| < 4.5$. In the case of the Z–jet balance in the forward region, the effects of in-time and out-of-time pile-up cannot be fully decoupled. Therefore, the N_{PV} uncertainty is assumed to be η-independent and is thus extrapolated from the central region. In the forward region, the uncertainty on the $\langle\mu\rangle$ dependence, $\Delta\,(\partial\langle\Delta p_{\mathrm{T}}\rangle/\partial\langle\mu\rangle)$, is taken to be the maximum difference between $\partial\langle\Delta p_{\mathrm{T}}\rangle/\partial\langle\mu\rangle$ in the central region and $\partial\langle\Delta p_{\mathrm{T}}\rangle/\partial\langle\mu\rangle$ in the forward region. In this way, the forward region $\Delta\,(\partial\langle\Delta p_{\mathrm{T}}\rangle/\partial\langle\mu\rangle)$ uncertainty implicitly includes any η dependence.

5.3 Pile-up shape subtraction

The jet shape subtraction method [51] determines the sensitivity of jet shape observables, such as the jet width or substructure shapes, to pile-up by evaluating the sensitivity of that shape to variations in infinitesimally soft energy depositions. This variation is evaluated numerically for each jet in each event and then extrapolated to zero to derive the correction.

The procedure uses a uniform distribution of infinitesimally soft particles, or *ghosts*, that are added to the event. These ghost particles are distributed with a number density ν_g per unit in y–ϕ space, yielding an individual ghost area $A_g = 1/\nu_g$. The four-momentum of ghost i is defined as

$$g_{\mu,i} = g_t \cdot [\cos\phi_i, \sin\phi_i, \sinh y_i, \cosh y_i], \tag{6}$$

where g_t is the ghost transverse momentum (initially set to 10^{-30}GeV), and the ghosts are defined to have zero mass. This creates a uniform ghost density given by g_t/A_g which is used as a proxy for the estimated pile-up contribution described by Eq. (4). These ghosts are then incorporated into the jet finding and participate in the jet clustering. By varying the amount of ghost p_{T} density incorporated into the jet finding and determining the sensitivity of a given jet's shape to that variation, a numerical correction can be derived. A given jet shape variable $\mathcal{V}$ is assumed to be a function of ghost p_{T}, $\mathcal{V}(g_t)$. The reconstructed (uncorrected) jet shape is then $\mathcal{V}(g_t = 0)$. The corrected jet shape can be obtained by extrapolating to the value of g_t which cancels the effect of the pile-up p_{T} density, namely $g_t = -\rho \cdot A_g$. The corrected shape is then given by $\mathcal{V}_{\mathrm{corr}} = \mathcal{V}(g_t = -\rho \cdot A_g)$. This solution can be achieved by using the Taylor expansion:

$$\mathcal{V}_{\mathrm{corr}} = \sum_{k=0}^{\infty} \left(-\rho \cdot A_g\right)^k \left.\frac{\partial^k \mathcal{V}(\rho, g_t)}{\partial g_t^k}\right|_{g_t=0}. \tag{7}$$

The derivatives are obtained numerically by evaluating several values of $\mathcal{V}(g_t)$ for $g_t \geq 0$. Only the first three terms in Eq. (7) are used for the studies presented here.

One set of shape variables which has been shown to significantly benefit from the correction defined by the expansion in Eq. (7) is the set of N-subjettiness observables τ_N [52,53]. These observables measure the extent to which the constituents of a jet are clustered around a given number of axes denoted by N (typically with $N = 1, 2, 3$) and are related to the corresponding subjet multiplicity of a jet. The ratios τ_2/τ_1 (τ_{21}) and τ_3/τ_2 (τ_{32}) can be used to provide discrimination between Standard Model jet backgrounds and boosted W/Z bosons [31,52,54], top quarks [31,52,54,55], or even gluinos [56]. For example, $\tau_{21} \simeq 1$ corresponds to a jet that is very well described by a single subjet whereas a lower value implies a jet that is much better described by two subjets rather than one.

Two approaches are tested for correcting the N-subjettiness ratios τ_{21} and τ_{32}. The first approach is to use the individu-

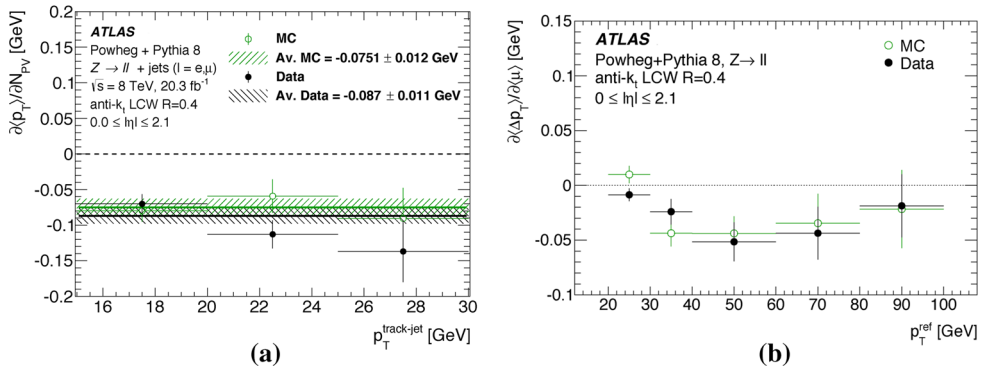

Fig. 7 **a** N_{PV} dependence of the reconstructed p_{T} of anti-k_t $R = 0.4$ LCW jets after the area subtraction as a function of track-jet p_{T}. **b** Validation results from Z+jets events showing the $\langle\mu\rangle$ dependence as a function of the Z boson p_{T}, denoted by $p_{\mathrm{T}}^{\mathrm{ref}}$, for anti-$k_t$ $R = 0.4$ LCW jets in the central region after the area subtraction. The *points* represent central values of the linear fit to $\partial\langle\Delta p_{\mathrm{T}}\rangle/\partial\langle\mu\rangle$ and the *error bars* correspond to the associated fitting error

ally corrected τ_N for the calculation of the numerators and denominators of the ratios. A second approach is also tested in which the full ratio is treated as a single observable and corrected directly. The resulting agreement between data and MC simulation is very similar in the two cases. However, for very high p_{T} jets (600 GeV $\leq p_{\mathrm{T}}^{\mathrm{jet}} <$ 800 GeV) the first approach is preferable since it yields final ratios that are closer to the values obtained for truth-particle jets and a mean $\langle\tau_{32}\rangle$ that is more stable against $\langle\mu\rangle$. On the other hand, at lower jet p_{T} (200 GeV $\leq p_{\mathrm{T}}^{\mathrm{jet}} <$ 300 GeV), applying the jet shape subtraction to the ratio itself performs better than the individual τ_N corrections according to the same figures of merit. Since substructure studies and the analysis of boosted hadronic objects typically focus on the high jet p_{T} regime, all results shown here use the individual corrections for τ_N in order to compute the corrected τ_{21} and τ_{32}.

Figure 8 presents the uncorrected and corrected distributions of τ_{32}, in both the observed data and MC simulation, as well as the truth-particle jet distributions. In the case of Fig. 8b, the mean value of τ_{32} is also presented for trimmed jets, using both the reconstructed and truth-particle jets. This comparison allows for a direct comparison of the shape subtraction method to trimming in terms of their relative effectiveness in reducing the pile-up dependence of the jet shape. Additional selections are applied to the jets used to study τ_{32} in this case: $\tau_{21} > 0.1$ (after correction) and jet mass $m^{\mathrm{jet}} > 30$ GeV (after correction). These selections provide protection against the case where τ_2 becomes very small and small variations in τ_3 can thus lead to large changes in the ratio. The requirement on τ_{21} rejects approximately 1% of jets, whereas the mass requirement removes approximately 9% of jets. As discussed above, the default procedure adopted here is to correct the ratio τ_{21} by correcting τ_1 and τ_2 separately. In cases where both the corrected τ_1 and τ_2 are negative, the sign of the corrected τ_{21} is set to negative.

The corrected N-subjettiness ratio τ_{32} shows a significant reduction in pile-up dependence, as well as a much closer agreement with the distribution expected from truth-particle jets. Figure 8b provides comparisons between the shape subtraction procedure and jet trimming. Trimming is very effective in removing the pile-up dependence of jet substructure variables (see Ref. [31] and Sect. 7). However, jet shape variables computed after jet trimming are considerably modified by the removal of soft subjets and must be directly compared to truth-level jet shape variables constructed with trimming at the truth level as well. Comparing the mean trimmed jet τ_{32} at truth level to the reconstructed quantity in Fig. 8b (open black triangles and open purple square markers, respectively), and similarly for the shape correction method (filled green triangles and filled red square markers, respectively) it is clear that the shape expansion correction obtains a mean value closer to the truth.

6 Pile-up jet suppression techniques and results

The suppression of pile-up jets is a crucial component of many physics analyses in ATLAS. Pile-up jets arise from two sources: hard QCD jets originating from a pile-up vertex, and local fluctuations of pile-up activity. The pile-up QCD jets are genuine jets and must be tagged and rejected using the vertex-pointing information of charged-particle tracks (out-of-time QCD jets have very few or no associated tracks since the ID reconstructs tracks only from the in-time events). Pile-up jets originating from local fluctuations are a superposition of random combinations of particles from multiple pile-up vertices, and they are generically referred to here as *stochastic* jets. Stochastic jets are preferentially produced in regions of the calorimeter where the global ρ estimate is smaller than the actual pile-up activity. Tracking information also plays a

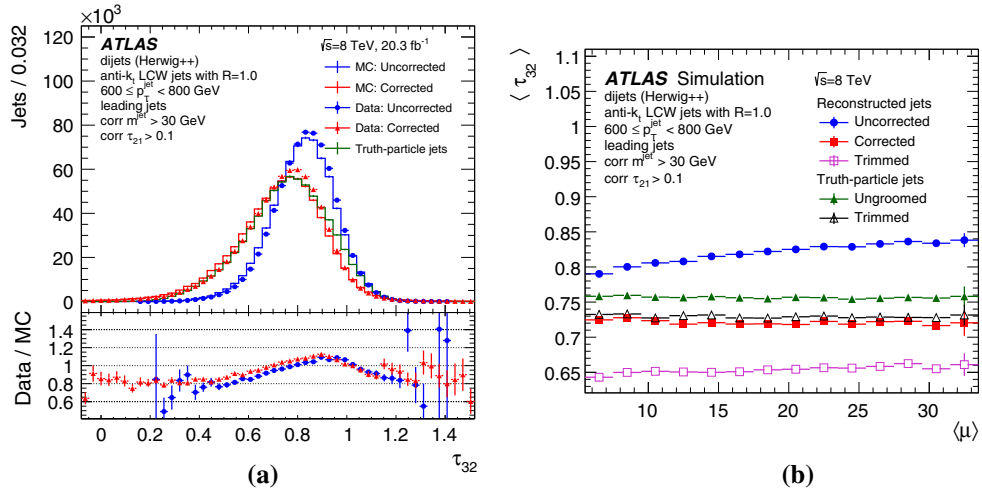

Fig. 8 **a** Comparisons of the uncorrected (*filled blue circles*), corrected (*red*) distributions of the ratio of 3-subjettiness to 2-subjettiness (τ_{32}) for data (*points*) and for MC simulation (*solid histogram*) for leading jets in the range $600 \leq p_{\mathrm{T}} < 800$ GeV. The distribution of τ_{32} computed using stable truth particles (*filled green triangles*) is also included. The *lower panel* displays the ratio of the data to the MC simulation. **b** Dependence of τ_{32} on $\langle\mu\rangle$ for the uncorrected (*filled blue circles*), corrected (*filled red squares*) and trimmed (*open purple squares*) distributions for reconstructed jets in MC simulation for leading jets in the range $600 \leq p_{\mathrm{T}} < 800$ GeV. The mean value of τ_{32} computed using stable truth particles (*green*) is also included

key role in tagging and rejecting stochastic jets. Since tracks can be precisely associated with specific vertices, track-based observables can provide information about the pile-up structure and vertex composition of jets within the tracking detector acceptance ($|\eta| < 2.5$) that can be used for discrimination. The composition of pile-up jets depends on both $\langle\mu\rangle$ and p_{T}. Stochastic jets have a much steeper p_{T} spectrum than pile-up QCD jets. Therefore, higher-p_{T} jets that are associated with a primary vertex which is not the hard-scatter vertex are more likely to be pile-up QCD jets, not stochastic jets. On the other hand, while the number of QCD pile-up jets increases linearly with $\langle\mu\rangle$, the rate of stochastic jets increases more rapidly such that at high luminosity the majority of pile-up jets at low p_{T} are expected to be stochastic in nature [57].

6.1 Pile-up jet suppression from subtraction

The number of reconstructed jets increases with the average number of pile-up interactions, as shown in Fig. 9 using the Z+jets event sample described in Sect. 5.1. Event-by-event pile-up subtraction based on jet areas, as described in Sect. 5.2, removes the majority of pile-up jets by shifting their p_{T} below the p_{T} threshold of 20 GeV. This has the effect of improving the level of agreement between data and MC simulation. The phenomenon of pile-up jets is generally not well modelled, as shown in the ratio plot of Fig. 9.

6.2 Pile-up jet suppression from tracking

Some pile-up jets remain even after pile-up subtraction mainly due to localised fluctuations in pile-up activity which

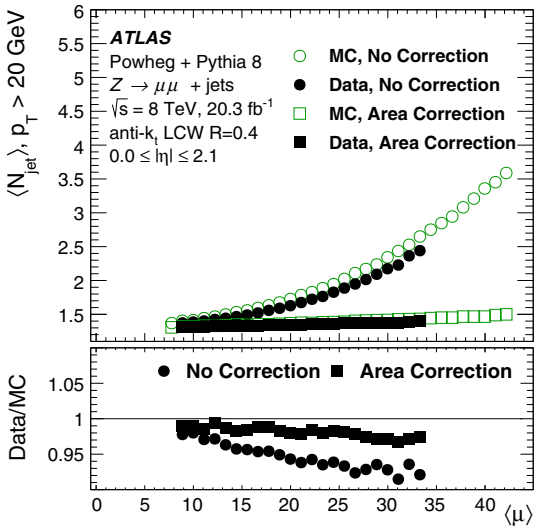

Fig. 9 The mean anti-k_t $R = 0.4$ LCW jet multiplicity as a function of $\langle\mu\rangle$ in Z+jets events for jets with $p_{\mathrm{T}} > 20$ GeV and $|\eta| < 2.1$. Events in this plot are required to have at least 1 jet both before and after the application of the jet-area based pile-up correction

are not fully corrected by ρ in Eq. (5). Information from the tracks matched to each jet may be used to further reject any jets not originating from the hard-scatter interaction. ATLAS has developed three different track-based tagging approaches for the identification of pile-up jets: The jet vertex fraction (JVF) algorithm, used in almost all physics analyses in Run 1, a set of two new variables (corrJVF, and R_{pT}) for improved performance, and a new combined discriminant, the jet vertex tagger (JVT) for optimal performance. While the last two approaches were developed using Run 1 data, most analyses

based on Run 1 data were completed before these new algorithms for pile-up suppression were developed. Their utility is already being demonstrated for use in high-luminosity LHC upgrade studies, and they will be available to all ATLAS analyses at the start of Run 2.

6.2.1 Jet vertex fraction

The jet vertex fraction (JVF) is a variable used in ATLAS to identify the primary vertex from which the jet originated. A cut on the JVF variable can help to remove jets which are not associated with the hard-scatter primary vertex. Using tracks reconstructed from the ID information, the JVF variable can be defined for each jet with respect to each identified primary vertex (PV) in the event, by identifying the PV associated with each of the charged-particle tracks pointing towards the given jet. Once the hard-scatter PV is identified, the JVF variable can be used to select jets having a high likelihood of originating from that vertex. Tracks are assigned to calorimeter jets following the ghost-association procedure [50], which consists of assigning tracks to jets by adding tracks with infinitesimal p_{T} to the jet clustering process. Then, the JVF is calculated as the ratio of the scalar sum of the p_{T} of matched tracks that originate from a given PV to the scalar sum of p_{T} of all matched tracks in the jet, independently of their origin.

JVF is defined for each jet with respect to each PV. For a given jet_i, its JVF with respect to the primary vertex PV_j is given by:

$$\mathrm{JVF}(\mathrm{jet}_i, \mathrm{PV}_j) = \frac{\sum_m p_{\mathrm{T}}(\mathrm{track}_m^{\mathrm{jet_i}}, \mathrm{PV}_j)}{\sum_n \sum_l p_{\mathrm{T}}(\mathrm{track}_l^{\mathrm{jet_i}}, \mathrm{PV}_n)}, \tag{8}$$

where m runs over all tracks originating from PV_j[2] matched to jet_i, n over all primary vertices in the event and l over all tracks originating from PV_n matched to jet_i. Only tracks with $p_{\mathrm{T}} > 500$ MeV are considered in the JVF calculation. JVF is bounded by 0 and 1, but a value of -1 is assigned to jets with no associated tracks.

For the purposes of this paper, JVF is defined from now on with respect to the hard-scatter primary vertex. In the Z+jets events used for these studies of pile-up suppression, this selection of the hard-scatter primary vertex is found to be correct in at least 98% of events. JVF may then be interpreted as an estimate of the fraction of p_{T} in the jet that can be associated with the hard-scatter interaction. The principle of the JVF variable is shown schematically in Fig. 10a. Figure 10b shows the JVF distribution in MC simulation for hard-scatter jets and for pile-up jets with $p_{\mathrm{T}} > 20$ GeV after pile-up subtraction and jet energy scale correction in a $Z(\rightarrow ee)$+jets sample with the $\langle\mu\rangle$ distribution shown in Fig. 1. Hard-scatter jets are calorimeter jets that have been matched to truth-particle jets from the hard-scatter with an angular separation of $\Delta R \leq 0.4$, whereas pile-up jets are defined as calorimeter jets with an angular separation to the nearest truth-particle jet of $\Delta R > 0.4$. The thresholds for truth-particle jets are $p_T > 10$ GeV for those originating from the hard-scatter, and $p_T > 4$ GeV for those originating in pile-up interactions. This comparison demonstrates the discriminating power of the JVF variable.

While JVF is highly correlated with the actual fraction of hard-scatter activity in a reconstructed calorimeter jet, it is important to note that the correspondence is imperfect. For example, a jet with significant neutral pile-up contributions may receive JVF $= 1$, while JVF $= 0$ may result from a fluctuation in the fragmentation of a hard-scatter jet such that its charged constituents all fall below the track p_{T} threshold. JVF also relies on the hard-scatter vertex being well separated along the beam axis from all of the pile-up vertices. In some events, a pile-up jet may receive a high value of JVF because its associated primary vertex is very close to the hard-scatter primary vertex. While this effect is very small for 2012 pile-up conditions, it will become more important at higher luminosities, as the average distance between interactions decreases as $1/\langle\mu\rangle$. For these reasons, as well as the lower probability for producing a pile-up QCD jet at high p_{T}, JVF selections are only applied to jets with $p_{\mathrm{T}} \leq 50$ GeV.

The modelling of JVF is investigated in $Z(\rightarrow \mu\mu)$+jets events using the same selection as discussed in Sect. 5.1, which yields a nearly pure sample of hard-scatter jets. By comparison to truth-particle jets in MC simulation, it was found that the level of pile-up jet contamination in this sample is close to 2% near 20 GeV and almost zero at the higher end of the range near 50 GeV. The JVF distribution for the jet balanced against the Z boson in these events is well modelled for hard-scatter jets. However, the total jet multiplicity in these events is overestimated in simulated events, due to mismodelling of pile-up jets. This is shown in Fig. 11, for several different choices of the minimum p_{T} cut applied at the fully calibrated jet energy scale (including jet-area-based pile-up subtraction). The application of a JVF cut significantly improves the data/MC agreement because the majority of pile-up jets fail the JVF cut: across all p_{T} bins, data and MC simulation are seen to agree within 1% following the application of a JVF cut. It is also observed that the application of a JVF cut results in stable values for the mean jet multiplicity as a function of $\langle\mu\rangle$.

Figure 11 also shows the systematic uncertainty bands, which are only visible for the lowest p_{T} selection of 20 GeV. These uncertainties are estimated by comparing the JVF distributions for hard-scatter jets in data and MC simulation. The efficiency of a nominal JVF cut of X is defined

[2] Tracks are assigned to vertices by requiring $|\Delta z \times \sin\theta| < 1$ mm. In cases where more than one vertex satisfies this criterion, ambiguity is resolved by choosing the vertex with the largest summed p_{T}^2 of tracks.

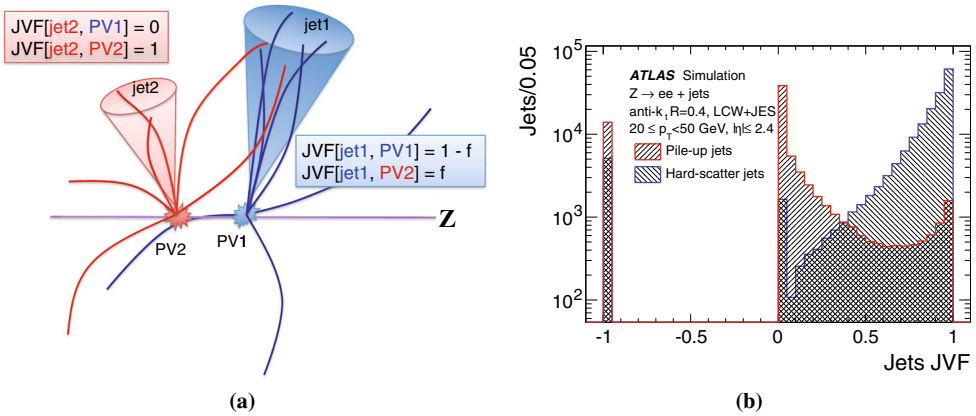

Fig. 10 **a** Schematic representation of the jet vertex fraction JVF principle where f denotes the fraction of track p_{T} contributed to jet 1 due to the second vertex (PV2). **b** JVF distribution for hard-scatter (*blue*) and pile-up (*red*) jets with $20 < p_{\mathrm{T}} < 50$ GeV and $|\eta| < 2.4$ after pile-up subtraction and jet energy scale correction in simulated Z+jets events

as the fraction of jets, well balanced against the Z boson, passing the cut, denoted by $\mathcal{E}_{\mathrm{MC}}^{\mathrm{nom}}$ and $\mathcal{E}_{\mathrm{data}}^{\mathrm{nom}}$ for MC events and data, respectively. The systematic uncertainty is derived by finding two JVF cuts with $\mathcal{E}_{\mathrm{MC}}$ differing from $\mathcal{E}_{\mathrm{MC}}^{\mathrm{nom}}$ by $\pm(\mathcal{E}_{\mathrm{MC}}^{\mathrm{nom}} - \mathcal{E}_{\mathrm{data}}^{\mathrm{nom}})$. The JVF uncertainty band is then formed by re-running the analysis with these up and down variations in the JVF cut value. Systematic uncertainties vary between 2 and 6% depending on jet p_{T} and η.

6.2.2 *Improved variables for pile-up jet vertex identification*

While a JVF selection is very effective in rejecting pile-up jets, it has limitations when used in higher (or varying) luminosity conditions. As the denominator of JVF increases with the number of reconstructed primary vertices in the event, the mean JVF for signal jets is shifted to smaller values. This explicit pile-up dependence of JVF results in an N_{PV}-dependent jet efficiency when a minimum JVF criterion is imposed to reject pile-up jets. This pile-up sensitivity is addressed in two different ways. First, by correcting JVF for the explicit pile-up dependence in its denominator (corrJVF) and, second, by introducing a new variable defined entirely from hard-scatter observables (R_{pT}).

The quantity corrJVF is a variable similar to JVF, but corrected for the N_{PV} dependence. It is defined as

$$\mathrm{corrJVF} = \frac{\sum_m p_{\mathrm{T},m}^{\mathrm{track}}(\mathrm{PV}_0)}{\sum_l p_{\mathrm{T},l}^{\mathrm{track}}(\mathrm{PV}_0) + \frac{\sum_{n\geq 1}\sum_l p_{\mathrm{T},l}^{\mathrm{track}}(\mathrm{PV}_n)}{(k\cdot n_{\mathrm{track}}^{\mathrm{PU}})}}, \tag{9}$$

where $\sum_m p_{\mathrm{T},m}^{\mathrm{track}}(\mathrm{PV}_0)$ is the scalar sum of the p_{T} of the tracks that are associated with the jet and originate from the hard-scatter vertex. The term $\sum_{n\geq 1}\sum_l p_{\mathrm{T},l}^{\mathrm{track}}(\mathrm{PV}_n) = p_{\mathrm{T}}^{\mathrm{PU}}$ denotes the scalar sum of the p_{T} of the associated tracks that originate from any of the pile-up interactions.

The corrJVF variable uses a modified track-to-vertex association method that is different from the one used for JVF. The new selection aims to improve the efficiency for b-quark jets and consists of two steps. In the first step, the vertex reconstruction is used to assign tracks to vertices. If a track is attached to more than one vertex, priority is given to the vertex with higher $\sum(p_{\mathrm{T}}^{\mathrm{track}})^2$. In the second step, if a track is not associated with any primary vertex after the first step but satisfies $|\Delta z| < 3$ mm with respect to the hard-scatter primary vertex, it is assigned to the hard-scatter primary vertex. The second step targets tracks from decays in flight of hadrons that originate from the hard-scatter but are not likely to be attached to any vertex. The $|\Delta z| < 3$ mm criterion was chosen based on the longitudinal impact parameter distribution of tracks from b-hadron decays, but no strong dependence of the performance on this particular criterion was observed when the cut value was altered within 1 mm. The new 2-step track-to-vertex association method results in a significant increase in the hard-scatter jet efficiency at fixed rate of fake pile-up jets, with a large performance gain for jets initiated by b-quarks.

To correct for the linear increase of $\langle p_{\mathrm{T}}^{\mathrm{PU}}\rangle$ with the total number of pile-up tracks per event ($n_{\mathrm{track}}^{\mathrm{PU}}$), $p_{\mathrm{T}}^{\mathrm{PU}}$ is divided by $(k \cdot n_{\mathrm{track}}^{\mathrm{PU}})$, with $k = 0.01$, in the corrJVF definition. The total number of pile-up tracks per event is computed from all tracks associated with vertices other than the hard-scatter vertex. The scaling factor k is approximated by the slope of $\langle p_{\mathrm{T}}^{\mathrm{PU}}\rangle$ with $n_{\mathrm{track}}^{\mathrm{PU}}$, but the resulting discrimination between hard-scatter and pile-up jets is insensitive to the choice of k.[3]

Figure 12a shows the corrJVF distribution for pile-up and hard-scatter jets in simulated dijet events. A value corrJVF $= -1$ is assigned to jets with no associated tracks. Jets with corrJVF $= 1$ are not included in the studies that follow due to use of signed corrJVF selections. About 1% of hard-scatter jets with $20 < p_{\mathrm{T}} < 30$ GeV have no associated hard-scatter tracks and thus corrJVF $= 0$.

Figure 12b shows the hard-scatter jet efficiency as a function of the number of reconstructed primary vertices in the

[3] With this particular choice of k, the resulting corrJVF shapes for hard-scatter and pile-up jets are similar to the corresponding ones for JVF.

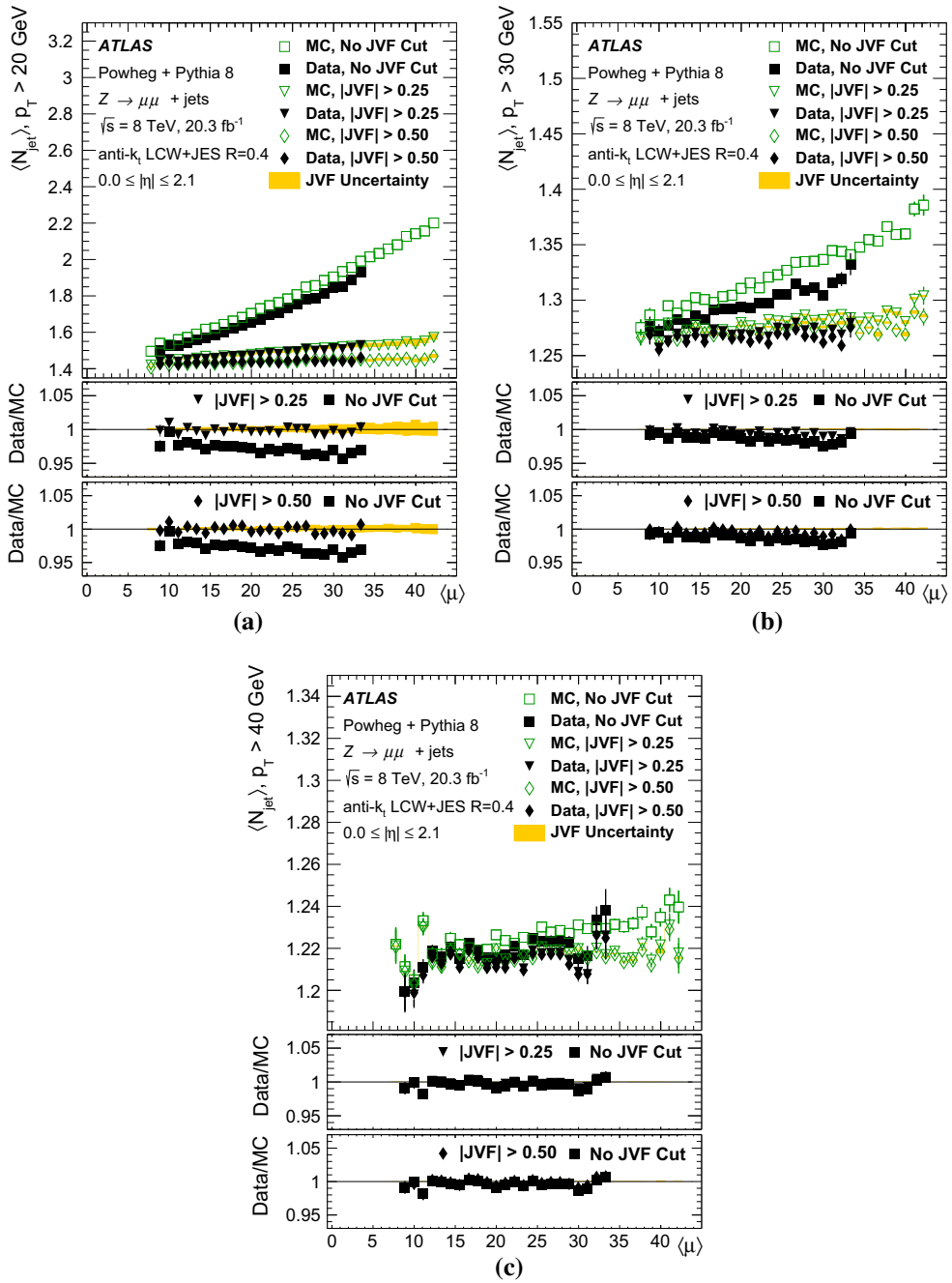

Fig. 11 The mean anti-k_t $R = 0.4$ LCW+JES jet multiplicity as a function of $\langle\mu\rangle$ in Z+jets events for jets with $|\eta| < 2.1$, back-to-back with the Z boson, before and after several |JVF| cuts were applied to jets with $p_{\mathrm{T}} < 50$ GeV. Results for jets with **a** $p_{\mathrm{T}} > 20$ GeV, **b** $p_{\mathrm{T}} > 30$ GeV and **c** $p_{\mathrm{T}} > 40$ GeV are shown requiring at least one jet of that p_{T}. To remove effects of hard-scatter modelling the dependence on $\langle\mu\rangle$ was fit and the MC simulation shifted so that data and simulation agree at zero pile-up, $\langle\mu\rangle = 0$. The *upper ratio plots* show results before and after applying a |JVF| cut of 0.25 and the *lower ratio plots* show the same for a cut of 0.50. The JVF uncertainty is very small when counting jets with $p_{\mathrm{T}} > 40$ GeV

event when imposing a minimum corrJVF or JVF requirement such that the efficiency measured across the full range of N_{PV} is 90%. For the full range of N_{PV} considered, the hard-scatter jet efficiency after a selection based on corrJVF is stable at $90\% \pm 1\%$, whereas for JVF the efficiency degrades by about 20%, from 97 to 75%. The choice of scaling factor k in the corrJVF distribution does not affect the stability of the hard-scatter jet efficiency with N_{PV}.

The variable R_{pT} is defined as the scalar sum of the p_{T} of the tracks that are associated with the jet and originate from the hard-scatter vertex divided by the fully calibrated jet p_{T}, which includes pile-up subtraction:

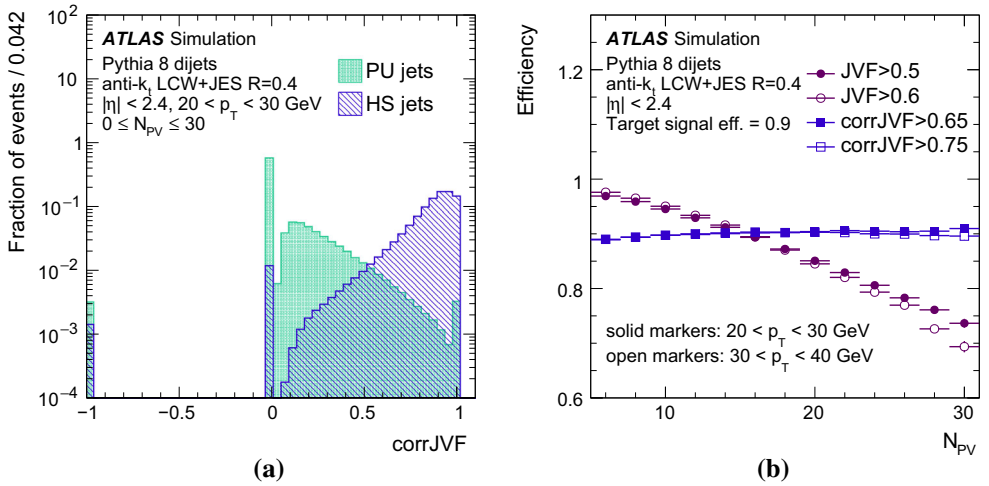

Fig. 12 **a** Distribution of corrJVF for pile-up (PU) and hard-scatter (HS) jets with $20 < p_{\mathrm{T}} < 30$ GeV. **b** Primary-vertex dependence of the hard-scatter jet efficiency for $20 < p_{\mathrm{T}} < 30$ GeV (*solid markers*) and $30 < p_{\mathrm{T}} < 40$ GeV (*open markers*) jets for fixed cuts of corrJVF (*blue square*) and JVF (*violet circle*) such that the inclusive efficiency is 90%. The selections placed on corrJVF and JVF, which depend on the p_{T} bin, are specified in the legend

$$R_{\mathrm{pT}} = \frac{\sum_k p_{\mathrm{T},k}^{\mathrm{track}}(\mathrm{PV}_0)}{p_{\mathrm{T}}^{\mathrm{jet}}}. \tag{10}$$

The R_{pT} distributions for pile-up and hard-scatter jets are shown in Fig. 13a. R_{pT} is peaked at 0 and is steeply falling for pile-up jets, since tracks from the hard-scatter vertex rarely contribute. For hard-scatter jets, however, R_{pT} has the meaning of a charged p_{T} fraction and its mean value and spread are larger than for pile-up jets. Since R_{pT} involves only tracks that are associated with the hard-scatter vertex, its definition is at first order independent of N_{PV}. Figure 13b shows the hard-scatter jet efficiency as a function of N_{PV} when imposing a minimum R_{pT} and JVF requirement such that the N_{PV} inclusive efficiency is 90%. For the full range of N_{PV} considered, the hard-scatter jet efficiency after a selection based on R_{pT} is stable at $90\% \pm 1\%$.

6.2.3 Jet vertex tagger

A new discriminant called the jet vertex tagger (JVT) is constructed using R_{pT} and corrJVF as a two-dimensional likelihood derived using simulated dijet events and based on a k-nearest neighbour (kNN) algorithm [58]. For each point in the two-dimensional corrJVF–R_{pT} plane, the relative probability for a jet at that point to be of signal type is computed as the ratio of the number of hard-scatter jets to the number of hard-scatter plus pile-up jets found in a local neighbourhood around the point using a training sample of signal and pile-up jets with $20 < p_{\mathrm{T}} < 50$ GeV and $|\eta| < 2.4$. The local neighbourhood is defined dynamically as the 100 nearest neighbours around the test point using a Euclidean metric in the R_{pT}–corrJVF space, where corrJVF and R_{pT} are rescaled so that the variables have the same range.

Figure 14a shows the fake rate versus efficiency curves comparing the performance of the four variables JVF, corrJVF, R_{pT} and JVT when selecting a sample of jets with $20 < p_{\mathrm{T}} < 50$ GeV, $|\eta| < 2.4$ in simulated dijet events.

The figure shows the fraction of pile-up jets passing a minimum JVF, corrJVF, R_{pT} or JVT requirement as a function of the signal-jet efficiency resulting from the same requirement. The JVT performance is driven by corrJVF (R_{pT}) in the region of high signal-jet efficiency (high pile-up rejection). Using JVT, signal jet efficiencies of 80, 90 and 95% are achieved for pile-up fake rates of respectively 0.4, 1.0 and 3%. When imposing cuts on JVF that result in the same jet efficiencies, the pile-up fake rates are 1.3, 2.2 and 4%.

The dependence of the hard-scatter jet efficiencies on N_{PV} is shown in Fig. 14b. For the full range of N_{PV} considered, the hard-scatter jet efficiencies after a selection based on JVT are stable within 1%.

The differences in fragmentation and showering between jets initiated by gluons and light quarks affect the shapes of the corrJVF and R_{pT} distributions and thus the performance of the JVT-based pile-up jet suppression. Jets initiated by light quarks (u, d, s) have on average a lower number of associated hard-scatter tracks but a slightly higher jet energy response [59] and both effects lead towards an increase in the number of jets with no associated tracks from the hard-scatter primary vertex relative to gluon-initiated jets.

Figure 15 shows the corrJVF, R_{pT} and JVT distributions for hard-scatter jets with $20 < p_{\mathrm{T}} < 30$ GeV initiated by gluons and light quarks. Using a leading-order notion of jet flavour, the parton-level flavour labelling refers to the highest-energy parton within a narrow cone of size $\Delta R = 0.3$ around the jet axis. The distributions for jets initiated by light quarks have more entries at low corrJVF, R_{pT} and JVT val-

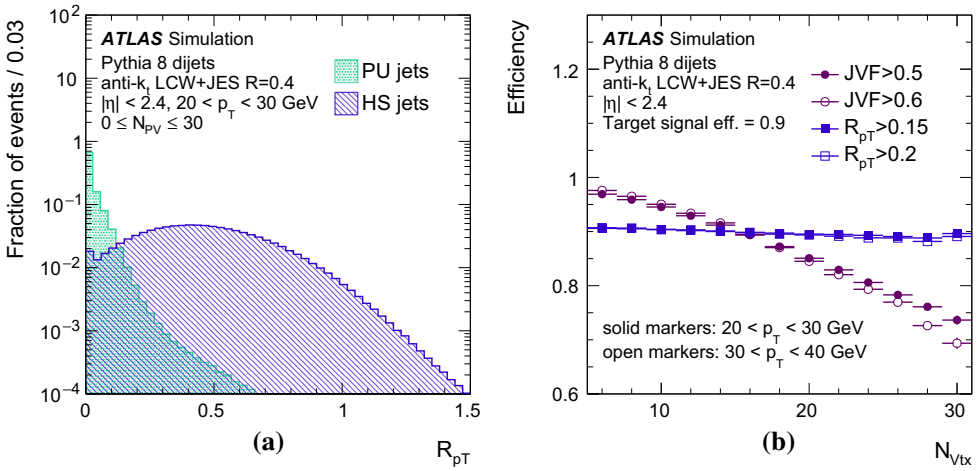

Fig. 13 **a** Distribution of R_{pT} for pile-up (PU) and hard-scatter (HS) jets with $20 < p_{\mathrm{T}} < 30$ GeV. **b** Primary-vertex dependence of the hard-scatter jet efficiency for $20 < p_{\mathrm{T}} < 30$GeV (*solid markers*) and $30 < p_{\mathrm{T}} < 40$ GeV (*open markers*) jets for fixed cuts of R_{pT} (*blue square*) and JVF (*violet circle*) such that the inclusive efficiency is 90%. The cut values imposed on R_{pT} and JVF, which depend on the p_{T} bin, are specified in the legend

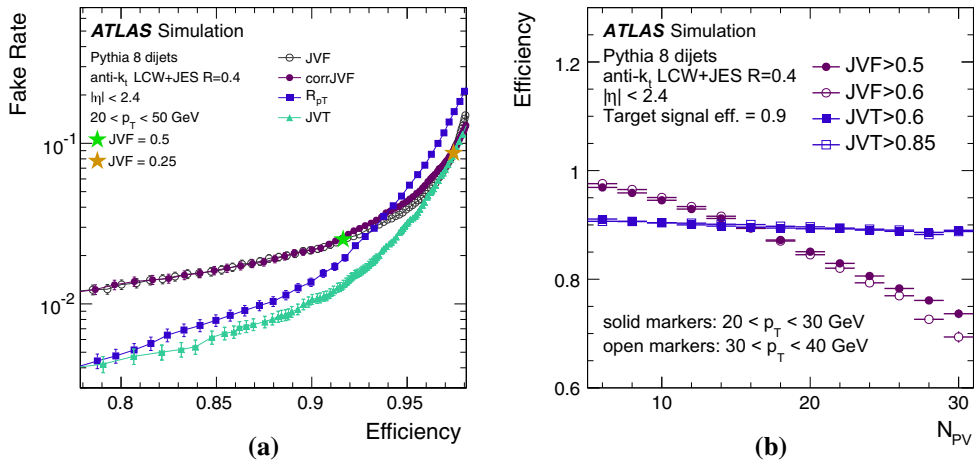

Fig. 14 **a** Fake rate from pile-up jets versus hard-scatter jet efficiency curves for JVF, corrJVF, R_{pT} and JVT. The widely used JVF working points with cut values 0.25 and 0.5 are indicated with *gold* and *green stars*. **b** Primary vertex dependence of the hard-scatter jet efficiency for $20 < p_{\mathrm{T}} < 30$ GeV (*solid markers*) and $30 < p_{\mathrm{T}} < 40$ GeV (*open markers*) jets for fixed cuts of JVT (*blue square*) and JVF (*violet circle*) such that the inclusive efficiency is 90%

ues and consequently a worse separation from pile-up jets. Most notably, about twice as many light-quark jets have no associated tracks from the hard-scatter primary vertex, that is corrJVF = JVT = 0.

Figure 16 shows the efficiency versus fake-rate curve for JVT for jets initiated by light quarks, gluons and b-quarks. As expected from Fig. 15, the performance is worse for jets initiated by light quarks. The pile-up versus hard-scatter jet discrimination performs best for hard-scatter jets initiated by b-quarks. The efficiency versus fake-rate curve for jets initiated by c-quarks is similar to that of gluon jets.

The stability of the hard-scatter efficiencies as a function of N_{PV} is found to be independent of the flavour of the parton initiating the jet.

To test the sample dependence of JVT, the likelihood was also derived using a sample of $20 < p_{\mathrm{T}} < 50$ GeV jets in simulated $Z(\rightarrow \mu\mu)$+jets events. The performance of the JVT-based pile-up jet suppression (evaluated in terms of fake rate versus efficiency curves) was found to be independent of the sample from which the likelihood is derived.

The hard-scatter jet efficiency for JVT in data was measured using the tag-and-probe method in $Z(\rightarrow \mu\mu)$+jets events, using a procedure similar to that described in Sect. 6.2.1 (see also Ref. [60]). Using the leading jet recoiling against the Z boson as a probe, a signal region for hard-scatter jets is defined as the back-to-back region specified by the requirement $|\Delta\phi(Z, \mathrm{jet})| > 2.8$. The pile-up contamination in the signal region is estimated from a pile-up control region, based on the assumption that the $|\Delta\phi(Z, \mathrm{jet})|$ distribution is flat for pile-up jets.

Figure 17a, b show the jet efficiencies for minimum JVT requirements of 0.2, 0.4 and 0.7 respectively, measured in bins of $p_{\mathrm{T}}^{\mathrm{ref}} = p_{\mathrm{T}}^{Z}$.

Good agreement is observed between data and simulation, although there is a very slight tendency for the MC simulation to predict an efficiency higher than that found in data at low $p_{\mathrm{T}}^{\mathrm{ref}}$, but this difference is within the statistical uncertainty. The simulation-to-data scale factors are consistent with unity within the uncertainties. The grey band reflects the total uncertainty on the efficiency in simulation, adding the statistical and the systematic uncertainties in quadrature. The systematic uncertainty is determined by accounting for the differences in efficiency observed between the SHERPA and the POWHEG+PYTHIA 8 $Z(\rightarrow \mu\mu)$+jets

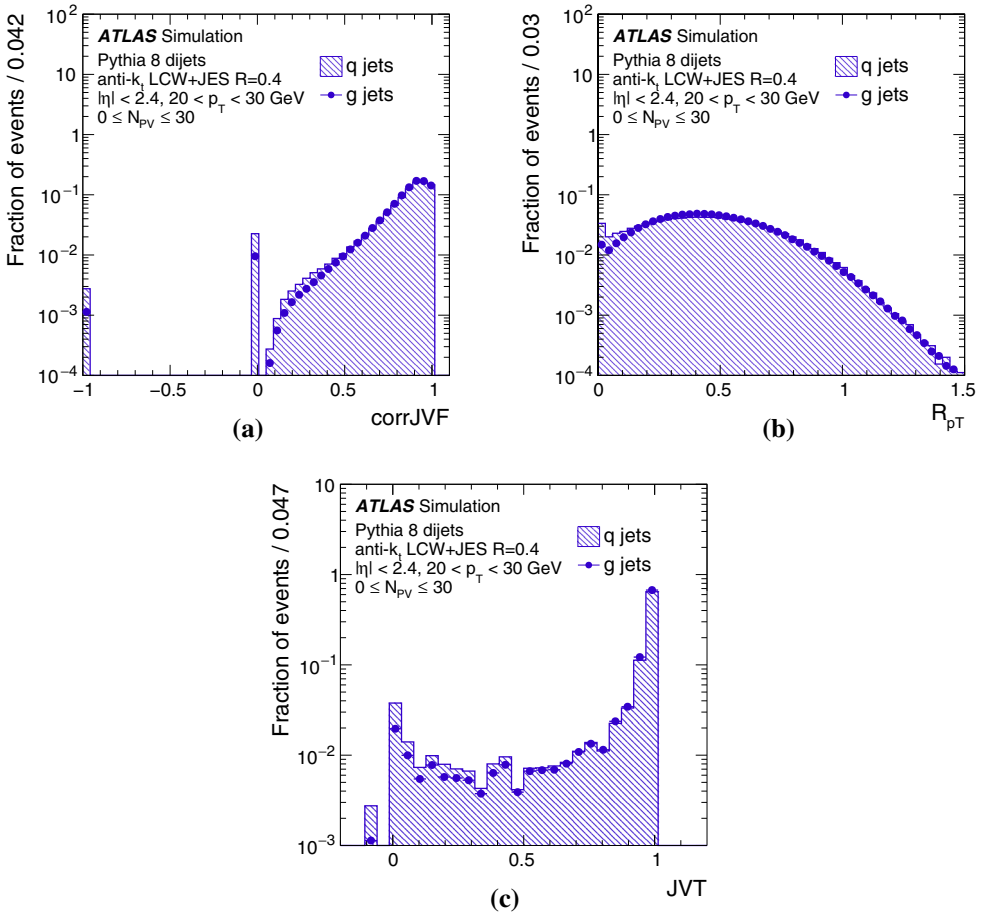

Fig. 15 The distributions of **a** corrJVF, **b** R_{pT} and **c** JVT for light-quark and gluon initiated hard-scatter jets

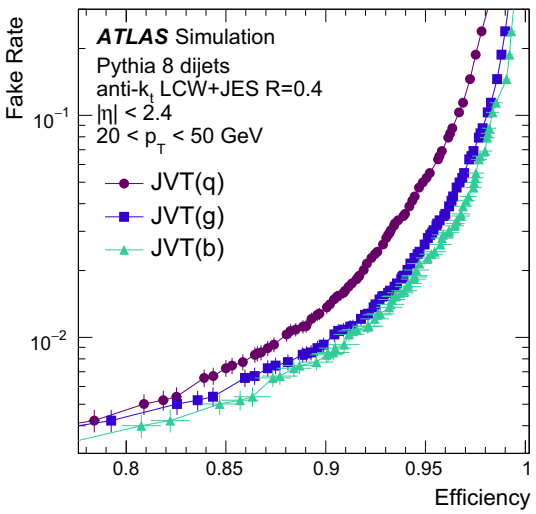

Fig. 16 The fake rate from pile-up jets versus hard-scatter jet efficiency curves for JVT separating jets initiated by light quarks, gluons and b-quarks

MC samples, and by the mismodelling in the simulation of the $\Delta\phi(Z, \mathrm{jet})$ shape for hard-scatter jets. The total uncertainty ranges from 2 to 1% when $p_{\mathrm{T}}^{\mathrm{ref}}$ varies from 20 to 60 GeV.

7 Jet grooming for pile-up mitigation and suppression

The algorithmic removal of substructures within a jet based on kinematic criteria is generally referred to as *jet grooming*. Several types of jet grooming have been explored in ATLAS [31] for their ability to reduce the backgrounds to boosted-object selection while maintaining high efficiencies for signal processes. Improving the individual jet mass resolution and mitigating the effects of pile-up are critical issues in these studies. Indeed, these measures of performance are used as some of the primary figures of merit in determining a subset of groomed-jet algorithms on which to focus for physics analysis in ATLAS.

Previous studies show that trimming and filtering both significantly reduce the dependence of the jet mass on pile-up [31]. As described in Sect. 3.1, trimming removes subjets with $p_{\mathrm{T}i}/p_{\mathrm{T}}^{\mathrm{jet}} < f_{\mathrm{cut}}$, where $p_{\mathrm{T}i}$ is the transverse momentum of the ith subjet and $f_{\mathrm{cut}} = 0.05$. Filtering proceeds similarly, but it utilises the relative masses of the subjets defined and the original jet. For at least one of the configurations tested, trimming and filtering are both able to approximately eliminate the pile-up dependence of the jet mass. Building upon the success of calorimeter-based grooming methods

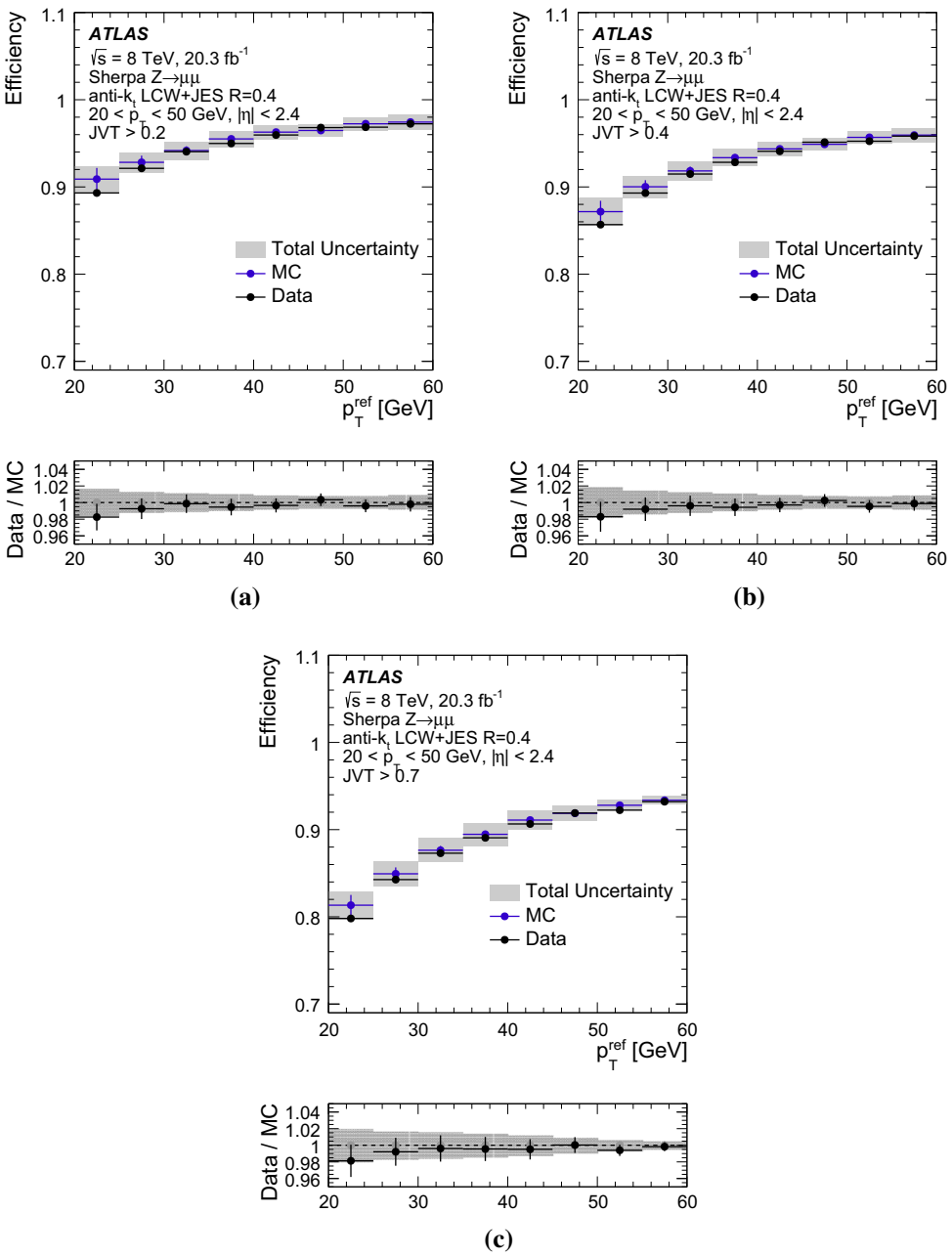

Fig. 17 Efficiency measured in $Z(\rightarrow \mu\mu)$+jets events as a function of $p_{\mathrm{T}}^{\mathrm{ref}}$ in data and MC simulation for **a** JVT > 0.2, **b** JVT > 0.4 and **c** JVT > 0.7, where $p_{\mathrm{T}}^{\mathrm{ref}} = p_{\mathrm{T}}^{Z}$. The *bottom panels* of each figure show the ratio of efficiencies measured in data and MC simulation

and track-based pile-up suppression of small-radius jets, a new, track-based, grooming technique can be designed by vetoing individual subjets of large-R jets that are associated with pile-up interactions using tracking information.

The implementations of track-based grooming in ATLAS have so far focused on corrJVF and so-called *jet cleansing* methods [61]. The algorithm which uses corrJVF relies on the application of corrJVF to the individual subjets of large-R jets wherein tracks matched to each subjet are used in the calculation of corrJVF for that subjet. In particular, track-based trimming is implemented by replacing the f_{cut} criterion with a requirement on the corrJVF of subjets.

The concept of track-based grooming can be illustrated in an event display. Figure 18 shows both calorimeter and tracking information in the rapidity (y) versus azimuthal angle (ϕ) plane of a simulated event where a W' boson with a mass of 1 TeV decays to a W boson and a Z boson, which decay hadronically. The orange star and blue triangle indicate the y–ϕ positions of the generated W and Z bosons. The large circles represent the active area boundaries of the anti-k_t $R = 1.0$ jets, built from topological clusters. In the following, these jets are referred to as ungroomed jets. The clusters are represented by small solid squares with colours ranging from blue to red encoding low to high transverse energies.

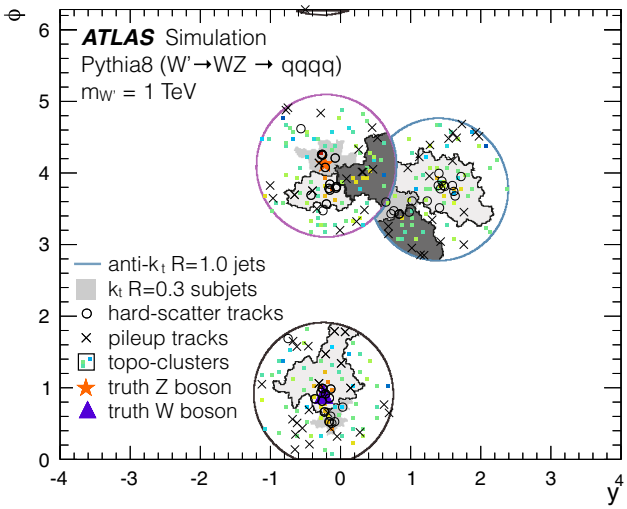

Fig. 18 Rapidity–ϕ view of a simulated event of a W' boson with a mass of 1 TeV decaying to a W boson and a Z boson, both of which decay to jet pairs

The grey regions indicate the active areas of the k_t $R = 0.3$ subjets reconstructed from the constituents of the ungroomed jets. Only subjets with a p_{T} of at least 5% of the ungroomed jet p_{T} are shown. Tracks associated with the jet and originating from the hard-scatter vertex (black open circles) or from pile-up vertices (black crosses) are also indicated. The violet ungroomed jet (with $\phi \approx 4.1$ and $y \approx -0.2$) has a p_{T} of 446 GeV and is matched in ΔR to the truth Z boson. While all three subjets have active areas overlapping with the y–ϕ positions of pile-up tracks, only two subjets have associated hard-scatter tracks. The invariant mass reconstructed from the two subjets with hard-scatter tracks is 89 GeV and the one from all three subjets is 119 GeV. This event display shows that tracking information can provide information complementary to calorimeter-based trimming. Track-assisted trimming would allow the rejection of the third subjet, which is likely to originate from pile-up, while keeping the two subjets from the Z boson.

Figure 19a shows the ratio of the subjet p_{T} to the ungroomed jet p_{T} on a logarithmic scale as a function of the subjet corrJVF in simulated $W' \to WZ \to qqqq$ events. The subjet p_{T} is defined as the four-momentum sum of the constituents contained within the k_t jet that forms the subjet. The ungroomed jet p_{T} is defined as the p_{T} of the large-R jet from which the subjets are then constructed. The two-dimensional distribution of this ratio is normalised to unit area. Approximately 4% of subjets have no associated tracks (corrJVF $= -1$) and are omitted. Most subjets with significant p_{T} ratio also have large corrJVF, indicating that most of their charged p_{T} comes from the hard-scatter vertex. A large fraction of subjets with a low p_{T} ratio $< 5\%$ ($\log_{10}[p_{\mathrm{T}}^{\mathrm{sub}}/p_{\mathrm{T}}^{\mathrm{ungroomed}}] < -1.3$) and a few subjets with a significant p_{T} ratio, however, have small corrJVF values. Most such subjets are consistent with pile-up and are excluded by the track-based jet grooming procedure. Similarly, subjets with small p_{T} ratio and large corrJVF that would be removed by calorimeter-based trimming, are kept by the track-based trimming algorithm.

For the 2012 pile-up conditions with an average of about 21 pp interactions per bunch crossing, an f_{cut} of 4% in addition to the requirement of corrJVF > 0.6 is found to be the optimal combination of trimming and corrJVF selection. A grooming configuration based solely on corrJVF (with no f_{cut} applied) is found to have a slightly worse mass resolution than trimming alone.

The jet cleansing approach is implemented in two forms: JVF cleansing and linear cleansing. In JVF cleansing, the four-momentum of each subjet is scaled by the subjet JVF, aiming to approximate the momentum of the subjet arising from neutral and charged particles from the hard-scatter vertex only. In linear cleansing, the subjet four-momentum from the hard-scatter vertex is approximated by scaling the reconstructed four-momentum based on the assumption that the ratio of charged to charged plus neutral pile-up p_{T} contributing to a subjet is 0.55 [61]. Each f_{cut} used in these procedures is chosen to optimise the mass resolution. For 2012 pile-up conditions, the application of track-assisted grooming achieves a similar mass resolution to that of calorimeter-based trimming.

Figure 19b compares the performance of the track-assisted grooming procedure with the variants of the jet cleansing concept. All of the methods studied show significant improvements in the jet mass resolution and stability with respect to pile-up. For the pile-up conditions expected during the LHC Run 1 and Run 2, studies using simulated data do not exhibit any significant difference between corrJVF and jet cleansing. However, for higher luminosity conditions expected beyond 2023 at the LHC the track-based grooming provides an alternative to calorimeter-only approaches. Another advantage of track-based grooming over standard calorimeter-based grooming is that no p_{T} threshold is involved in the removal of subjets. This means that in the limit of no pile-up, track-based grooming does not remove any signal, unlike for example trimming, which always rejects subjets that fall below the f_{cut} threshold.

8 Conclusions

The presence of multiple simultaneous proton-proton interactions, known as pile-up, is one of the major challenges for jet reconstruction at the LHC. ATLAS has implemented three main techniques to mitigate the effect of pile-up on jets and jet measurements: topological clustering, event-by-event jet pile-up subtraction, and jet vertex tagging pile-up jet suppression. The first method reduces the impact of pile-up at the constituent level, whereas the latter two techniques are

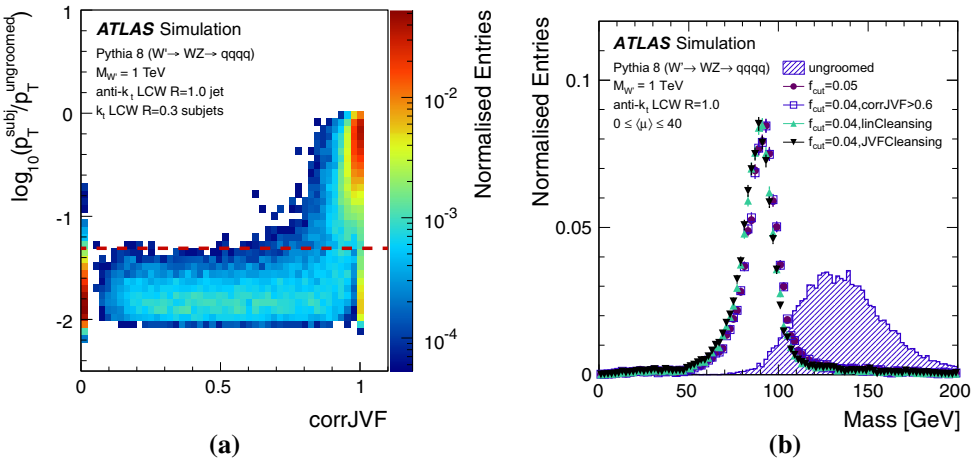

Fig. 19 **a** Correlation of subjet p_{T} fraction, defined as the ratio of the subjet p_{T} to the ungroomed jet p_{T}, and subjet corrJVF for anti-k_t $R = 1.0$ jets with $p_{\mathrm{T}} > 300$ GeV and $|\eta| < 1.5$. The *dotted line* indicates the standard calorimeter-based trimming f_{cut} of 5%. **b** Distribution of jet mass for calorimeter- and track-based trimming configurations and jet cleansing. The default trimmed jet mass (*purple filled circles*) with $f_{\mathrm{cut}} = 0.05$ is compared to calorimeter-based trimming with ($f_{\mathrm{cut}} = 0.04$) and corrJVF > 0.6 (*blue open squares*), linear cleansing (*green upward triangles*) and JVF cleansing (*black downward triangles*). The *dashed blue histogram* is the mass distribution for ungroomed jets, with no pile-up subtraction applied

applied after jet reconstruction, to correct jet kinematic and substructure variables and to suppress jets induced by pile-up.

Topological clustering partially suppresses the formation of calorimeter clusters from pile-up activity, before jet reconstruction, by considering pile-up as a form of noise in the definition of the energy significance thresholds for cells. This acts as a constituent-level pile-up suppression and significantly reduces the contribution of pile-up to the inputs to jet reconstruction. For the 20.3 fb^{-1} of pp data collected at $\sqrt{s} = 8$ TeV, topological clustering used a fixed pile-up noise corresponding to $\langle\mu\rangle = 30$. Fluctuations of pile-up due to different luminosity conditions as well as global and local event pile-up fluctuations can still affect the seeding and growth of clusters and require jet-level pile-up corrections.

The jet-area pile-up subtraction method reduces global fluctuations of pile-up in jets and allows the correction of jet shape variables. This method uses a direct measure of the pile-up activity in the calorimeter on an event-by-event basis (the p_{T} density ρ in η–ϕ space), as well as a jet-by-jet measure of pile-up susceptibility (the jet area, A^{jet}). A residual pile-up correction is necessary to fully accommodate the impact of pile-up on jet p_{T} as the high-occupancy jet core contributes some extra sensitivity to both in-time and out-of-time pile-up, and the effects of pile-up on forward jets are not fully described by the median p_{T} density as calculated from topological clusters in the central calorimeter. The combination of $\rho \times A^{\mathrm{jet}}$ subtraction and residual correction results in a stable jet p_{T} response across the full range of pile-up conditions in 2012, and it significantly reduces the degradation in jet p_{T} resolution associated with fluctuations in pile-up. It also reduces the dependence of jet multiplicity on pile-up, shifting the majority of pile-up jets below the minimum jet p_{T} threshold. For $p_{\mathrm{T}} > 50$ GeV, the pile-up subtraction procedure alone is sufficient to make the jet multiplicity stable as a function of $\langle\mu\rangle$ and N_{PV} within statistical errors. Systematic uncertainties are typically below 2% for $R = 0.4$ anti-k_t jets with $p_{\mathrm{T}} > 40$ GeV in the central region of the calorimeters; they reach up to 6% at low p_{T} and higher η. Jet-area subtraction also significantly reduces the pile-up dependence of jet shape variables.

Jet vertex tagging enables the identification and rejection of pile-up jets arising from local fluctuations of pile-up within events, as well as from QCD jets originating from pile-up vertices. A fundamental feature of the JVT algorithm, introduced in this paper, is that its discrimination power is independent of the pile-up conditions, leading to hard-scatter jet selection efficiencies that are stable within 1% for up to 35 interactions per bunch crossing. This pile-up stability implies that there is no need to re-optimise selections based on JVT as pile-up conditions change, even as the LHC transitions to $\sqrt{s} = 13$ TeV and 25 ns bunch spacing in Run 2. The JVT selection efficiency, measured as a function of p_{T} and η, is found to agree between data and simulation within 1–2%.

Jet vertex tagging has also been extended to the case of large-R jets by introducing a track-based trimming algorithm at the subjet level. The new track-based grooming achieves performance similar to that of calorimeter-based trimming, while using complementary tracking information. In particular, track-based grooming does not need to rely on subjet p_{T} selection cuts as in the case of standard grooming methods.

Jet cleansing has also been studied and results in performance similar to that of all other methods considered.

The suite of algorithms discussed in this paper has provided the capability to manage and suppress pile-up, both at the level already observed during the LHC Run 1 and at the level expected for Run 2. The impact on jet reconstruction and measurement is significant and has thus improved many aspects of the physics program in ATLAS. Pile-up corrections and suppression algorithms both for small and large radius jets have enhanced the discovery potential of the ATLAS experiment and improved the precision for Standard Model measurements. New and more advanced methods that are presented in this paper and developed towards the end of the LHC Run 1 will provide additional handles and improved precision for pile-up mitigation for the upcoming LHC Run 2 and the future high-luminosity upgrades.

Acknowledgements We thank CERN for the very successful operation of the LHC, as well as the support staff from our institutions without whom ATLAS could not be operated efficiently. We acknowledge the support of ANPCyT, Argentina; YerPhI, Armenia; ARC, Australia; BMWFW and FWF, Austria; ANAS, Azerbaijan; SSTC, Belarus; CNPq and FAPESP, Brazil; NSERC, NRC and CFI, Canada; CERN; CONICYT, Chile; CAS, MOST and NSFC, China; COLCIENCIAS, Colombia; MSMT CR, MPO CR and VSC CR, Czech Republic; DNRF and DNSRC, Denmark; IN2P3-CNRS, CEA-DSM/IRFU, France; GNSF, Georgia; BMBF, HGF, and MPG, Germany; GSRT, Greece; RGC, Hong Kong SAR, China; ISF, I-CORE and Benoziyo Center, Israel; INFN, Italy; MEXT and JSPS, Japan; CNRST, Morocco; FOM and NWO, Netherlands; RCN, Norway; MNiSW and NCN, Poland; FCT, Portugal; MNE/IFA, Romania; MES of Russia and NRC KI, Russian Federation; JINR; MESTD, Serbia; MSSR, Slovakia; ARRS and MIZŠ, Slovenia; DST/NRF, South Africa; MINECO, Spain; SRC and Wallenberg Foundation, Sweden; SERI, SNSF and Cantons of Bern and Geneva, Switzerland; MOST, Taiwan; TAEK, Turkey; STFC, United Kingdom; DOE and NSF, United States of America. In addition, individual groups and members have received support from BCKDF, the Canada Council, CANARIE, CRC, Compute Canada, FQRNT, and the Ontario Innovation Trust, Canada; EPLANET, ERC, FP7, Horizon 2020 and Marie Skłodowska-Curie Actions, European Union; Investissements d'Avenir Labex and Idex, ANR, Région Auvergne and Fondation Partager le Savoir, France; DFG and AvH Foundation, Germany; Herakleitos, Thales and Aristeia programmes co-financed by EU-ESF and the Greek NSRF; BSF, GIF and Minerva, Israel; BRF, Norway; the Royal Society and Leverhulme Trust, United Kingdom. The crucial computing support from all WLCG partners is acknowledged gratefully, in particular from CERN and the ATLAS Tier-1 facilities at TRIUMF (Canada), NDGF (Denmark, Norway, Sweden), CC-IN2P3 (France), KIT/GridKA (Germany), INFN-CNAF (Italy), NL-T1 (Netherlands), PIC (Spain), ASGC (Taiwan), RAL (UK) and BNL (USA) and in the Tier-2 facilities worldwide.

Funded by SCOAP[3].

References

1. O.S. Brüning et al., LHC Design report Vol.1: the LHC main ring, CERN-2004-003-V-1 (2004). https://cdsweb.cern.ch/record/782076
2. M. Cacciari, G.P. Salam, Pileup subtraction using jet areas. Phys. Lett. B **659**, 119 (2008). doi:10.1016/j.physletb.2007.09.077. arXiv:0707.1378 [hep-ph]
3. ATLAS Collaboration,Jet energy measurement with the ATLAS detector in proton-proton collisions at $\sqrt{s} = 7$ TeV. Eur. Phys. J. C **73**, 2304 (2013). doi:10.1140/epjc/s10052-013-2304-2. arXiv:1112.6426 [hep-ex]
4. ATLAS Collaboration, Jet energy measurement and its systematic uncertainty in proton-proton collisions at $\sqrt{s} = 7$ TeV with the ATLAS detector. Eur. Phys. J. C **75**, 17 (2015). doi:10.1140/epjc/s10052-014-3190-y. arXiv:1406.0076 [hep-ex]
5. ATLAS Collaboration, Fiducial and differential cross sections of Higgs boson production measured in the four-lepton decay channel in pp collisions at $\sqrt{s}$=8 TeV with the ATLAS detector. Phys. Lett. B **738**, 234 (2014). doi:10.1016/j.physletb.2014.09.054. arXiv:1408.3226 [hep-ex]
6. ATLAS Collaboration, Measurements of Higgs boson production and couplings in the four-lepton channel in pp collisions at center-of-mass energies of 7 and 8 TeV with the ATLAS detector. Phys. Rev. D **91**, 012006 (2015). doi:10.1103/PhysRevD.91.012006. arXiv:1408.5191 [hep-ex]
7. ATLAS Collaboration, Measurement of Higgs boson production in the diphoton decay channel in pp collisions at center-of-mass energies of 7 and 8 TeV with the ATLAS detector. Phys. Rev. D **90**, 112015 (2014). doi:10.1103/PhysRevD.90.112015. arXiv:1408.7084 [hep-ex]
8. ATLAS Collaboration, Search for the $b\bar{b}$ decay of the Standard Model Higgs boson in associated $(W/Z)H$ production with the ATLAS detector. JHEP **1501**, 069 (2015). doi:10.1007/JHEP01(2015)069. arXiv:1409.6212 [hep-ex]
9. ATLAS Collaboration, Observation and measurement of Higgs boson decays to WW* with the ATLAS detector. Phys. Rev. D **92**, 012006 (2015). doi:10.1103/PhysRevD.92.012006. arXiv:1412.2641 [hep-ex]
10. ATLAS Collaboration, The ATLAS experiment at the CERN large hadron collider. JINST **3**, S08003 (2008). doi:10.1088/1748-0221/3/08/S08003
11. ATLAS Collaboration, Performance of the ATLAS detector using first collision data. JHEP **09**, 056 (2010). doi:10.1007/JHEP09(2010)056. arXiv:1005.5254 [hep-ex]
12. ATLAS Collaboration, Charged-particle multiplicities in pp interactions measured with the ATLAS detector at the LHC. New J. Phys. **13**, 053033 (2011). doi:10.1088/1367-2630/13/5/053033. arXiv:1012.5104 [hep-ex]
13. ATLAS Collaboration, Performance of the ATLAS inner detector track and vertex reconstruction in the high Pile-Up LHC environment, ATLAS-CONF-2012-042 (2012). http://cdsweb.cern.ch/record/1435196
14. ATLAS Collaboration, Alignment of the ATLAS inner detector and its performance in 2012, ATLAS-CONF-2014-047 (2014). https://cdsweb.cern.ch/record/1741021
15. ATLAS Collaboration,A measurement of single hadron response using data at $\sqrt{s} = 8$ TeV with the ATLAS detector, ATL-PHYS-PUB-2014-002 (2014). http://cds.cern.ch/record/1668961
16. N. Buchanan et al., ATLAS liquid argon calorimeter front end electronics. JINST **3**, P09003 (2008). doi:10.1088/1748-0221/3/09/P09003
17. H. Abreu et al., Performance of the electronic readout of the ATLAS liquid argon calorimeters. JINST **5**, P09003 (2010). doi:10.1088/1748-0221/5/09/P09003

18. W.E. Cleland, E.G. Stern, Signal processing considerations for liquid ionization calorimeters in a high rate environment. Nucl. Instrum. Methods A **338**, 467 (1994). doi:10.1016/0168-9002(94)91332-3
19. ATLAS Collaboration, Readiness of the ATLAS Tile calorimeter for LHC collisions. Eur. Phys. J. C **70**, 1193 (2010). doi:10.1140/epjc/s10052-010-1508-y. arXiv:1007.5423 [physics.ins-det]
20. ATLAS Collaboration, Monitoring and data quality assessment of the ATLAS liquid argon calorimeter. JINST **9**, P07024 (2014). doi:10.1088/1748-0221/9/07/P07024. arXiv:1405.3768 [hep-ex]
21. ATLAS Collaboration, Improved luminosity determination in pp collisions at $\sqrt{s}$ = 7 TeV using the ATLAS detector at the LHC. Eur. Phys. J. C **73**, 2518 (2013). doi:10.1140/epjc/s10052-013-2518-3. arXiv:1302.4393 [hep-ex]
22. ATLAS Collaboration, Characterisation and mitigation of beam-induced backgrounds observed in the ATLAS detector during the 2011 proton-proton run. JINST **8**, P07004 (2013). doi:10.1088/1748-0221/8/07/P07004. arXiv:1303.0223 [hep-ex]
23. M. Cacciari, G.P. Salam, Dispelling the N^3 myth for the k_t jet-finder. Phys. Lett. B **641**, 57 (2006). doi:10.1016/j.physletb.2006.08.037. arXiv:hep-ph/0512210 [hep-ph]
24. M. Cacciari, G.P. Salam, G. Soyez, The anti-k_t jet clustering algorithm. JHEP **04**, 063 (2008). doi:10.1088/1126-6708/2008/04/063. arXiv:0802.1189 [hep-ph]
25. W. Lampl et al., Calorimeter clustering algorithms: description and performance, ATL-LARG-PUB-2008-002 (2008). http://cdsweb.cern.ch/record/1099735
26. ATLAS Collaboration, Search for dark matter in events with a Z boson and missing transverse momentum in pp collisions at $\sqrt{s}$=8 TeV with the ATLAS detector. Phys. Rev. D **90**, 012004 (2014). doi:10.1103/PhysRevD.90.012004. arXiv:1404.0051 [hep-ex]
27. ATLAS Collaboration, Search for $W' \to tb \to qqbb$ decays in pp collisions at $\sqrt{s}$ = 8 TeV with the ATLAS detector. Eur. Phys. J. C **75**, 165 (2015). doi:10.1140/epjc/s10052-015-3372-2. arXiv:1408.0886 [hep-ex]
28. D. Krohn, J. Thaler, L.-T. Wang, Jet trimming. JHEP **2010**, 20 (2010). doi:10.1007/JHEP02(2010)084. arXiv:0912.1342 [hep-ph]
29. S.D. Ellis, D.E. Soper, Successive combination jet algorithm for hadron collisions. Phys. Rev. D **48**, 3160 (1993). doi:10.1103/PhysRevD.48.3160. arXiv:hep-ph/9305266 [hep-ph]
30. S. Catani, Y.L. Dokshitzer, M. Seymour, B. Webber, Longitudinally invariant K_t clustering algorithms for hadron hadron collisions. Nucl. Phys. B **406**, 187 (1993). doi:10.1016/0550-3213(93)90166-M
31. ATLAS Collaboration, Performance of jet substructure techniques for large-R jets in proton-proton collisions at $\sqrt{s}$ = 7 TeV using the ATLAS detector. JHEP **1309**, 076 (2013). doi:10.1007/JHEP09(2013)076. arXiv:1306.4945 [hep-ex]
32. T. Sjöstrand, S. Mrenna, P.Z. Skands, A brief introduction to PYTHIA 8.1. Comput. Phys. Commun. **178**, 852–867 (2008). doi:10.1016/j.cpc.2008.01.036. arXiv:0710.3820 [hep-ph]
33. ATLAS Collaboration, Summary of ATLAS Pythia 8 tunes, ATL-PHYS-PUB-2012-003 (2012). http://cdsweb.cern.ch/record/1474107
34. H.-L. Lai et al., New parton distributions for collider physics. Phys. Rev. D **82**, 074024 (2010). doi:10.1103/PhysRevD.82.074024. arXiv:1007.2241 [hep-ph]
35. M. Bähr et al., Herwig++ physics and manual. Eur. Phys. J. C **58**, 639–707 (2008). doi:10.1140/epjc/s10052-008-0798-9. arXiv:0803.0883 [hep-ph]
36. J. Pumplin et al., New generation of parton distributions with uncertainties from global QCD analysis. JHEP **07**, 012 (2002). doi:10.1088/1126-6708/2002/07/012. arXiv:0201195 [hep-ph]
37. S. Gieseke, C. Rohr, A. Siodmok, Colour reconnections in Herwig++. Eur. Phys. J. C **72**, 2225 (2012). doi:10.1140/epjc/s10052-012-2225-5. arXiv:1206.0041 [hep-ph]
38. GEANT4 Collaboration, S. Agostinelli et al., GEANT4: A simulation toolkit. Nucl. Instrum. Methods A **506**, 250 (2003). doi:10.1016/S0168-9002(03)01368-8
39. ATLAS Collaboration, The ATLAS simulation infrastructure. Eur. Phys. J. C **70**, 823 (2010). doi:10.1140/epjc/s10052-010-1429-9. arXiv:1005.4568 [physics.ins-det]
40. S. Alioli, P. Nason, C. Oleari, E. Re, A general framework for implementing NLO calculations in shower Monte Carlo programs: the POWHEG BOX. JHEP **1006**, 043 (2010). doi:10.1007/JHEP06(2010)043. arXiv:1002.2581 [hep-ph]
41. S. Frixione, P. Nason, C. Oleari, Matching NLO QCD computations with Parton Shower simulations: the POWHEG method. JHEP **0711**, 070 (2007). doi:10.1088/1126-6708/2007/11/070. arXiv:0709.2092 [hep-ph]
42. P. Nason, A New method for combining NLO QCD with shower Monte Carlo algorithms. JHEP **0411**, 040 (2004). doi:10.1088/1126-6708/2004/11/040. arXiv:hep-ph/0409146 [hep-ph]
43. T. Gleisberg et al.,Event generation with SHERPA 1.1. JHEP **02**, 007 (2009). doi:10.1088/1126-6708/2009/02/007. arXiv:0811.4622 [hep-ph]
44. P. Golonka, Z. Was, PHOTOS Monte Carlo: a precision tool for QED corrections in Z and W decays. Eur. Phys. J. C **45**, 97–107 (2006). doi:10.1140/epjc/s2005-02396-4. arXiv:hep-ph/0506026 [hep-ph]
45. G. Watt, R. Thorne, Study of Monte Carlo approach to experimental uncertainty propagation with MSTW 2008 PDFs. JHEP **1208**, 052 (2012). doi:10.1007/JHEP08(2012)052. arXiv:1205.4024 [hep-ph]
46. ATLAS Collaboration, Luminosity determination in p-p collisions at $\sqrt{s}$ = 7 TeV using the ATLAS detector at the LHC. Eur. Phys. J. C **71**, 1630 (2011). doi:10.1140/epjc/s10052-011-1630-5. arXiv:1101.2185 [hep-ex]
47. C.M.S. Collaboration, Determination of jet energy calibration and transverse momentum resolution in CMS. JINST **6**, P11002 (2011). doi:10.1088/1748-0221/6/11/P11002. arXiv:1107.4277 [physics.ins-det]
48. P. Berta, M. Spousta, D.W. Miller, R. Leitner, Particle-level pileup subtraction for jets and jet shapes. JHEP **06**, 092 (2014). doi:10.1007/JHEP06(2014)092. arXiv:1403.3108 [hep-ex]
49. D. Bertolini, P. Harris, M. Low, N. Tran, Pileup per particle identification. JHEP **10**, 59 (2014). doi:10.1007/JHEP10(2014)059. arXiv:1407.6013 [hep-ph]
50. M. Cacciari, G.P. Salam, The catchment area of jets. JHEP **04**, 005 (2008). doi:10.1088/1126-6708/2008/04/005. arXiv:0802.1188 [hep-ph]
51. G. Soyez, G.P. Salam, J. Kim, S. Dutta, M. Cacciari, Pileup subtraction for jet shapes. Phys. Rev. Lett. **110**, 162001 (2013). doi:10.1103/PhysRevLett.110.162001. arXiv:1211.2811 [hep-ph]
52. J. Thaler, K. Van Tilburg, Identifying boosted objects with N-subjettiness. JHEP **1103**, 015 (2011). doi:10.1007/JHEP03(2011)015. arXiv:1011.2268 [hep-ph]
53. J. Thaler, K. Van Tilburg, Maximizing boosted top identification by minimizing N-subjettiness. JHEP **1202**, 093 (2012). doi:10.1007/JHEP02(2012)093. arXiv:1108.2701 [hep-ph]
54. J. Thaler, L.-T. Wang, Strategies to identify boosted tops. JHEP **07**, 092 (2008). doi:10.1088/1126-6708/2008/07/092. arXiv:0806.0023 [hep-ph]
55. A. Altheimer et al., Jet substructure at the Tevatron and LHC: new results, new tools, new benchmarks (BOOST 2011 Working Group Report). J. Phys. G **39**, 063001 (2012). doi:10.1088/0954-3899/39/6/063001. arXiv:1201.0008 [hep-ph]
56. ATLAS Collaboration, Search for pair production of massive particles decaying into three quarks with the ATLAS detector in $\sqrt{s} = 7$

58. A. Hoecker et al., TMVA: toolkit for multivariate data analysis. PoS **ACAT**, 040 (2007). arXiv:physics/0703039
59. ATLAS Collaboration, Light-quark and gluon jet discrimination in pp collisions at $\sqrt{s} = 7$ TeV with the ATLAS detector. Eur. Phys. J. C **74**, 3023 (2014). doi:10.1140/epjc/s10052-014-3023-z. arXiv:1405.6583 [hep-ex]
60. CMS Collaboration, Pileup jet identification, CMS-PAS-JME-13-005 (2013). http://cdsweb.cern.ch/record/1581583
61. D. Krohn, M.D. Schwartz, M. Low, L.-T. Wang, Jet cleansing: pileup removal at high luminosity. Phys. Rev. D **90**, 065020 (2014). doi:10.1103/PhysRevD.90.065020. arXiv:1309.4777 [hep-ph]

ATLAS Collaboration

G. Aad[85], B. Abbott[113], J. Abdallah[151], O. Abdinov[11], R. Aben[107], M. Abolins[90], O. S. AbouZeid[158], H. Abramowicz[153], H. Abreu[152], R. Abreu[116], Y. Abulaiti[146a,146b], B. S. Acharya[164a,164b,a], L. Adamczyk[38a], D. L. Adams[25], J. Adelman[108], S. Adomeit[100], T. Adye[131], A. A. Affolder[74], T. Agatonovic-Jovin[13], J. Agricola[54], J. A. Aguilar-Saavedra[126a,126f], S. P. Ahlen[22], F. Ahmadov[65,b], G. Aielli[133a,133b], H. Akerstedt[146a,146b], T. P. A. Åkesson[81], A. V. Akimov[96], G. L. Alberghi[20a,20b], J. Albert[169], S. Albrand[55], M. J. Alconada Verzini[71], M. Aleksa[30], I. N. Aleksandrov[65], C. Alexa[26a], G. Alexander[153], T. Alexopoulos[10], M. Alhroob[113], G. Alimonti[91a], L. Alio[85], J. Alison[31], S. P. Alkire[35], B. M. M. Allbrooke[149], P. P. Allport[18], A. Aloisio[104a,104b], A. Alonso[36], F. Alonso[71], C. Alpigiani[76], A. Altheimer[35], B. Alvarez Gonzalez[30], D. Álvarez Piqueras[167], M. G. Alviggi[104a,104b], B. T. Amadio[15], K. Amako[66], Y. Amaral Coutinho[24a], C. Amelung[23], D. Amidei[89], S. P. Amor Dos Santos[126a,126c], A. Amorim[126a,126b], S. Amoroso[48], N. Amram[153], G. Amundsen[23], C. Anastopoulos[139], L. S. Ancu[49], N. Andari[108], T. Andeen[35], C. F. Anders[58b], G. Anders[30], J. K. Anders[74], K. J. Anderson[31], A. Andreazza[91a,91b], V. Andrei[58a], S. Angelidakis[9], I. Angelozzi[107], P. Anger[44], A. Angerami[35], F. Anghinolfi[30], A. V. Anisenkov[109,c], N. Anjos[12], A. Annovi[124a,124b], M. Antonelli[47], A. Antonov[98], J. Antos[144b], F. Anulli[132a], M. Aoki[66], L. Aperio Bella[18], G. Arabidze[90], Y. Arai[66], J. P. Araque[126a], A. T. H. Arce[45], F. A. Arduh[71], J.-F. Arguin[95], S. Argyropoulos[42], M. Arik[19a], A. J. Armbruster[30], O. Arnaez[30], V. Arnal[82], H. Arnold[48], M. Arratia[28], O. Arslan[21], A. Artamonov[97], G. Artoni[23], S. Asai[155], N. Asbah[42], A. Ashkenazi[153], B. Åsman[146a,146b], L. Asquith[149], K. Assamagan[25], R. Astalos[144a], M. Atkinson[165], N. B. Atlay[141], K. Augsten[128], M. Aurousseau[145b], G. Avolio[30], B. Axen[15], M. K. Ayoub[117], G. Azuelos[95,d], M. A. Baak[30], A. E. Baas[58a], M. J. Baca[18], C. Bacci[134a,134b], H. Bachacou[136], K. Bachas[154], M. Backes[30], M. Backhaus[30], P. Bagiacchi[132a,132b], P. Bagnaia[132a,132b], Y. Bai[33a], T. Bain[35], J. T. Baines[131], O. K. Baker[176], E. M. Baldin[109,c], P. Balek[129], T. Balestri[148], F. Balli[84], E. Banas[39], Sw. Banerjee[173], A. A. E. Bannoura[175], H. S. Bansil[18], L. Barak[30], E. L. Barberio[88], D. Barberis[50a,50b], M. Barbero[85], T. Barillari[101], M. Barisonzi[164a,164b], T. Barklow[143], N. Barlow[28], S. L. Barnes[84], B. M. Barnett[131], R. M. Barnett[15], Z. Barnovska[5], A. Baroncelli[134a], G. Barone[23], A. J. Barr[120], F. Barreiro[82], J. Barreiro Guimarães da Costa[57], R. Bartoldus[143], A. E. Barton[72], P. Bartos[144a], A. Basalaev[123], A. Bassalat[117], A. Basye[165], R. L. Bates[53], S. J. Batista[158], J. R. Batley[28], M. Battaglia[137], M. Bauce[132a,132b], F. Bauer[136], H. S. Bawa[143,e], J. B. Beacham[111], M. D. Beattie[72], T. Beau[80], P. H. Beauchemin[161], R. Beccherle[124a,124b], P. Bechtle[21], H. P. Beck[17,f], K. Becker[120], M. Becker[83], S. Becker[100], M. Beckingham[170], C. Becot[117], A. J. Beddall[19b], A. Beddall[19b], V. A. Bednyakov[65], C. P. Bee[148], L. J. Beemster[107], T. A. Beermann[175], M. Begel[25], J. K. Behr[120], C. Belanger-Champagne[87], W. H. Bell[49], G. Bella[153], L. Bellagamba[20a], A. Bellerive[29], M. Bellomo[86], K. Belotskiy[98], O. Beltramello[30], O. Benary[153], D. Benchekroun[135a], M. Bender[100], K. Bendtz[146a,146b], N. Benekos[10], Y. Benhammou[153], E. Benhar Noccioli[49], J. A. Benitez Garcia[159b], D. P. Benjamin[45], J. R. Bensinger[23], S. Bentvelsen[107], L. Beresford[120], M. Beretta[47], D. Berge[107], E. Bergeaas Kuutmann[166], N. Berger[5], F. Berghaus[169], J. Beringer[15], C. Bernard[22], N. R. Bernard[86], C. Bernius[110], F. U. Bernlochner[21], T. Berry[77], P. Berta[129], C. Bertella[83], G. Bertoli[146a,146b], F. Bertolucci[124a,124b], C. Bertsche[113], D. Bertsche[113], M. I. Besana[91a], G. J. Besjes[36], O. Bessidskaia Bylund[146a,146b], M. Bessner[42], N. Besson[136], C. Betancourt[48], S. Bethke[101], A. J. Bevan[76], W. Bhimji[15], R. M. Bianchi[125], L. Bianchini[23], M. Bianco[30], O. Biebel[100], D. Biedermann[16], S. P. Bieniek[78], M. Biglietti[134a], J. Bilbao De Mendizabal[49], H. Bilokon[47], M. Bindi[54], S. Binet[117], A. Bingul[19b], C. Bini[132a,132b], S. Biondi[20a,20b], C. W. Black[150], J. E. Black[143], K. M. Black[22], D. Blackburn[138], R. E. Blair[6], J. -B. Blanchard[136], J. E. Blanco[77], T. Blazek[144a], I. Bloch[42], C. Blocker[23], W. Blum[83,*], U. Blumenschein[54], G. J. Bobbink[107], V. S. Bobrovnikov[109,c], S. S. Bocchetta[81], A. Bocci[45], C. Bock[100], M. Boehler[48], J. A. Bogaerts[30], D. Bogavac[13], A. G. Bogdanchikov[109], C. Bohm[146a], V. Boisvert[77], T. Bold[38a], V. Boldea[26a], A. S. Boldyrev[99], M. Bomben[80], M. Bona[76], M. Boonekamp[136], A. Borisov[130], G. Borissov[72], S. Borroni[42], J. Bortfeldt[100], V. Bortolotto[60a,60b,60c], K. Bos[107], D. Boscherini[20a], M. Bosman[12], J. Boudreau[125], J. Bouffard[2], E. V. Bouhova-Thacker[72], D. Boumediene[34], C. Bourdarios[117], N. Bousson[114], A. Boveia[30], J. Boyd[30], I. R. Boyko[65], I. Bozic[13], J. Bracinik[18], A. Brandt[8], G. Brandt[54], O. Brandt[58a], U. Bratzler[156], B. Brau[86], J. E. Brau[116], H. M. Braun[175,*], S. F. Brazzale[164a,164c], W. D. Breaden Madden[53], K. Brendlinger[122], A. J. Brennan[88], L. Brenner[107], R. Brenner[166], S. Bressler[172], K. Bristow[145c], T. M. Bristow[46], D. Britton[53], D. Britzger[42],

F. M. Brochu[28], I. Brock[21], R. Brock[90], J. Bronner[101], G. Brooijmans[35], T. Brooks[77], W. K. Brooks[32b], J. Brosamer[15], E. Brost[116], J. Brown[55], P. A. Bruckman de Renstrom[39], D. Bruncko[144b], R. Bruneliere[48], A. Bruni[20a], G. Bruni[20a], M. Bruschi[20a], N. Bruscino[21], L. Bryngemark[81], T. Buanes[14], Q. Buat[142], P. Buchholz[141], A. G. Buckley[53], S. I. Buda[26a], I. A. Budagov[65], F. Buehrer[48], L. Bugge[119], M. K. Bugge[119], O. Bulekov[98], D. Bullock[8], H. Burckhart[30], S. Burdin[74], B. Burghgrave[108], S. Burke[131], I. Burmeister[43], E. Busato[34], D. Büscher[48], V. Büscher[83], P. Bussey[53], J. M. Butler[22], A. I. Butt[3], C. M. Buttar[53], J. M. Butterworth[78], P. Butti[107], W. Buttinger[25], A. Buzatu[53], A. R. Buzykaev[109,c], S. Cabrera Urbán[167], D. Caforio[128], V. M. Cairo[37a,37b], O. Cakir[4a], N. Calace[49], P. Calafiura[15], A. Calandri[136], G. Calderini[80], P. Calfayan[100], L. P. Caloba[24a], D. Calvet[34], S. Calvet[34], R. Camacho Toro[31], S. Camarda[42], P. Camarri[133a,133b], D. Cameron[119], R. Caminal Armadans[165], S. Campana[30], M. Campanelli[78], A. Campoverde[148], V. Canale[104a,104b], A. Canepa[159a], M. Cano Bret[33e], J. Cantero[82], R. Cantrill[126a], T. Cao[40], M. D. M. Capeans Garrido[30], I. Caprini[26a], M. Caprini[26a], M. Capua[37a,37b], R. Caputo[83], R. Cardarelli[133a], F. Cardillo[48], T. Carli[30], G. Carlino[104a], L. Carminati[91a,91b], S. Caron[106], E. Carquin[32a], G. D. Carrillo-Montoya[8], J. R. Carter[28], J. Carvalho[126a,126c], D. Casadei[78], M. P. Casado[12], M. Casolino[12], E. Castaneda-Miranda[145b], A. Castelli[107], V. Castillo Gimenez[167], N. F. Castro[126a,g], P. Catastini[57], A. Catinaccio[30], J. R. Catmore[119], A. Cattai[30], J. Caudron[83], V. Cavaliere[165], D. Cavalli[91a], M. Cavalli-Sforza[12], V. Cavasinni[124a,124b], F. Ceradini[134a,134b], B. C. Cerio[45], K. Cerny[129], A. S. Cerqueira[24b], A. Cerri[149], L. Cerrito[76], F. Cerutti[15], M. Cerv[30], A. Cervelli[17], S. A. Cetin[19c], A. Chafaq[135a], D. Chakraborty[108], I. Chalupkova[129], P. Chang[165], J. D. Chapman[28], D. G. Charlton[18], C. C. Chau[158], C. A. Chavez Barajas[149], S. Cheatham[152], A. Chegwidden[90], S. Chekanov[6], S. V. Chekulaev[159a], G. A. Chelkov[65,h], M. A. Chelstowska[89], C. Chen[64], H. Chen[25], K. Chen[148], L. Chen[33d,i], S. Chen[33c], X. Chen[33f], Y. Chen[67], H. C. Cheng[89], Y. Cheng[31], A. Cheplakov[65], E. Cheremushkina[130], R. Cherkaoui El Moursli[135e], V. Chernyatin[25,*], E. Cheu[7], L. Chevalier[136], V. Chiarella[47], G. Chiarelli[124a,124b], J. T. Childers[6], G. Chiodini[73a], A. S. Chisholm[18], R. T. Chislett[78], A. Chitan[26a], M. V. Chizhov[65], K. Choi[61], S. Chouridou[9], B. K. B. Chow[100], V. Christodoulou[78], D. Chromek-Burckhart[30], J. Chudoba[127], A. J. Chuinard[87], J. J. Chwastowski[39], L. Chytka[115], G. Ciapetti[132a,132b], A. K. Ciftci[4a], D. Cinca[53], V. Cindro[75], I. A. Cioara[21], A. Ciocio[15], Z. H. Citron[172], M. Ciubancan[26a], A. Clark[49], B. L. Clark[57], P. J. Clark[46], R. N. Clarke[15], W. Cleland[125], C. Clement[146a,146b], Y. Coadou[85], M. Cobal[164a,164c], A. Coccaro[49], J. Cochran[64], L. Coffey[23], J. G. Cogan[143], L. Colasurdo[106], B. Cole[35], S. Cole[108], A. P. Colijn[107], J. Collot[55], T. Colombo[58c], G. Compostella[101], P. Conde Muiño[126a,126b], E. Coniavitis[48], S. H. Connell[145b], I. A. Connelly[77], S. M. Consonni[91a,91b], V. Consorti[48], S. Constantinescu[26a], C. Conta[121a,121b], G. Conti[30], F. Conventi[104a,j], M. Cooke[15], B. D. Cooper[78], A. M. Cooper-Sarkar[120], T. Cornelissen[175], M. Corradi[20a], F. Corriveau[87,k], A. Corso-Radu[163], A. Cortes-Gonzalez[12], G. Cortiana[101], G. Costa[91a], M. J. Costa[167], D. Costanzo[139], D. Côté[8], G. Cottin[28], G. Cowan[77], B. E. Cox[84], K. Cranmer[110], G. Cree[29], S. Crépé-Renaudin[55], F. Crescioli[80], W. A. Cribbs[146a,146b], M. Crispin Ortuzar[120], M. Cristinziani[21], V. Croft[106], G. Crosetti[37a,37b], T. Cuhadar Donszelmann[139], J. Cummings[176], M. Curatolo[47], C. Cuthbert[150], H. Czirr[141], P. Czodrowski[3], S. D'Auria[53], M. D'Onofrio[74], M. J. Da Cunha Sargedas De Sousa[126a,126b], C. Da Via[84], W. Dabrowski[38a], A. Dafinca[120], T. Dai[89], O. Dale[14], F. Dallaire[95], C. Dallapiccola[86], M. Dam[36], J. R. Dandoy[31], N. P. Dang[48], A. C. Daniells[18], M. Danninger[168], M. Dano Hoffmann[136], V. Dao[48], G. Darbo[50a], S. Darmora[8], J. Dassoulas[3], A. Dattagupta[61], W. Davey[21], C. David[169], T. Davidek[129], E. Davies[120,l], M. Davies[153], P. Davison[78], Y. Davygora[58a], E. Dawe[88], I. Dawson[139], R. K. Daya-Ishmukhametova[86], K. De[8], R. de Asmundis[104a], A. De Benedetti[113], S. De Castro[20a,20b], S. De Cecco[80], N. De Groot[106], P. de Jong[107], H. De la Torre[82], F. De Lorenzi[64], L. De Nooij[107], D. De Pedis[132a], A. De Salvo[132a], U. De Sanctis[149], A. De Santo[149], J. B. De Vivie De Regie[117], W. J. Dearnaley[72], R. Debbe[25], C. Debenedetti[137], D. V. Dedovich[65], I. Deigaard[107], J. Del Peso[82], T. Del Prete[124a,124b], D. Delgove[117], F. Deliot[136], C. M. Delitzsch[49], M. Deliyergiyev[75], A. Dell'Acqua[30], L. Dell'Asta[22], M. Dell'Orso[124a,124b], M. Della Pietra[104a,j], D. della Volpe[49], M. Delmastro[5], P. A. Delsart[55], C. Deluca[107], D. A. DeMarco[158], S. Demers[176], M. Demichev[65], A. Demilly[80], S. P. Denisov[130], D. Derendarz[39], J. E. Derkaoui[135d], F. Derue[80], P. Dervan[74], K. Desch[21], C. Deterre[42], P. O. Deviveiros[30], A. Dewhurst[131], S. Dhaliwal[23], A. Di Ciaccio[133a,133b], L. Di Ciaccio[5], A. Di Domenico[132a,132b], C. Di Donato[104a,104b], A. Di Girolamo[30], B. Di Girolamo[30], A. Di Mattia[152], B. Di Micco[134a,134b], R. Di Nardo[47], A. Di Simone[48], R. Di Sipio[158], D. Di Valentino[29], C. Diaconu[85], M. Diamond[158], F. A. Dias[46], M. A. Diaz[32a], E. B. Diehl[89], J. Dietrich[16], S. Diglio[85], A. Dimitrievska[13], J. Dingfelder[21], P. Dita[26a], S. Dita[26a], F. Dittus[30], F. Djama[85], T. Djobava[51b], J. I. Djuvsland[58a], M. A. B. do Vale[24c], D. Dobos[30], M. Dobre[26a], C. Doglioni[81], T. Dohmae[155], J. Dolejsi[129], Z. Dolezal[129], B. A. Dolgoshein[98,*], M. Donadelli[24d], S. Donati[124a,124b], P. Dondero[121a,121b], J. Donini[34], J. Dopke[131], A. Doria[104a], M. T. Dova[71], A. T. Doyle[53], E. Drechsler[54], M. Dris[10], E. Dubreuil[34], E. Duchovni[172], G. Duckeck[100], O. A. Ducu[26a,85], D. Duda[107], A. Dudarev[30], L. Duflot[117], L. Duguid[77], M. Dührssen[30], M. Dunford[58a], H. Duran Yildiz[4a], M. Düren[52], A. Durglishvili[51b], D. Duschinger[44], M. Dyndal[38a], C. Eckardt[42], K. M. Ecker[101], R. C. Edgar[89], W. Edson[2], N. C. Edwards[46], W. Ehrenfeld[21], T. Eifert[30], G. Eigen[14],

K. Einsweiler[15], T. Ekelof[166], M. El Kacimi[135c], M. Ellert[166], S. Elles[5], F. Ellinghaus[175], A. A. Elliot[169], N. Ellis[30], J. Elmsheuser[100], M. Elsing[30], D. Emeliyanov[131], Y. Enari[155], O. C. Endner[83], M. Endo[118], J. Erdmann[43], A. Ereditato[17], G. Ernis[175], J. Ernst[2], M. Ernst[25], S. Errede[165], E. Ertel[83], M. Escalier[117], H. Esch[43], C. Escobar[125], B. Esposito[47], A. I. Etienvre[136], E. Etzion[153], H. Evans[61], A. Ezhilov[123], L. Fabbri[20a,20b], G. Facini[31], R. M. Fakhrutdinov[130], S. Falciano[132a], R. J. Falla[78], J. Faltova[129], Y. Fang[33a], M. Fanti[91a,91b], A. Farbin[8], A. Farilla[134a], T. Farooque[12], S. Farrell[15], S. M. Farrington[170], P. Farthouat[30], F. Fassi[135e], P. Fassnacht[30], D. Fassouliotis[9], M. Faucci Giannelli[77], A. Favareto[50a,50b], L. Fayard[117], P. Federic[144a], O. L. Fedin[123,m], W. Fedorko[168], S. Feigl[30], L. Feligioni[85], C. Feng[33d], E. J. Feng[6], H. Feng[89], A. B. Fenyuk[130], L. Feremenga[8], P. Fernandez Martinez[167], S. Fernandez Perez[30], J. Ferrando[53], A. Ferrari[166], P. Ferrari[107], R. Ferrari[121a], D. E. Ferreira de Lima[53], A. Ferrer[167], D. Ferrere[49], C. Ferretti[89], A. Ferretto Parodi[50a,50b], M. Fiascaris[31], F. Fiedler[83], A. Filipčič[75], M. Filipuzzi[42], F. Filthaut[106], M. Fincke-Keeler[169], K. D. Finelli[150], M. C. N. Fiolhais[126a,126c], L. Fiorini[167], A. Firan[40], A. Fischer[2], C. Fischer[12], J. Fischer[175], W. C. Fisher[90], E. A. Fitzgerald[23], N. Flaschel[42], I. Fleck[141], P. Fleischmann[89], S. Fleischmann[175], G. T. Fletcher[139], G. Fletcher[76], R. R. M. Fletcher[122], T. Flick[175], A. Floderus[81], L. R. Flores Castillo[60a], M. J. Flowerdew[101], A. Formica[136], A. Forti[84], D. Fournier[117], H. Fox[72], S. Fracchia[12], P. Francavilla[80], M. Franchini[20a,20b], D. Francis[30], L. Franconi[119], M. Franklin[57], M. Frate[163], M. Fraternali[121a,121b], D. Freeborn[78], S. T. French[28], F. Friedrich[44], D. Froidevaux[30], J. A. Frost[120], C. Fukunaga[156], E. Fullana Torregrosa[83], B. G. Fulsom[143], T. Fusayasu[102], J. Fuster[167], C. Gabaldon[55], O. Gabizon[175], A. Gabrielli[20a,20b], A. Gabrielli[132a,132b], G. P. Gach[18], S. Gadatsch[107], S. Gadomski[49], G. Gagliardi[50a,50b], P. Gagnon[61], C. Galea[106], B. Galhardo[126a,126c], E. J. Gallas[120], B. J. Gallop[131], P. Gallus[128], G. Galster[36], K. K. Gan[111], J. Gao[33b,85], Y. Gao[46], Y. S. Gao[143,e], F. M. Garay Walls[46], F. Garberson[176], C. García[167], J. E. García Navarro[167], M. Garcia-Sciveres[15], R. W. Gardner[31], N. Garelli[143], V. Garonne[119], C. Gatti[47], A. Gaudiello[50a,50b], G. Gaudio[121a], B. Gaur[141], L. Gauthier[95], P. Gauzzi[132a,132b], I. L. Gavrilenko[96], C. Gay[168], G. Gaycken[21], E. N. Gazis[10], P. Ge[33d], Z. Gecse[168], C. N. P. Gee[131], D. A. A. Geerts[107], Ch. Geich-Gimbel[21], M. P. Geisler[58a], C. Gemme[50a], M. H. Genest[55], S. Gentile[132a,132b], M. George[54], S. George[77], D. Gerbaudo[163], A. Gershon[153], S. Ghasemi[141], H. Ghazlane[135b], B. Giacobbe[20a], S. Giagu[132a,132b], V. Giangiobbe[12], P. Giannetti[124a,124b], B. Gibbard[25], S. M. Gibson[77], M. Gilchriese[15], T. P. S. Gillam[28], D. Gillberg[30], G. Gilles[34], D. M. Gingrich[3,d], N. Giokaris[9], M. P. Giordani[164a,164c], F. M. Giorgi[20a], F. M. Giorgi[16], P. F. Giraud[136], P. Giromini[47], D. Giugni[91a], C. Giuliani[48], M. Giulini[58b], B. K. Gjelsten[119], S. Gkaitatzis[154], I. Gkialas[154], E. L. Gkougkousis[117], L. K. Gladilin[99], C. Glasman[82], J. Glatzer[30], P. C. F. Glaysher[46], A. Glazov[42], M. Goblirsch-Kolb[101], J. R. Goddard[76], J. Godlewski[39], S. Goldfarb[89], T. Golling[49], D. Golubkov[130], A. Gomes[126a,126b,126d], R. Gonçalo[126a], J. Goncalves Pinto Firmino Da Costa[136], L. Gonella[21], S. González de la Hoz[167], G. Gonzalez Parra[12], S. Gonzalez-Sevilla[49], L. Goossens[30], P. A. Gorbounov[97], H. A. Gordon[25], I. Gorelov[105], B. Gorini[30], E. Gorini[73a,73b], A. Gorišek[75], E. Gornicki[39], A. T. Goshaw[45], C. Gössling[43], M. I. Gostkin[65], D. Goujdami[135c], A. G. Goussiou[138], N. Govender[145b], E. Gozani[152], H. M. X. Grabas[137], L. Graber[54], I. Grabowska-Bold[38a], P. O. J. Gradin[166], P. Grafström[20a,20b], K-J. Grahn[42], J. Gramling[49], E. Gramstad[119], S. Grancagnolo[16], V. Grassi[148], V. Gratchev[123], H. M. Gray[30], E. Graziani[134a], Z. D. Greenwood[79,n], K. Gregersen[78], I. M. Gregor[42], P. Grenier[143], J. Griffiths[8], A. A. Grillo[137], K. Grimm[72], S. Grinstein[12,o], Ph. Gris[34], J. -F. Grivaz[117], J. P. Grohs[44], A. Grohsjean[42], E. Gross[172], J. Grosse-Knetter[54], G. C. Grossi[79], Z. J. Grout[149], L. Guan[89], J. Guenther[128], F. Guescini[49], D. Guest[176], O. Gueta[153], E. Guido[50a,50b], T. Guillemin[117], S. Guindon[2], U. Gul[53], C. Gumpert[44], J. Guo[33e], Y. Guo[33b,p], S. Gupta[120], G. Gustavino[132a,132b], P. Gutierrez[113], N. G. Gutierrez Ortiz[78], C. Gutschow[44], C. Guyot[136], C. Gwenlan[120], C. B. Gwilliam[74], A. Haas[110], C. Haber[15], H. K. Hadavand[8], N. Haddad[135e], P. Haefner[21], S. Hageböck[21], Z. Hajduk[39], H. Hakobyan[177], M. Haleem[42], J. Haley[114], D. Hall[120], G. Halladjian[90], G. D. Hallewell[85], K. Hamacher[175], P. Hamal[115], K. Hamano[169], M. Hamer[54], A. Hamilton[145a], G. N. Hamity[145c], P. G. Hamnett[42], L. Han[33b], K. Hanagaki[66,q], K. Hanawa[155], M. Hance[15], P. Hanke[58a], R. Hanna[136], J. B. Hansen[36], J. D. Hansen[36], M. C. Hansen[21], P. H. Hansen[36], K. Hara[160], A. S. Hard[173], T. Harenberg[175], F. Hariri[117], S. Harkusha[92], R. D. Harrington[46], P. F. Harrison[170], F. Hartjes[107], M. Hasegawa[67], S. Hasegawa[103], Y. Hasegawa[140], A. Hasib[113], S. Hassani[136], S. Haug[17], R. Hauser[90], L. Hauswald[44], M. Havranek[127], C. M. Hawkes[18], R. J. Hawkings[30], A. D. Hawkins[81], T. Hayashi[160], D. Hayden[90], C. P. Hays[120], J. M. Hays[76], H. S. Hayward[74], S. J. Haywood[131], S. J. Head[18], T. Heck[83], V. Hedberg[81], L. Heelan[8], S. Heim[122], T. Heim[175], B. Heinemann[15], L. Heinrich[110], J. Hejbal[127], L. Helary[22], S. Hellman[146a,146b], D. Hellmich[21], C. Helsens[12], J. Henderson[120], R. C. W. Henderson[72], Y. Heng[173], C. Hengler[42], S. Henkelmann[168], A. Henrichs[176], A. M. Henriques Correia[30], S. Henrot-Versille[117], G. H. Herbert[16], Y. Hernández Jiménez[167], R. Herrberg-Schubert[16], G. Herten[48], R. Hertenberger[100], L. Hervas[30], G. G. Hesketh[78], N. P. Hessey[107], J. W. Hetherly[40], R. Hickling[76], E. Higón-Rodriguez[167], E. Hill[169], J. C. Hill[28], K. H. Hiller[42], S. J. Hillier[18], I. Hinchliffe[15], E. Hines[122], R. R. Hinman[15], M. Hirose[157], D. Hirschbuehl[175], J. Hobbs[148], N. Hod[107], M. C. Hodgkinson[139], P. Hodgson[139], A. Hoecker[30], M. R. Hoeferkamp[105], F. Hoenig[100], M. Hohlfeld[83], D. Hohn[21], T. R. Holmes[15], M. Homann[43],

T. M. Hong[125], L. Hooft van Huysduynen[110], W. H. Hopkins[116], Y. Horii[103], A. J. Horton[142], J-Y. Hostachy[55], S. Hou[151], A. Hoummada[135a], J. Howard[120], J. Howarth[42], M. Hrabovsky[115], I. Hristova[16], J. Hrivnac[117], T. Hryn'ova[5], A. Hrynevich[93], C. Hsu[145c], P. J. Hsu[151,r], S. -C. Hsu[138], D. Hu[35], Q. Hu[33b], X. Hu[89], Y. Huang[42], Z. Hubacek[128], F. Hubaut[85], F. Huegging[21], T. B. Huffman[120], E. W. Hughes[35], G. Hughes[72], M. Huhtinen[30], T. A. Hülsing[83], N. Huseynov[65,b], J. Huston[90], J. Huth[57], G. Iacobucci[49], G. Iakovidis[25], I. Ibragimov[141], L. Iconomidou-Fayard[117], E. Ideal[176], Z. Idrissi[135e], P. Iengo[30], O. Igonkina[107], T. Iizawa[171], Y. Ikegami[66], K. Ikematsu[141], M. Ikeno[66], Y. Ilchenko[31,s], D. Iliadis[154], N. Ilic[143], T. Ince[101], G. Introzzi[121a,121b], P. Ioannou[9], M. Iodice[134a], K. Iordanidou[35], V. Ippolito[57], A. Irles Quiles[167], C. Isaksson[166], M. Ishino[68], M. Ishitsuka[157], R. Ishmukhametov[111], C. Issever[120], S. Istin[19a], J. M. Iturbe Ponce[84], R. Iuppa[133a,133b], J. Ivarsson[81], W. Iwanski[39], H. Iwasaki[66], J. M. Izen[41], V. Izzo[104a], S. Jabbar[3], B. Jackson[122], M. Jackson[74], P. Jackson[1], M. R. Jaekel[30], V. Jain[2], K. Jakobs[48], S. Jakobsen[30], T. Jakoubek[127], J. Jakubek[128], D. O. Jamin[114], D. K. Jana[79], E. Jansen[78], R. Jansky[62], J. Janssen[21], M. Janus[170], G. Jarlskog[81], N. Javadov[65,b], T. Javůrek[48], L. Jeanty[15], J. Jejelava[51a,t], G. -Y. Jeng[150], D. Jennens[88], P. Jenni[48,u], J. Jentzsch[43], C. Jeske[170], S. Jézéquel[5], H. Ji[173], J. Jia[148], Y. Jiang[33b], S. Jiggins[78], J. Jimenez Pena[167], S. Jin[33a], A. Jinaru[26a], O. Jinnouchi[157], M. D. Joergensen[36], P. Johansson[139], K. A. Johns[7], K. Jon-And[146a,146b], G. Jones[170], R. W. L. Jones[72], T. J. Jones[74], J. Jongmanns[58a], P. M. Jorge[126a,126b], K. D. Joshi[84], J. Jovicevic[159a], X. Ju[173], C. A. Jung[43], P. Jussel[62], A. Juste Rozas[12,o], M. Kaci[167], A. Kaczmarska[39], M. Kado[117], H. Kagan[111], M. Kagan[143], S. J. Kahn[85], E. Kajomovitz[45], C. W. Kalderon[120], S. Kama[40], A. Kamenshchikov[130], N. Kanaya[155], S. Kaneti[28], V. A. Kantserov[98], J. Kanzaki[66], B. Kaplan[110], L. S. Kaplan[173], A. Kapliy[31], D. Kar[53], K. Karakostas[10], A. Karamaoun[3], N. Karastathis[10,107], M. J. Kareem[54], E. Karentzos[10], M. Karnevskiy[83], S. N. Karpov[65], Z. M. Karpova[65], K. Karthik[110], V. Kartvelishvili[72], A. N. Karyukhin[130], L. Kashif[173], R. D. Kass[111], A. Kastanas[14], Y. Kataoka[155], C. Kato[155], A. Katre[49], J. Katzy[42], K. Kawagoe[70], T. Kawamoto[155], G. Kawamura[54], S. Kazama[155], V. F. Kazanin[109,c], R. Keeler[169], R. Kehoe[40], J. S. Keller[42], J. J. Kempster[77], H. Keoshkerian[84], O. Kepka[127], B. P. Kerševan[75], S. Kersten[175], R. A. Keyes[87], F. Khalil-zada[11], H. Khandanyan[146a,146b], A. Khanov[114], A. G. Kharlamov[109,c], T. J. Khoo[28], V. Khovanskiy[97], E. Khramov[65], J. Khubua[51b,v], H. Y. Kim[8], H. Kim[146a,146b], S. H. Kim[160], Y. K. Kim[31], N. Kimura[154], O. M. Kind[16], B. T. King[74], M. King[167], S. B. King[168], J. Kirk[131], A. E. Kiryunin[101], T. Kishimoto[67], D. Kisielewska[38a], F. Kiss[48], K. Kiuchi[160], O. Kivernyk[136], E. Kladiva[144b], M. H. Klein[35], M. Klein[74], U. Klein[74], K. Kleinknecht[83], P. Klimek[146a,146b], A. Klimentov[25], R. Klingenberg[43], J. A. Klinger[139], T. Klioutchnikova[30], E. -E. Kluge[58a], P. Kluit[107], S. Kluth[101], J. Knapik[39], E. Kneringer[62], E. B. F. G. Knoops[85], A. Knue[53], A. Kobayashi[155], D. Kobayashi[157], T. Kobayashi[155], M. Kobel[44], M. Kocian[143], P. Kodys[129], T. Koffas[29], E. Koffeman[107], L. A. Kogan[120], S. Kohlmann[175], Z. Kohout[128], T. Kohriki[66], T. Koi[143], H. Kolanoski[16], I. Koletsou[5], A. A. Komar[96,*], Y. Komori[155], T. Kondo[66], N. Kondrashova[42], K. Köneke[48], A. C. König[106], T. Kono[66], R. Konoplich[110,w], N. Konstantinidis[78], R. Kopeliansky[152], S. Koperny[38a], L. Köpke[83], A. K. Kopp[48], K. Korcyl[39], K. Kordas[154], A. Korn[78], A. A. Korol[109,c], I. Korolkov[12], E. V. Korolkova[139], O. Kortner[101], S. Kortner[101], T. Kosek[129], V. V. Kostyukhin[21], V. M. Kotov[65], A. Kotwal[45], A. Kourkoumeli-Charalampidi[154], C. Kourkoumelis[9], V. Kouskoura[25], A. Koutsman[159a], R. Kowalewski[169], T. Z. Kowalski[38a], W. Kozanecki[136], A. S. Kozhin[130], V. A. Kramarenko[99], G. Kramberger[75], D. Krasnopevtsev[98], M. W. Krasny[80], A. Krasznahorkay[30], J. K. Kraus[21], A. Kravchenko[25], S. Kreiss[110], M. Kretz[58c], J. Kretzschmar[74], K. Kreutzfeldt[52], P. Krieger[158], K. Krizka[31], K. Kroeninger[43], H. Kroha[101], J. Kroll[122], J. Kroseberg[21], J. Krstic[13], U. Kruchonak[65], H. Krüger[21], N. Krumnack[64], A. Kruse[173], M. C. Kruse[45], M. Kruskal[22], T. Kubota[88], H. Kucuk[78], S. Kuday[4b], S. Kuehn[48], A. Kugel[58c], F. Kuger[174], A. Kuhl[137], T. Kuhl[42], V. Kukhtin[65], Y. Kulchitsky[92], S. Kuleshov[32b], M. Kuna[132a,132b], T. Kunigo[68], A. Kupco[127], H. Kurashige[67], Y. A. Kurochkin[92], V. Kus[127], E. S. Kuwertz[169], M. Kuze[157], J. Kvita[115], T. Kwan[169], D. Kyriazopoulos[139], A. La Rosa[137], J. L. La Rosa Navarro[24d], L. La Rotonda[37a,37b], C. Lacasta[167], F. Lacava[132a,132b], J. Lacey[29], H. Lacker[16], D. Lacour[80], V. R. Lacuesta[167], E. Ladygin[65], R. Lafaye[5], B. Laforge[80], T. Lagouri[176], S. Lai[54], L. Lambourne[78], S. Lammers[61], C. L. Lampen[7], W. Lampl[7], E. Lançon[136], U. Landgraf[48], M. P. J. Landon[76], V. S. Lang[58a], J. C. Lange[12], A. J. Lankford[163], F. Lanni[25], K. Lantzsch[21], A. Lanza[121a], S. Laplace[80], C. Lapoire[30], J. F. Laporte[136], T. Lari[91a], F. Lasagni Manghi[20a,20b], M. Lassnig[30], P. Laurelli[47], W. Lavrijsen[15], A. T. Law[137], P. Laycock[74], T. Lazovich[57], O. Le Dortz[80], E. Le Guirriec[85], E. Le Menedeu[12], M. LeBlanc[169], T. LeCompte[6], F. Ledroit-Guillon[55], C. A. Lee[145b], S. C. Lee[151], L. Lee[1], G. Lefebvre[80], M. Lefebvre[169], F. Legger[100], C. Leggett[15], A. Lehan[74], G. Lehmann Miotto[30], X. Lei[7], W. A. Leight[29], A. Leisos[154,x], A. G. Leister[176], M. A. L. Leite[24d], R. Leitner[129], D. Lellouch[172], B. Lemmer[54], K. J. C. Leney[78], T. Lenz[21], B. Lenzi[30], R. Leone[7], S. Leone[124a,124b], C. Leonidopoulos[46], S. Leontsinis[10], C. Leroy[95], C. G. Lester[28], M. Levchenko[123], J. Levêque[5], D. Levin[89], L. J. Levinson[172], M. Levy[18], A. Lewis[120], A. M. Leyko[21], M. Leyton[41], B. Li[33b,y], H. Li[148], H. L. Li[31], L. Li[45], L. Li[33e], S. Li[45], Y. Li[33c,z], Z. Liang[137], H. Liao[34], B. Liberti[133a], A. Liblong[158], P. Lichard[30], K. Lie[165], J. Liebal[21], W. Liebig[14], C. Limbach[21], A. Limosani[150], S. C. Lin[151,aa], T. H. Lin[83], F. Linde[107], B. E. Lindquist[148], J. T. Linnemann[90], E. Lipeles[122], A. Lipniacka[14], M. Lisovyi[58b], T. M. Liss[165], D. Lissauer[25], A. Lister[168], A. M. Litke[137],

B. Liu[151,ab], D. Liu[151], H. Liu[89], J. Liu[85], J. B. Liu[33b], K. Liu[85], L. Liu[165], M. Liu[45], M. Liu[33b], Y. Liu[33b], M. Livan[121a,121b], A. Lleres[55], J. Llorente Merino[82], S. L. Lloyd[76], F. Lo Sterzo[151], E. Lobodzinska[42], P. Loch[7], W. S. Lockman[137], F. K. Loebinger[84], A. E. Loevschall-Jensen[36], A. Loginov[176], T. Lohse[16], K. Lohwasser[42], M. Lokajicek[127], B. A. Long[22], J. D. Long[89], R. E. Long[72], K. A. Looper[111], L. Lopes[126a], D. Lopez Mateos[57], B. Lopez Paredes[139], I. Lopez Paz[12], J. Lorenz[100], N. Lorenzo Martinez[61], M. Losada[162], P. Loscutoff[15], P. J. Lösel[100], X. Lou[33a], A. Lounis[117], J. Love[6], P. A. Love[72], N. Lu[89], H. J. Lubatti[138], C. Luci[132a,132b], A. Lucotte[55], F. Luehring[61], W. Lukas[62], L. Luminari[132a], O. Lundberg[146a,146b], B. Lund-Jensen[147], D. Lynn[25], R. Lysak[127], E. Lytken[81], H. Ma[25], L. L. Ma[33d], G. Maccarrone[47], A. Macchiolo[101], C. M. Macdonald[139], J. Machado Miguens[122,126b], D. Macina[30], D. Madaffari[85], R. Madar[34], H. J. Maddocks[72], W. F. Mader[44], A. Madsen[166], S. Maeland[14], T. Maeno[25], A. Maevskiy[99], E. Magradze[54], K. Mahboubi[48], J. Mahlstedt[107], C. Maiani[136], C. Maidantchik[24a], A. A. Maier[101], T. Maier[100], A. Maio[126a,126b,126d], S. Majewski[116], Y. Makida[66], N. Makovec[117], B. Malaescu[80], Pa. Malecki[39], V. P. Maleev[123], F. Malek[55], U. Mallik[63], D. Malon[6], C. Malone[143], S. Maltezos[10], V. M. Malyshev[109], S. Malyukov[30], J. Mamuzic[42], G. Mancini[47], B. Mandelli[30], L. Mandelli[91a], I. Mandić[75], R. Mandrysch[63], J. Maneira[126a,126b], A. Manfredini[101], L. Manhaes de Andrade Filho[24b], J. Manjarres Ramos[159b], A. Mann[100], P. M. Manning[137], A. Manousakis-Katsikakis[9], B. Mansoulie[136], R. Mantifel[87], M. Mantoani[54], L. Mapelli[30], L. March[145c], G. Marchiori[80], M. Marcisovsky[127], C. P. Marino[169], M. Marjanovic[13], D. E. Marley[89], F. Marroquim[24a], S. P. Marsden[84], Z. Marshall[15], L. F. Marti[17], S. Marti-Garcia[167], B. Martin[90], T. A. Martin[170], V. J. Martin[46], B. Martin dit Latour[14], M. Martinez[12,o], S. Martin-Haugh[131], V. S. Martoiu[26a], A. C. Martyniuk[78], M. Marx[138], F. Marzano[132a], A. Marzin[30], L. Masetti[83], T. Mashimo[155], R. Mashinistov[96], J. Masik[84], A. L. Maslennikov[109,c], I. Massa[20a,20b], L. Massa[20a,20b], N. Massol[5], P. Mastrandrea[148], A. Mastroberardino[37a,37b], T. Masubuchi[155], P. Mättig[175], J. Mattmann[83], J. Maurer[26a], S. J. Maxfield[74], D. A. Maximov[109,c], R. Mazini[151], S. M. Mazza[91a,91b], L. Mazzaferro[133a,133b], G. Mc Goldrick[158], S. P. Mc Kee[89], A. McCarn[89], R. L. McCarthy[148], T. G. McCarthy[29], N. A. McCubbin[131], K. W. McFarlane[56,*], J. A. Mcfayden[78], G. Mchedlidze[54], S. J. McMahon[131], R. A. McPherson[169,k], M. Medinnis[42], S. Meehan[145a], S. Mehlhase[100], A. Mehta[74], K. Meier[58a], C. Meineck[100], B. Meirose[41], B. R. Mellado Garcia[145c], F. Meloni[17], A. Mengarelli[20a,20b], S. Menke[101], E. Meoni[161], K. M. Mercurio[57], S. Mergelmeyer[21], P. Mermod[49], L. Merola[104a,104b], C. Meroni[91a], F. S. Merritt[31], A. Messina[132a,132b], J. Metcalfe[25], A. S. Mete[163], C. Meyer[83], C. Meyer[122], J-P. Meyer[136], J. Meyer[107], R. P. Middleton[131], S. Miglioranzi[164a,164c], L. Mijović[21], G. Mikenberg[172], M. Mikestikova[127], M. Mikuž[75], M. Milesi[88], A. Milic[30], D. W. Miller[31], C. Mills[46], A. Milov[172], D. A. Milstead[146a,146b], A. A. Minaenko[130], Y. Minami[155], I. A. Minashvili[65], A. I. Mincer[110], B. Mindur[38a], M. Mineev[65], Y. Ming[173], L. M. Mir[12], T. Mitani[171], J. Mitrevski[100], V. A. Mitsou[167], A. Miucci[49], P. S. Miyagawa[139], J. U. Mjörnmark[81], T. Moa[146a,146b], K. Mochizuki[85], S. Mohapatra[35], W. Mohr[48], S. Molander[146a,146b], R. Moles-Valls[21], K. Mönig[42], C. Monini[55], J. Monk[36], E. Monnier[85], J. Montejo Berlingen[12], F. Monticelli[71], S. Monzani[132a,132b], R. W. Moore[3], N. Morange[117], D. Moreno[162], M. Moreno Llácer[54], P. Morettini[50a], M. Morgenstern[44], D. Mori[142], M. Morii[57], M. Morinaga[155], V. Morisbak[119], S. Moritz[83], A. K. Morley[150], G. Mornacchi[30], J. D. Morris[76], S. S. Mortensen[36], A. Morton[53], L. Morvaj[103], M. Mosidze[51b], J. Moss[111], K. Motohashi[157], R. Mount[143], E. Mountricha[25], S. V. Mouraviev[96,*], E. J. W. Moyse[86], S. Muanza[85], R. D. Mudd[18], F. Mueller[101], J. Mueller[125], R. S. P. Mueller[100], T. Mueller[28], D. Muenstermann[49], P. Mullen[53], G. A. Mullier[17], J. A. Murillo Quijada[18], W. J. Murray[170,131], H. Musheghyan[54], E. Musto[152], A. G. Myagkov[130,ac], M. Myska[128], B. P. Nachman[143], O. Nackenhorst[54], J. Nadal[54], K. Nagai[120], R. Nagai[157], Y. Nagai[85], K. Nagano[66], A. Nagarkar[111], Y. Nagasaka[59], K. Nagata[160], M. Nagel[101], E. Nagy[85], A. M. Nairz[30], Y. Nakahama[30], K. Nakamura[66], T. Nakamura[155], I. Nakano[112], H. Namasivayam[41], R. F. Naranjo Garcia[42], R. Narayan[31], T. Naumann[42], G. Navarro[162], R. Nayyar[7], H. A. Neal[89], P. Yu. Nechaeva[96], T. J. Neep[84], P. D. Nef[143], A. Negri[121a,121b], M. Negrini[20a], S. Nektarijevic[106], C. Nellist[117], A. Nelson[163], S. Nemecek[127], P. Nemethy[110], A. A. Nepomuceno[24a], M. Nessi[30,ad], M. S. Neubauer[165], M. Neumann[175], R. M. Neves[110], P. Nevski[25], P. R. Newman[18], D. H. Nguyen[6], R. B. Nickerson[120], R. Nicolaidou[136], B. Nicquevert[30], J. Nielsen[137], N. Nikiforou[35], A. Nikiforov[16], V. Nikolaenko[130,ac], I. Nikolic-Audit[80], K. Nikolopoulos[18], J. K. Nilsen[119], P. Nilsson[25], Y. Ninomiya[155], A. Nisati[132a], R. Nisius[101], T. Nobe[155], M. Nomachi[118], I. Nomidis[29], T. Nooney[76], S. Norberg[113], M. Nordberg[30], O. Novgorodova[44], S. Nowak[101], M. Nozaki[66], L. Nozka[115], K. Ntekas[10], G. Nunes Hanninger[88], T. Nunnemann[100], E. Nurse[78], F. Nuti[88], B. J. O'Brien[46], F. O'grady[7], D. C. O'Neil[142], V. O'Shea[53], F. G. Oakham[29,d], H. Oberlack[101], T. Obermann[21], J. Ocariz[80], A. Ochi[67], I. Ochoa[78], J. P. Ochoa-Ricoux[32a], S. Oda[70], S. Odaka[66], H. Ogren[61], A. Oh[84], S. H. Oh[45], C. C. Ohm[15], H. Ohman[166], H. Oide[30], W. Okamura[118], H. Okawa[160], Y. Okumura[31], T. Okuyama[66], A. Olariu[26a], S. A. Olivares Pino[46], D. Oliveira Damazio[25], E. Oliver Garcia[167], A. Olszewski[39], J. Olszowska[39], A. Onofre[126a,126e], P. U. E. Onyisi[31,s], C. J. Oram[159a], M. J. Oreglia[31], Y. Oren[153], D. Orestano[134a,134b], N. Orlando[154], C. Oropeza Barrera[53], R. S. Orr[158], B. Osculati[50a,50b], R. Ospanov[84], G. Otero y Garzon[27], H. Otono[70], M. Ouchrif[135d], E. A. Ouellette[169], F. Ould-Saada[119], A. Ouraou[136], K. P. Oussoren[107], Q. Ouyang[33a], A. Ovcharova[15], M. Owen[53], R. E. Owen[18],

V. E. Ozcan[19a], N. Ozturk[8], K. Pachal[142], A. Pacheco Pages[12], C. Padilla Aranda[12], M. Pagáčová[48], S. Pagan Griso[15], E. Paganis[139], F. Paige[25], P. Pais[86], K. Pajchel[119], G. Palacino[159b], S. Palestini[30], M. Palka[38b], D. Pallin[34], A. Palma[126a,126b], Y. B. Pan[173], E. Panagiotopoulou[10], C. E. Pandini[80], J. G. Panduro Vazquez[77], P. Pani[146a,146b], S. Panitkin[25], D. Pantea[26a], L. Paolozzi[49], Th. D. Papadopoulou[10], K. Papageorgiou[154], A. Paramonov[6], D. Paredes Hernandez[154], M. A. Parker[28], K. A. Parker[139], F. Parodi[50a,50b], J. A. Parsons[35], U. Parzefall[48], E. Pasqualucci[132a], S. Passaggio[50a], F. Pastore[134a,134b,*], Fr. Pastore[77], G. Pásztor[29], S. Pataraia[175], N. D. Patel[150], J. R. Pater[84], T. Pauly[30], J. Pearce[169], B. Pearson[113], L. E. Pedersen[36], M. Pedersen[119], S. Pedraza Lopez[167], R. Pedro[126a,126b], S. V. Peleganchuk[109,c], D. Pelikan[166], O. Penc[127], C. Peng[33a], H. Peng[33b], B. Penning[31], J. Penwell[61], D. V. Perepelitsa[25], E. Perez Codina[159a], M. T. Pérez García-Estañ[167], L. Perini[91a,91b], H. Pernegger[30], S. Perrella[104a,104b], R. Peschke[42], V. D. Peshekhonov[65], K. Peters[30], R. F. Y. Peters[84], B. A. Petersen[30], T. C. Petersen[36], E. Petit[42], A. Petridis[146a,146b], C. Petridou[154], P. Petroff[117], E. Petrolo[132a], F. Petrucci[134a,134b], N. E. Pettersson[157], R. Pezoa[32b], P. W. Phillips[131], G. Piacquadio[143], E. Pianori[170], A. Picazio[49], E. Piccaro[76], M. Piccinini[20a,20b], M. A. Pickering[120], R. Piegaia[27], D. T. Pignotti[111], J. E. Pilcher[31], A. D. Pilkington[84], J. Pina[126a,126b,126d], M. Pinamonti[164a,164c,ae], J. L. Pinfold[3], A. Pingel[36], B. Pinto[126a], S. Pires[80], H. Pirumov[42], M. Pitt[172], C. Pizio[91a,91b], L. Plazak[144a], M. -A. Pleier[25], V. Pleskot[129], E. Plotnikova[65], P. Plucinski[146a,146b], D. Pluth[64], R. Poettgen[146a,146b], L. Poggioli[117], D. Pohl[21], G. Polesello[121a], A. Poley[42], A. Policicchio[37a,37b], R. Polifka[158], A. Polini[20a], C. S. Pollard[53], V. Polychronakos[25], K. Pommès[30], L. Pontecorvo[132a], B. G. Pope[90], G. A. Popeneciu[26b], D. S. Popovic[13], A. Poppleton[30], S. Pospisil[128], K. Potamianos[15], I. N. Potrap[65], C. J. Potter[149], C. T. Potter[116], G. Poulard[30], J. Poveda[30], V. Pozdnyakov[65], P. Pralavorio[85], A. Pranko[15], S. Prasad[30], S. Prell[64], D. Price[84], L. E. Price[6], M. Primavera[73a], S. Prince[87], M. Proissl[46], K. Prokofiev[60c], F. Prokoshin[32b], E. Protopapadaki[136], S. Protopopescu[25], J. Proudfoot[6], M. Przybycien[38a], E. Ptacek[116], D. Puddu[134a,134b], E. Pueschel[86], D. Puldon[148], M. Purohit[25,af], P. Puzo[117], J. Qian[89], G. Qin[53], Y. Qin[84], A. Quadt[54], D. R. Quarrie[15], W. B. Quayle[164a,164b], M. Queitsch-Maitland[84], D. Quilty[53], S. Raddum[119], V. Radeka[25], V. Radescu[42], S. K. Radhakrishnan[148], P. Radloff[116], P. Rados[88], F. Ragusa[91a,91b], G. Rahal[178], S. Rajagopalan[25], M. Rammensee[30], C. Rangel-Smith[166], F. Rauscher[100], S. Rave[83], T. Ravenscroft[53], M. Raymond[30], A. L. Read[119], N. P. Readioff[74], D. M. Rebuzzi[121a,121b], A. Redelbach[174], G. Redlinger[25], R. Reece[137], K. Reeves[41], L. Rehnisch[16], J. Reichert[122], H. Reisin[27], M. Relich[163], C. Rembser[30], H. Ren[33a], A. Renaud[117], M. Rescigno[132a], S. Resconi[91a], O. L. Rezanova[109,c], P. Reznicek[129], R. Rezvani[95], R. Richter[101], S. Richter[78], E. Richter-Was[38b], O. Ricken[21], M. Ridel[80], P. Rieck[16], C. J. Riegel[175], J. Rieger[54], M. Rijssenbeek[148], A. Rimoldi[121a,121b], L. Rinaldi[20a], B. Ristić[49], E. Ritsch[30], I. Riu[12], F. Rizatdinova[114], E. Rizvi[76], S. H. Robertson[87,k], A. Robichaud-Veronneau[87], D. Robinson[28], J. E. M. Robinson[42], A. Robson[53], C. Roda[124a,124b], S. Roe[30], O. Røhne[119], S. Rolli[161], A. Romaniouk[98], M. Romano[20a,20b], S. M. Romano Saez[34], E. Romero Adam[167], N. Rompotis[138], M. Ronzani[48], L. Roos[80], E. Ros[167], S. Rosati[132a], K. Rosbach[48], P. Rose[137], P. L. Rosendahl[14], O. Rosenthal[141], V. Rossetti[146a,146b], E. Rossi[104a,104b], L. P. Rossi[50a], R. Rosten[138], M. Rotaru[26a], I. Roth[172], J. Rothberg[138], D. Rousseau[117], C. R. Royon[136], A. Rozanov[85], Y. Rozen[152], X. Ruan[145c], F. Rubbo[143], I. Rubinskiy[42], V. I. Rud[99], C. Rudolph[44], M. S. Rudolph[158], F. Rühr[48], A. Ruiz-Martinez[30], Z. Rurikova[48], N. A. Rusakovich[65], A. Ruschke[100], H. L. Russell[138], J. P. Rutherfoord[7], N. Ruthmann[48], Y. F. Ryabov[123], M. Rybar[165], G. Rybkin[117], N. C. Ryder[120], A. F. Saavedra[150], G. Sabato[107], S. Sacerdoti[27], A. Saddique[3], H. F-W. Sadrozinski[137], R. Sadykov[65], F. Safai Tehrani[132a], M. Sahinsoy[19a], M. Saimpert[136], T. Saito[155], H. Sakamoto[155], Y. Sakurai[171], G. Salamanna[134a,134b], A. Salamon[133a], M. Saleem[113], D. Salek[107], P. H. Sales De Bruin[138], D. Salihagic[101], A. Salnikov[143], J. Salt[167], D. Salvatore[37a,37b], F. Salvatore[149], A. Salvucci[106], A. Salzburger[30], D. Sammel[48], D. Sampsonidis[154], A. Sanchez[104a,104b], J. Sánchez[167], V. Sanchez Martinez[167], H. Sandaker[119], R. L. Sandbach[76], H. G. Sander[83], M. P. Sanders[100], M. Sandhoff[175], C. Sandoval[162], R. Sandstroem[101], D. P. C. Sankey[131], M. Sannino[50a,50b], A. Sansoni[47], C. Santoni[34], R. Santonico[133a,133b], H. Santos[126a], I. Santoyo Castillo[149], K. Sapp[125], A. Sapronov[65], J. G. Saraiva[126a,126d], B. Sarrazin[21], O. Sasaki[66], Y. Sasaki[155], K. Sato[160], G. Sauvage[5,*], E. Sauvan[5], G. Savage[77], P. Savard[158,d], C. Sawyer[131], L. Sawyer[79,n], J. Saxon[31], C. Sbarra[20a], A. Sbrizzi[20a,20b], T. Scanlon[78], D. A. Scannicchio[163], M. Scarcella[150], V. Scarfone[37a,37b], J. Schaarschmidt[172], P. Schacht[101], D. Schaefer[30], R. Schaefer[42], J. Schaeffer[83], S. Schaepe[21], S. Schaetzel[58b], U. Schäfer[83], A. C. Schaffer[117], D. Schaile[100], R. D. Schamberger[148], V. Scharf[58a], V. A. Schegelsky[123], D. Scheirich[129], M. Schernau[163], C. Schiavi[50a,50b], C. Schillo[48], M. Schioppa[37a,37b], S. Schlenker[30], E. Schmidt[48], K. Schmieden[30], C. Schmitt[83], S. Schmitt[58b], S. Schmitt[42], B. Schneider[159a], Y. J. Schnellbach[74], U. Schnoor[44], L. Schoeffel[136], A. Schoening[58b], B. D. Schoenrock[90], E. Schopf[21], A. L. S. Schorlemmer[54], M. Schott[83], D. Schouten[159a], J. Schovancova[8], S. Schramm[49], M. Schreyer[174], C. Schroeder[83], N. Schuh[83], M. J. Schultens[21], H.-C. Schultz-Coulon[58a], H. Schulz[16], M. Schumacher[48], B. A. Schumm[137], Ph. Schune[136], C. Schwanenberger[84], A. Schwartzman[143], T. A. Schwarz[89], Ph. Schwegler[101], H. Schweiger[84], Ph. Schwemling[136], R. Schwienhorst[90], J. Schwindling[136], T. Schwindt[21], F. G. Sciacca[17], E. Scifo[117], G. Sciolla[23], F. Scuri[124a,124b], F. Scutti[21], J. Searcy[89], G. Sedov[42], E. Sedykh[123], P. Seema[21], S. C. Seidel[105],

A. Seiden[137], F. Seifert[128], J. M. Seixas[24a], G. Sekhniaidze[104a], K. Sekhon[89], S. J. Sekula[40], D. M. Seliverstov[123,*], N. Semprini-Cesari[20a,20b], C. Serfon[30], L. Serin[117], L. Serkin[164a,164b], T. Serre[85], M. Sessa[134a,134b], R. Seuster[159a], H. Severini[113], T. Sfiligoj[75], F. Sforza[30], A. Sfyrla[30], E. Shabalina[54], M. Shamim[116], L. Y. Shan[33a], R. Shang[165], J. T. Shank[22], M. Shapiro[15], P. B. Shatalov[97], K. Shaw[164a,164b], S. M. Shaw[84], A. Shcherbakova[146a,146b], C. Y. Shehu[149], P. Sherwood[78], L. Shi[151,ag], S. Shimizu[67], C. O. Shimmin[163], M. Shimojima[102], M. Shiyakova[65], A. Shmeleva[96], D. Shoaleh Saadi[95], M. J. Shochet[31], S. Shojaii[91a,91b], S. Shrestha[111], E. Shulga[98], M. A. Shupe[7], S. Shushkevich[42], P. Sicho[127], P. E. Sidebo[147], O. Sidiropoulou[174], D. Sidorov[114], A. Sidoti[20a,20b], F. Siegert[44], Dj. Sijacki[13], J. Silva[126a,126d], Y. Silver[153], S. B. Silverstein[146a], V. Simak[128], O. Simard[5], Lj. Simic[13], S. Simion[117], E. Simioni[83], B. Simmons[78], D. Simon[34], R. Simoniello[91a,91b], P. Sinervo[158], N. B. Sinev[116], M. Sioli[20a,20b], G. Siragusa[174], A. N. Sisakyan[65,*], S. Yu. Sivoklokov[99], J. Sjölin[146a,146b], T. B. Sjursen[14], M. B. Skinner[72], H. P. Skottowe[57], P. Skubic[113], M. Slater[18], T. Slavicek[128], M. Slawinska[107], K. Sliwa[161], V. Smakhtin[172], B. H. Smart[46], L. Smestad[14], S. Yu. Smirnov[98], Y. Smirnov[98], L. N. Smirnova[99,ah], O. Smirnova[81], M. N. K. Smith[35], R. W. Smith[35], M. Smizanska[72], K. Smolek[128], A. A. Snesarev[96], G. Snidero[76], S. Snyder[25], R. Sobie[169,k], F. Socher[44], A. Soffer[153], D. A. Soh[151,ag], C. A. Solans[30], M. Solar[128], J. Solc[128], E. Yu. Soldatov[98], U. Soldevila[167], A. A. Solodkov[130], A. Soloshenko[65], O. V. Solovyanov[130], V. Solovyev[123], P. Sommer[48], H. Y. Song[33b,y], N. Soni[1], A. Sood[15], A. Sopczak[128], B. Sopko[128], V. Sopko[128], V. Sorin[12], D. Sosa[58b], M. Sosebee[8], C. L. Sotiropoulou[124a,124b], R. Soualah[164a,164c], A. M. Soukharev[109,c], D. South[42], B. C. Sowden[77], S. Spagnolo[73a,73b], M. Spalla[124a,124b], F. Spanò[77], W. R. Spearman[57], D. Sperlich[16], F. Spettel[101], R. Spighi[20a], G. Spigo[30], L. A. Spiller[88], M. Spousta[129], T. Spreitzer[158], R. D. St. Denis[53,*], S. Staerz[44], J. Stahlman[122], R. Stamen[58a], S. Stamm[16], E. Stanecka[39], C. Stanescu[134a], M. Stanescu-Bellu[42], M. M. Stanitzki[42], S. Stapnes[119], E. A. Starchenko[130], J. Stark[55], P. Staroba[127], P. Starovoitov[42], R. Staszewski[39], P. Stavina[144a,*], P. Steinberg[25], B. Stelzer[142], H. J. Stelzer[30], O. Stelzer-Chilton[159a], H. Stenzel[52], G. A. Stewart[53], J. A. Stillings[21], M. C. Stockton[87], M. Stoebe[87], G. Stoicea[26a], P. Stolte[54], S. Stonjek[101], A. R. Stradling[8], A. Straessner[44], M. E. Stramaglia[17], J. Strandberg[147], S. Strandberg[146a,146b], A. Strandlie[119], E. Strauss[143], M. Strauss[113], P. Strizenec[144b], R. Ströhmer[174], D. M. Strom[116], R. Stroynowski[40], A. Strubig[106], S. A. Stucci[17], B. Stugu[14], N. A. Styles[42], D. Su[143], J. Su[125], R. Subramaniam[79], A. Succurro[12], Y. Sugaya[118], C. Suhr[108], M. Suk[128], V. V. Sulin[96], S. Sultansoy[4c], T. Sumida[68], S. Sun[57], X. Sun[33a], J. E. Sundermann[48], K. Suruliz[149], G. Susinno[37a,37b], M. R. Sutton[149], S. Suzuki[66], M. Svatos[127], S. Swedish[168], M. Swiatlowski[143], I. Sykora[144a], T. Sykora[129], D. Ta[90], C. Taccini[134a,134b], K. Tackmann[42], J. Taenzer[158], A. Taffard[163], R. Tafirout[159a], N. Taiblum[153], H. Takai[25], R. Takashima[69], H. Takeda[67], T. Takeshita[140], Y. Takubo[66], M. Talby[85], A. A. Talyshev[109,c], J. Y. C. Tam[174], K. G. Tan[88], J. Tanaka[155], R. Tanaka[117], S. Tanaka[66], B. B. Tannenwald[111], N. Tannoury[21], S. Tapprogge[83], S. Tarem[152], F. Tarrade[29], G. F. Tartarelli[91a], P. Tas[129], M. Tasevsky[127], T. Tashiro[68], E. Tassi[37a,37b], A. Tavares Delgado[126a,126b], Y. Tayalati[135d], F. E. Taylor[94], G. N. Taylor[88], W. Taylor[159b], F. A. Teischinger[30], M. Teixeira Dias Castanheira[76], P. Teixeira-Dias[77], K. K. Temming[48], H. Ten Kate[30], P. K. Teng[151], J. J. Teoh[118], F. Tepel[175], S. Terada[66], K. Terashi[155], J. Terron[82], S. Terzo[101], M. Testa[47], R. J. Teuscher[158,k], T. Theveneaux-Pelzer[34], J. P. Thomas[18], J. Thomas-Wilsker[77], E. N. Thompson[35], P. D. Thompson[18], R. J. Thompson[84], A. S. Thompson[53], L. A. Thomsen[176], E. Thomson[122], M. Thomson[28], R. P. Thun[89,*], M. J. Tibbetts[15], R. E. Ticse Torres[85], V. O. Tikhomirov[96,ai], Yu. A. Tikhonov[109,c], S. Timoshenko[98], E. Tiouchichine[85], P. Tipton[176], S. Tisserant[85], K. Todome[157], T. Todorov[5,*], S. Todorova-Nova[129], J. Tojo[70], S. Tokár[144a], K. Tokushuku[66], K. Tollefson[90], E. Tolley[57], L. Tomlinson[84], M. Tomoto[103], L. Tompkins[143,aj], K. Toms[105], E. Torrence[116], H. Torres[142], E. Torró Pastor[167], J. Toth[85,ak], F. Touchard[85], D. R. Tovey[139], T. Trefzger[174], L. Tremblet[30], A. Tricoli[30], I. M. Trigger[159a], S. Trincaz-Duvoid[80], M. F. Tripiana[12], W. Trischuk[158], B. Trocmé[55], C. Troncon[91a], M. Trottier-McDonald[15], M. Trovatelli[169], P. True[90], L. Truong[164a,164c], M. Trzebinski[39], A. Trzupek[39], C. Tsarouchas[30], J. C-L. Tseng[120], P. V. Tsiareshka[92], D. Tsionou[154], G. Tsipolitis[10], N. Tsirintanis[9], S. Tsiskaridze[12], V. Tsiskaridze[48], E. G. Tskhadadze[51a], I. I. Tsukerman[97], V. Tsulaia[15], S. Tsuno[66], D. Tsybychev[148], A. Tudorache[26a], V. Tudorache[26a], A. N. Tuna[122], S. A. Tupputi[20a,20b], S. Turchikhin[99,ah], D. Turecek[128], R. Turra[91a,91b], A. J. Turvey[40], P. M. Tuts[35], A. Tykhonov[49], M. Tylmad[146a,146b], M. Tyndel[131], I. Ueda[155], R. Ueno[29], M. Ughetto[146a,146b], M. Ugland[14], M. Uhlenbrock[21], F. Ukegawa[160], G. Unal[30], A. Undrus[25], G. Unel[163], F. C. Ungaro[48], Y. Unno[66], C. Unverdorben[100], J. Urban[144b], P. Urquijo[88], P. Urrejola[83], G. Usai[8], A. Usanova[62], L. Vacavant[85], V. Vacek[128], B. Vachon[87], C. Valderanis[83], N. Valencic[107], S. Valentinetti[20a,20b], A. Valero[167], L. Valery[12], S. Valkar[129], E. Valladolid Gallego[167], S. Vallecorsa[49], J. A. Valls Ferrer[167], W. Van Den Wollenberg[107], P. C. Van Der Deijl[107], R. van der Geer[107], H. van der Graaf[107], R. Van Der Leeuw[107], N. van Eldik[152], P. van Gemmeren[6], J. Van Nieuwkoop[142], I. van Vulpen[107], M. C. van Woerden[30], M. Vanadia[132a,132b], W. Vandelli[30], R. Vanguri[122], A. Vaniachine[6], F. Vannucci[80], G. Vardanyan[177], R. Vari[132a], E. W. Varnes[7], T. Varol[40], D. Varouchas[80], A. Vartapetian[8], K. E. Varvell[150], V. I. Vassilakopoulos[56], F. Vazeille[34], T. Vazquez Schroeder[87], J. Veatch[7], L. M. Veloce[158], F. Veloso[126a,126c], T. Velz[21], S. Veneziano[132a], A. Ventura[73a,73b], D. Ventura[86], M. Venturi[169], N. Venturi[158], A. Venturini[23], V. Vercesi[121a], M. Verducci[132a,132b], W. Verkerke[107],

J. C. Vermeulen[107], A. Vest[44], M. C. Vetterli[142,d], O. Viazlo[81], I. Vichou[165], T. Vickey[139], O. E. Vickey Boeriu[139], G. H. A. Viehhauser[120], S. Viel[15], R. Vigne[62], M. Villa[20a,20b], M. Villaplana Perez[91a,91b], E. Vilucchi[47], M. G. Vincter[29], V. B. Vinogradov[65], I. Vivarelli[149], F. Vives Vaque[3], S. Vlachos[10], D. Vladoiu[100], M. Vlasak[128], M. Vogel[32a], P. Vokac[128], G. Volpi[124a,124b], M. Volpi[88], H. von der Schmitt[101], H. von Radziewski[48], E. von Toerne[21], V. Vorobel[129], K. Vorobev[98], M. Vos[167], R. Voss[30], J. H. Vossebeld[74], N. Vranjes[13], M. Vranjes Milosavljevic[13], V. Vrba[127], M. Vreeswijk[107], R. Vuillermet[30], I. Vukotic[31], Z. Vykydal[128], P. Wagner[21], W. Wagner[175], H. Wahlberg[71], S. Wahrmund[44], J. Wakabayashi[103], J. Walder[72], R. Walker[100], W. Walkowiak[141], C. Wang[151], F. Wang[173], H. Wang[15], H. Wang[40], J. Wang[42], J. Wang[33a], K. Wang[87], R. Wang[6], S. M. Wang[151], T. Wang[21], T. Wang[35], X. Wang[176], C. Wanotayaroj[116], A. Warburton[87], C. P. Ward[28], D. R. Wardrope[78], M. Warsinsky[48], A. Washbrook[46], C. Wasicki[42], P. M. Watkins[18], A. T. Watson[18], I. J. Watson[150], M. F. Watson[18], G. Watts[138], S. Watts[84], B. M. Waugh[78], S. Webb[84], M. S. Weber[17], S. W. Weber[174], J. S. Webster[31], A. R. Weidberg[120], B. Weinert[61], J. Weingarten[54], C. Weiser[48], H. Weits[107], P. S. Wells[30], T. Wenaus[25], T. Wengler[30], S. Wenig[30], N. Wermes[21], M. Werner[48], P. Werner[30], M. Wessels[58a], J. Wetter[161], K. Whalen[116], A. M. Wharton[72], A. White[8], M. J. White[1], R. White[32b], S. White[124a,124b], D. Whiteson[163], F. J. Wickens[131], W. Wiedenmann[173], M. Wielers[131], P. Wienemann[21], C. Wiglesworth[36], L. A. M. Wiik-Fuchs[21], A. Wildauer[101], H. G. Wilkens[30], H. H. Williams[122], S. Williams[107], C. Willis[90], S. Willocq[86], A. Wilson[89], J. A. Wilson[18], I. Wingerter-Seez[5], F. Winklmeier[116], B. T. Winter[21], M. Wittgen[143], J. Wittkowski[100], S. J. Wollstadt[83], M. W. Wolter[39], H. Wolters[126a,126c], B. K. Wosiek[39], J. Wotschack[30], M. J. Woudstra[84], K. W. Wozniak[39], M. Wu[55], M. Wu[31], S. L. Wu[173], X. Wu[49], Y. Wu[89], T. R. Wyatt[84], B. M. Wynne[46], S. Xella[36], D. Xu[33a], L. Xu[33b,p], B. Yabsley[150], S. Yacoob[145a], R. Yakabe[67], M. Yamada[66], Y. Yamaguchi[118], A. Yamamoto[66], S. Yamamoto[155], T. Yamanaka[155], K. Yamauchi[103], Y. Yamazaki[67], Z. Yan[22], H. Yang[33e], H. Yang[173], Y. Yang[151], W-M. Yao[15], Y. Yasu[66], E. Yatsenko[5], K. H. Yau Wong[21], J. Ye[40], S. Ye[25], I. Yeletskikh[65], A. L. Yen[57], E. Yildirim[42], K. Yorita[171], R. Yoshida[6], K. Yoshihara[122], C. Young[143], C. J. S. Young[30], S. Youssef[22], D. R. Yu[15], J. Yu[8], J. M. Yu[89], J. Yu[114], L. Yuan[67], S. P. Y. Yuen[21], A. Yurkewicz[108], I. Yusuff[28,al], B. Zabinski[39], R. Zaidan[63], A. M. Zaitsev[130,ac], J. Zalieckas[14], A. Zaman[148], S. Zambito[57], L. Zanello[132a,132b], D. Zanzi[88], C. Zeitnitz[175], M. Zeman[128], A. Zemla[38a], K. Zengel[23], O. Zenin[130], T. Ženiš[144a], D. Zerwas[117], D. Zhang[89], F. Zhang[173], H. Zhang[33c], J. Zhang[6], L. Zhang[48], R. Zhang[33b,i], X. Zhang[33d], Z. Zhang[117], X. Zhao[40], Y. Zhao[33d,117], Z. Zhao[33b], A. Zhemchugov[65], J. Zhong[120], B. Zhou[89], C. Zhou[45], L. Zhou[35], L. Zhou[40], N. Zhou[163], C. G. Zhu[33d], H. Zhu[33a], J. Zhu[89], Y. Zhu[33b], X. Zhuang[33a], K. Zhukov[96], A. Zibell[174], D. Zieminska[61], N. I. Zimine[65], C. Zimmermann[83], S. Zimmermann[48], Z. Zinonos[54], M. Zinser[83], M. Ziolkowski[141], L. Živković[13], G. Zobernig[173], A. Zoccoli[20a,20b], M. zur Nedden[16], G. Zurzolo[104a,104b], L. Zwalinski[30]

[1] Department of Physics, University of Adelaide, Adelaide, Australia
[2] Physics Department, SUNY Albany, Albany, NY, USA
[3] Department of Physics, University of Alberta, Edmonton, AB, Canada
[4] [(a)]Department of Physics, Ankara University, Ankara, Turkey; [(b)]Istanbul Aydin University, Istanbul, Turkey; [(c)]Division of Physics, TOBB University of Economics and Technology, Ankara, Turkey
[5] LAPP, CNRS/IN2P3 and Université Savoie Mont Blanc, Annecy-le-Vieux, France
[6] High Energy Physics Division, Argonne National Laboratory, Argonne, IL, USA
[7] Department of Physics, University of Arizona, Tucson, AZ, USA
[8] Department of Physics, The University of Texas at Arlington, Arlington, TX, USA
[9] Physics Department, University of Athens, Athens, Greece
[10] Physics Department, National Technical University of Athens, Zografou, Greece
[11] Institute of Physics, Azerbaijan Academy of Sciences, Baku, Azerbaijan
[12] Departament de Física de la Universitat Autònoma de Barcelona, Institut de Física d'Altes Energies, Barcelona, Spain
[13] Institute of Physics, University of Belgrade, Belgrade, Serbia
[14] Department for Physics and Technology, University of Bergen, Bergen, Norway
[15] Physics Division, Lawrence Berkeley National Laboratory, University of California, Berkeley, CA, USA
[16] Department of Physics, Humboldt University, Berlin, Germany
[17] Albert Einstein Center for Fundamental Physics and Laboratory for High Energy Physics, University of Bern, Bern, Switzerland
[18] School of Physics and Astronomy, University of Birmingham, Birmingham, UK
[19] [(a)]Department of Physics, Bogazici University, Istanbul, Turkey; [(b)]Department of Physics Engineering, Gaziantep University, Gaziantep, Turkey; [(c)]Department of Physics, Dogus University, Istanbul, Turkey

[20] [(a)]INFN Sezione di Bologna, Bologna, Italy; [(b)]Dipartimento di Fisica e Astronomia, Università di Bologna, Bologna, Italy
[21] Physikalisches Institut, University of Bonn, Bonn, Germany
[22] Department of Physics, Boston University, Boston, MA, USA
[23] Department of Physics, Brandeis University, Waltham, MA, USA
[24] [(a)]Universidade Federal do Rio De Janeiro COPPE/EE/IF, Rio de Janeiro, Brazil; [(b)]Electrical Circuits Department, Federal University of Juiz de Fora (UFJF), Juiz de Fora, Brazil; [(c)]Federal University of Sao Joao del Rei (UFSJ), Sao Joao del Rei, Brazil; [(d)]Instituto de Fisica, Universidade de Sao Paulo, Sao Paulo, Brazil
[25] Physics Department, Brookhaven National Laboratory, Upton, NY, USA
[26] [(a)]National Institute of Physics and Nuclear Engineering, Bucharest, Romania; [(b)]Physics Department, National Institute for Research and Development of Isotopic and Molecular Technologies, Cluj Napoca, Romania; [(c)]University Politehnica Bucharest, Bucharest, Romania; [(d)]West University in Timisoara, Timisoara, Romania
[27] Departamento de Física, Universidad de Buenos Aires, Buenos Aires, Argentina
[28] Cavendish Laboratory, University of Cambridge, Cambridge, UK
[29] Department of Physics, Carleton University, Ottawa, ON, Canada
[30] CERN, Geneva, Switzerland
[31] Enrico Fermi Institute, University of Chicago, Chicago, IL, USA
[32] [(a)]Departamento de Física, Pontificia Universidad Católica de Chile, Santiago, Chile; [(b)]Departamento de Física, Universidad Técnica Federico Santa María, Valparaiso, Chile
[33] [(a)]Institute of High Energy Physics, Chinese Academy of Sciences, Beijing, China; [(b)]Department of Modern Physics, University of Science and Technology of China, Hefei, Anhui, China; [(c)]Department of Physics, Nanjing University, Jiangsu, China; [(d)]School of Physics, Shandong University, Shandong, China; [(e)]Department of Physics and Astronomy, Shanghai Key Laboratory for Particle Physics and Cosmology, Shanghai Jiao Tong University, Shanghai, China ; [(f)]Physics Department, Tsinghua University, Beijing 100084, China
[34] Laboratoire de Physique Corpusculaire, Clermont Université and Université Blaise Pascal and CNRS/IN2P3, Clermont-Ferrand, France
[35] Nevis Laboratory, Columbia University, Irvington, NY, USA
[36] Niels Bohr Institute, University of Copenhagen, Copenhagen, Denmark
[37] [(a)]INFN Gruppo Collegato di Cosenza, Laboratori Nazionali di Frascati, Rende, Italy; [(b)]Dipartimento di Fisica, Università della Calabria, Rende, Italy
[38] [(a)]Faculty of Physics and Applied Computer Science, AGH University of Science and Technology, Kraków, Poland ; [(b)]Marian Smoluchowski Institute of Physics, Jagiellonian University, Kraków, Poland
[39] Institute of Nuclear Physics , Polish Academy of Sciences, Kraków, Poland
[40] Physics Department, Southern Methodist University, Dallas, TX, USA
[41] Physics Department, University of Texas at Dallas, Richardson, TX, USA
[42] DESY, Hamburg and Zeuthen, Germany
[43] Institut für Experimentelle Physik IV, Technische Universität Dortmund, Dortmund, Germany
[44] Institut für Kern-und Teilchenphysik, Technische Universität Dresden, Dresden, Germany
[45] Department of Physics, Duke University, Durham, NC, USA
[46] SUPA-School of Physics and Astronomy, University of Edinburgh, Edinburgh, UK
[47] INFN Laboratori Nazionali di Frascati, Frascati, Italy
[48] Fakultät für Mathematik und Physik, Albert-Ludwigs-Universität, Freiburg, Germany
[49] Section de Physique, Université de Genève, Geneva, Switzerland
[50] [(a)]INFN Sezione di Genova, Genoa, Italy; [(b)]Dipartimento di Fisica, Università di Genova, Genoa, Italy
[51] [(a)]E. Andronikashvili Institute of Physics, Iv. Javakhishvili Tbilisi State University, Tbilisi, Georgia; [(b)]High Energy Physics Institute, Tbilisi State University, Tbilisi, Georgia
[52] II Physikalisches Institut, Justus-Liebig-Universität Giessen, Giessen, Germany
[53] SUPA-School of Physics and Astronomy, University of Glasgow, Glasgow, UK
[54] II Physikalisches Institut, Georg-August-Universität, Göttingen, Germany
[55] Laboratoire de Physique Subatomique et de Cosmologie, Université Grenoble-Alpes, CNRS/IN2P3, Grenoble, France
[56] Department of Physics, Hampton University, Hampton, VA, USA
[57] Laboratory for Particle Physics and Cosmology, Harvard University, Cambridge, MA, USA

[58] [(a)]Kirchhoff-Institut für Physik, Ruprecht-Karls-Universität Heidelberg, Heidelberg, Germany; [(b)]Physikalisches Institut, Ruprecht-Karls-Universität Heidelberg, Heidelberg, Germany; [(c)]ZITI Institut für technische Informatik, Ruprecht-Karls-Universität Heidelberg, Mannheim, Germany
[59] Faculty of Applied Information Science, Hiroshima Institute of Technology, Hiroshima, Japan
[60] [(a)]Department of Physics, The Chinese University of Hong Kong, Shatin, N.T., Hong Kong; [(b)]Department of Physics, The University of Hong Kong, Pokfulam, Hong Kong; [(c)]Department of Physics, The Hong Kong University of Science and Technology, Clear Water Bay, Kowloon, Hong Kong, China
[61] Department of Physics, Indiana University, Bloomington, IN, USA
[62] Institut für Astro- und Teilchenphysik, Leopold-Franzens-Universität, Innsbruck, Austria
[63] University of Iowa, Iowa City, IA, USA
[64] Department of Physics and Astronomy, Iowa State University, Ames, IA, USA
[65] Joint Institute for Nuclear Research, JINR Dubna, Dubna, Russia
[66] KEK, High Energy Accelerator Research Organization, Tsukuba, Japan
[67] Graduate School of Science, Kobe University, Kobe, Japan
[68] Faculty of Science, Kyoto University, Kyoto, Japan
[69] Kyoto University of Education, Kyoto, Japan
[70] Department of Physics, Kyushu University, Fukuoka, Japan
[71] Instituto de Física La Plata, Universidad Nacional de La Plata and CONICET, La Plata, Argentina
[72] Physics Department, Lancaster University, Lancaster, UK
[73] [(a)]INFN Sezione di Lecce, Lecce, Italy; [(b)]Dipartimento di Matematica e Fisica, Università del Salento, Lecce, Italy
[74] Oliver Lodge Laboratory, University of Liverpool, Liverpool, UK
[75] Department of Physics, Jožef Stefan Institute and University of Ljubljana, Ljubljana, Slovenia
[76] School of Physics and Astronomy, Queen Mary University of London, London, UK
[77] Department of Physics, Royal Holloway University of London, Surrey, UK
[78] Department of Physics and Astronomy, University College London, London, UK
[79] Louisiana Tech University, Ruston, LA, USA
[80] Laboratoire de Physique Nucléaire et de Hautes Energies, UPMC and Université Paris-Diderot and CNRS/IN2P3, Paris, France
[81] Fysiska institutionen, Lunds universitet, Lund, Sweden
[82] Departamento de Fisica Teorica C-15, Universidad Autonoma de Madrid, Madrid, Spain
[83] Institut für Physik, Universität Mainz, Mainz, Germany
[84] School of Physics and Astronomy, University of Manchester, Manchester, UK
[85] CPPM, Aix-Marseille Université and CNRS/IN2P3, Marseille, France
[86] Department of Physics, University of Massachusetts, Amherst, MA, USA
[87] Department of Physics, McGill University, Montreal, QC, Canada
[88] School of Physics, University of Melbourne, Melbourne, VIC, Australia
[89] Department of Physics, The University of Michigan, Ann Arbor, MI, USA
[90] Department of Physics and Astronomy, Michigan State University, East Lansing, MI, USA
[91] [(a)]INFN Sezione di Milano, Milan, Italy; [(b)]Dipartimento di Fisica, Università di Milano, Milan, Italy
[92] B.I. Stepanov Institute of Physics, National Academy of Sciences of Belarus, Minsk, Republic of Belarus
[93] National Scientific and Educational Centre for Particle and High Energy Physics, Minsk, Republic of Belarus
[94] Department of Physics, Massachusetts Institute of Technology, Cambridge, MA, USA
[95] Group of Particle Physics, University of Montreal, Montreal, QC, Canada
[96] P.N. Lebedev Physical Institute of the Russian, Academy of Sciences, Moscow, Russia
[97] Institute for Theoretical and Experimental Physics (ITEP), Moscow, Russia
[98] National Research Nuclear University MEPhI, Moscow, Russia
[99] D.V. Skobeltsyn Institute of Nuclear Physics, M.V. Lomonosov Moscow State University, Moscow, Russia
[100] Fakultät für Physik, Ludwig-Maximilians-Universität München, Munich, Germany
[101] Max-Planck-Institut für Physik (Werner-Heisenberg-Institut), Munich, Germany
[102] Nagasaki Institute of Applied Science, Nagasaki, Japan
[103] Graduate School of Science and Kobayashi-Maskawa Institute, Nagoya University, Nagoya, Japan
[104] [(a)]INFN Sezione di Napoli, Naples, Italy; [(b)]Dipartimento di Fisica, Università di Napoli, Naples, Italy
[105] Department of Physics and Astronomy, University of New Mexico, Albuquerque, NM, USA

[106] Institute for Mathematics, Astrophysics and Particle Physics, Radboud University Nijmegen/Nikhef, Nijmegen, The Netherlands
[107] Nikhef National Institute for Subatomic Physics and University of Amsterdam, Amsterdam, The Netherlands
[108] Department of Physics, Northern Illinois University, DeKalb, IL, USA
[109] Budker Institute of Nuclear Physics, SB RAS, Novosibirsk, Russia
[110] Department of Physics, New York University, New York, NY, USA
[111] Ohio State University, Columbus, OH, USA
[112] Faculty of Science, Okayama University, Okayama, Japan
[113] Homer L. Dodge Department of Physics and Astronomy, University of Oklahoma, Norman, OK, USA
[114] Department of Physics, Oklahoma State University, Stillwater, OK, USA
[115] Palacký University, RCPTM, Olomouc, Czech Republic
[116] Center for High Energy Physics, University of Oregon, Eugene, OR, USA
[117] LAL, Université Paris-Sub and CNRS/IN2P3, Orsay, France
[118] Graduate School of Science, Osaka University, Osaka, Japan
[119] Department of Physics, University of Oslo, Oslo, Norway
[120] Department of Physics, Oxford University, Oxford, UK
[121] [(a)]INFN Sezione di Pavia, Pavia, Italy; [(b)]Dipartimento di Fisica, Università di Pavia, Pavia, Italy
[122] Department of Physics, University of Pennsylvania, Philadelphia, PA, USA
[123] National Research Centre "Kurchatov Institute" B.P. Konstantinov Petersburg Nuclear Physics Institute, St. Petersburg, Russia
[124] [(a)]INFN Sezione di Pisa, Pisa, Italy; [(b)]Dipartimento di Fisica E. Fermi, Università di Pisa, Pisa, Italy
[125] Department of Physics and Astronomy, University of Pittsburgh, Pittsburgh, PA, USA
[126] [(a)]Laboratório de Instrumentação e Física Experimental de Partículas-LIP, Lisbon, Portugal; [(b)]Faculdade de Ciências, Universidade de Lisboa, Lisbon, Portugal; [(c)]Department of Physics, University of Coimbra, Coimbra, Portugal; [(d)]Centro de Física Nuclear da Universidade de Lisboa, Lisbon, Portugal; [(e)]Departamento de Fisica, Universidade do Minho, Braga, Portugal; [(f)]Departamento de Fisica Teorica y del Cosmos and CAFPE, Universidad de Granada, Granada, Spain ; [(g)]Dep Fisica and CEFITEC of Faculdade de Ciencias e Tecnologia, Universidade Nova de Lisboa, Caparica, Portugal
[127] Institute of Physics, Academy of Sciences of the Czech Republic, Prague, Czech Republic
[128] Czech Technical University in Prague, Prague, Czech Republic
[129] Faculty of Mathematics and Physics, Charles University in Prague, Prague, Czech Republic
[130] State Research Center Institute for High Energy Physics, Protvino, Russia
[131] Particle Physics Department, Rutherford Appleton Laboratory, Didcot, UK
[132] [(a)]INFN Sezione di Roma, Rome, Italy; [(b)]Dipartimento di Fisica, Sapienza Università di Roma, Rome, Italy
[133] [(a)]INFN Sezione di Roma Tor Vergata, Rome, Italy; [(b)]Dipartimento di Fisica, Università di Roma Tor Vergata, Rome, Italy
[134] [(a)]INFN Sezione di Roma Tre, Rome, Italy; [(b)]Dipartimento di Matematica e Fisica, Università Roma Tre, Rome, Italy
[135] [(a)]Faculté des Sciences Ain Chock, Réseau Universitaire de Physique des Hautes Energies-Université Hassan II, Casablanca, Morocco; [(b)]Centre National de l'Energie des Sciences Techniques Nucleaires, Rabat, Morocco; [(c)]Faculté des Sciences Semlalia, Université Cadi Ayyad, LPHEA-Marrakech, Marrakesh, Morocco; [(d)]Faculté des Sciences, Université Mohamed Premier and LPTPM, Oujda, Morocco; [(e)]Faculté des , Sciences, Université Mohammed V, Rabat, Morocco
[136] DSM/IRFU (Institut de Recherches sur les Lois Fondamentales de l'Univers), CEA Saclay (Commissariat à l'Energie Atomique et aux Energies Alternatives), Gif-sur-Yvette, France
[137] Santa Cruz Institute for Particle Physics, University of California Santa Cruz, Santa Cruz, CA, USA
[138] Department of Physics, University of Washington, Seattle, WA, USA
[139] Department of Physics and Astronomy, University of Sheffield, Sheffield, UK
[140] Department of Physics, Shinshu University, Nagano, Japan
[141] Fachbereich Physik, Universität Siegen, Siegen, Germany
[142] Department of Physics, Simon Fraser University, Burnaby, BC, Canada
[143] SLAC National Accelerator Laboratory, Stanford, CA, USA
[144] [(a)]Faculty of Mathematics, Physics and Informatics, Comenius University, Bratislava, Slovakia; [(b)]Department of Subnuclear Physics, Institute of Experimental Physics of the Slovak Academy of Sciences, Kosice, Slovak Republic

[145] [(a)]Department of Physics, University of Cape Town, Cape Town, South Africa; [(b)]Department of Physics, University of Johannesburg, Johannesburg, South Africa; [(c)]School of Physics, University of the Witwatersrand, Johannesburg, South Africa
[146] [(a)]Department of Physics, Stockholm University, Stockholm, Sweden; [(b)]The Oskar Klein Centre, Stockholm, Sweden
[147] Physics Department, Royal Institute of Technology, Stockholm, Sweden
[148] Departments of Physics and Astronomy and Chemistry, Stony Brook University, Stony Brook, NY, USA
[149] Department of Physics and Astronomy, University of Sussex, Brighton, UK
[150] School of Physics, University of Sydney, Sydney, Australia
[151] Institute of Physics, Academia Sinica, Taipei, Taiwan
[152] Department of Physics, Technion: Israel Institute of Technology, Haifa, Israel
[153] Raymond and Beverly Sackler School of Physics and Astronomy, Tel Aviv University, Tel Aviv, Israel
[154] Department of Physics, Aristotle University of Thessaloniki, Thessaloniki, Greece
[155] International Center for Elementary Particle Physics and Department of Physics, The University of Tokyo, Tokyo, Japan
[156] Graduate School of Science and Technology, Tokyo Metropolitan University, Tokyo, Japan
[157] Department of Physics, Tokyo Institute of Technology, Tokyo, Japan
[158] Department of Physics, University of Toronto, Toronto, ON, Canada
[159] [(a)]TRIUMF, Vancouver, BC, Canada; [(b)]Department of Physics and Astronomy, York University, Toronto, ON, Canada
[160] Faculty of Pure and Applied Sciences, University of Tsukuba, Tsukuba, Japan
[161] Department of Physics and Astronomy, Tufts University, Medford, MA, USA
[162] Centro de Investigaciones, Universidad Antonio Narino, Bogota, Colombia
[163] Department of Physics and Astronomy, University of California Irvine, Irvine, CA, USA
[164] [(a)]INFN Gruppo Collegato di Udine, Sezione di Trieste, Udine, Italy; [(b)]ICTP, Trieste, Italy; [(c)]Dipartimento di Chimica, Fisica e Ambiente, Università di Udine, Udine, Italy
[165] Department of Physics, University of Illinois, Urbana, IL, USA
[166] Department of Physics and Astronomy, University of Uppsala, Uppsala, Sweden
[167] Instituto de Física Corpuscular (IFIC) and Departamento de Física Atómica, Molecular y Nuclear and Departamento de Ingeniería Electrónica and Instituto de Microelectrónica de Barcelona (IMB-CNM), University of Valencia and CSIC, Valencia, Spain
[168] Department of Physics, University of British Columbia, Vancouver, BC, Canada
[169] Department of Physics and Astronomy, University of Victoria, Victoria, BC, Canada
[170] Department of Physics, University of Warwick, Coventry, UK
[171] Waseda University, Tokyo, Japan
[172] Department of Particle Physics, The Weizmann Institute of Science, Rehovot, Israel
[173] Department of Physics, University of Wisconsin, Madison, WI, USA
[174] Fakultät für Physik und Astronomie, Julius-Maximilians-Universität, Würzburg, Germany
[175] Fachbereich C Physik, Bergische Universität Wuppertal, Wuppertal, Germany
[176] Department of Physics, Yale University, New Haven, CT, USA
[177] Yerevan Physics Institute, Yerevan, Armenia
[178] Centre de Calcul de l'Institut National de Physique Nucléaire et de Physique des Particules (IN2P3), Villeurbanne, France

[a] Also at Department of Physics, King's College London, London, United Kingdom
[b] Also at Institute of Physics, Azerbaijan Academy of Sciences, Baku, Azerbaijan
[c] Also at Novosibirsk State University, Novosibirsk, Russia
[d] Also at TRIUMF, Vancouver BC, Canada
[e] Also at Department of Physics, California State University, Fresno CA, United States of America
[f] Also at Department of Physics, University of Fribourg, Fribourg, Switzerland
[g] Also at Departamento de Fisica e Astronomia, Faculdade de Ciencias, Universidade do Porto, Portugal
[h] Also at Tomsk State University, Tomsk, Russia
[i] Also at CPPM, Aix-Marseille Université and CNRS/IN2P3, Marseille, France
[j] Also at Universita di Napoli Parthenope, Napoli, Italy
[k] Also at Institute of Particle Physics (IPP), Canada
[l] Also at Particle Physics Department, Rutherford Appleton Laboratory, Didcot, United Kingdom
[m] Also at Department of Physics, St. Petersburg State Polytechnical University, St. Petersburg, Russia

[n] Also at Louisiana Tech University, Ruston LA, United States of America
[o] Also at Institucio Catalana de Recerca i Estudis Avancats, ICREA, Barcelona, Spain
[p] Also at Department of Physics, The University of Michigan, Ann Arbor MI, United States of America
[q] Also at Graduate School of Science, Osaka University, Osaka, Japan
[r] Also at Department of Physics, National Tsing Hua University, Taiwan
[s] Also at Department of Physics, The University of Texas at Austin, Austin TX, United States of America
[t] Also at Institute of Theoretical Physics, Ilia State University, Tbilisi, Georgia
[u] Also at CERN, Geneva, Switzerland
[v] Also at Georgian Technical University (GTU),Tbilisi, Georgia
[w] Also at Manhattan College, New York NY, United States of America
[x] Also at Hellenic Open University, Patras, Greece
[y] Also at Institute of Physics, Academia Sinica, Taipei, Taiwan
[z] Also at LAL, Université Paris-Sud and CNRS/IN2P3, Orsay, France
[aa] Also at Academia Sinica Grid Computing, Institute of Physics, Academia Sinica, Taipei, Taiwan
[ab] Also at School of Physics, Shandong University, Shandong, China
[ac] Also at Moscow Institute of Physics and Technology State University, Dolgoprudny, Russia
[ad] Also at Section de Physique, Université de Genève, Geneva, Switzerland
[ae] Also at International School for Advanced Studies (SISSA), Trieste, Italy
[af] Also at Department of Physics and Astronomy, University of South Carolina, Columbia SC, United States of America
[ag] Also at School of Physics and Engineering, Sun Yat-sen University, Guangzhou, China
[ah] Also at Faculty of Physics, M.V.Lomonosov Moscow State University, Moscow, Russia
[ai] Also at National Research Nuclear University MEPhI, Moscow, Russia
[aj] Also at Department of Physics, Stanford University, Stanford CA, United States of America
[ak] Also at Institute for Particle and Nuclear Physics, Wigner Research Centre for Physics, Budapest, Hungary
[al] Also at University of Malaya, Department of Physics, Kuala Lumpur, Malaysia
[*] Deceased